MULTIFUNCTIONAL CARBON NANOTUBE SENSORS FOR ENVIRONMENTAL MONITORING

A Dissertation Presented by

Yu Liu

to

The Department of Electrical and Computer Engineering

in partial fulfillment of the requirements

for the degree of

Doctor of Philosophy

in

Electrical Engineering

in the field of

Microsystems and Electron Devices

Northeastern University

Boston, MA. USA

March 2012

This thesis is dedicated to my parents, family and friends who taught me that love is an endless source of energy

ACKNOWLEDGMENTS

I would like to take this opportunity to thank the people who have helped me and cooperated me through the completion of this thesis for their generous contributions and continuous supports.

First of all, I want to express my deep gratitude to my advisors, Prof. Ming L. Wang and Prof. Mehmet R. Dokmeci, who continuously helped me and motivated me in all aspect of my work. Their broad knowledge and experiences, coupled with their energetic and persistent personality offered me invaluable guidance and kept me in the right track to finish this thesis. I learned a lot from their active mind, strong motivation and intelligence working attitude and I am very proud to be their student.

I wish to express my appreciation to Prof. Vincent Harris, Prof. Nian X. Sun, and Prof. Sameer Sonkusale for evaluating my thesis and defense, sharing their expertise with me and helping me during my studies at Northeastern.

I am happy to acknowledge my colleagues and friends in Snell 008, Dana 325 and CHN, especially Chia-Ling, Selvapraba, Dr. Y. Zhang, Dr. X. Li, Dr. L. Chen, Chenfu, Huiyan and Wunjun for sharing their valuable knowledge and experiences with me as well as providing me a collaborative, friendly and enjoyable environment to work.

I also want to thank all the staffs at Kostas facility, especially D. McKee, S. McNamara and R. Devito, for their help with the facility and experimental issues. Many thank to my collaborators Prof. Muftu for their generous help and collaboration and Dr. Michelle Chen for sharing her invaluable knowledge in DNA and RNA decoration.

Finally, special thanks to my family, for their continuous encouragement and for being a great spiritual support.

ABSTRACT

As a one dimensional material, a Single-walled Carbon Nanotube (SWNT) is made of a rolled up graphene sheet. With a diameter of 1~2 nm, the SWNTs exhibit many unique properties, such as high aspect ratios, ballistic carrier transport, high mechanical strength and thermal stability. These properties enable SWNTs to have superior performances in various applications including electronics and sensors. SWNT based sensors are extremely sensitive to slight electrostatic changes in their environment and have a fast response where conductance of an SWNT is observed to change in less than 2 sec upon exposure. In addition, SWNT sensors have size advantage over traditional sensors. Hence, SWNTs have been widely explored as active sensing elements for chemical and biomolecule detection.

Despite high sensitivities observed from nanotube sensors, one drawback is their lack of selectivity. The conductance of SWNTs is susceptible to many gas molecules in air, including oxygen and moisture which are abundantly present in the ambient environment. Due to this nonspecificity, the presence of any type of gas vapors can possibly interfere with the induced signals from the target gas vapors and hence reduce S/N ratio during detection. To minimize the effects of undesirable interference signals from the environment, several functionalization methods have been developed to customize the affinities of SWNTs to specific targets, including metal nano particles, conducting polymers and biomolecules.

The objective of this thesis is to utilize SWNTs in environmental applications. The proposed research topics include: investigating the sensing characteristics of RNA oligomers on carbon nanotubes; analyzing the sensing characteristics of DNA with

different sequence lengths on carbon nanotubes; integration of DNA decorated SWNTs onto CMOS chip for toxic and explosive gas monitoring; building nanosensor array based on multi-functionalized SWNTs for air quality monitoring and exploring the sensing mechanism of DNA decorated SWNTs; integration of SWNTs inside microfluidic channels for water quality monitoring. The essential procedures are composed of device fabrication (post CMOS and zincation process for CMOS chip; photolithography for silicon chip), SWNTs assembly, functionalization of SWNTs by DNA or RNA molecules, building setup for signal acquisition and processing and the measurement of sensing response to gases and liquids. These investigations will pave the way toward remote-controlled sensing arrays made of functionalized SWNTs for air and water quality monitoring. Finally a nanotube based electronic device embedded in flexible and stretchable polymer thin films is demonstrated which shows great potential to encapsulate SWNT based sensors inside flexible and stretchable substrates for structural health monitoring.

TABLE OF CONTENTS

LIST OF TABLES

LIST OF FIGURES

CHAPTER 1

INTRODUCTION

In the past few years, carbon nanotubes (CNTs) have attracted intensive interests from researchers in a wide variety of scientific fields. As a one dimensional nanomaterial, carbon nanotubes exhibit remarkable mechanical strength, unique electrical properties and efficient thermal conductivity. These inherent properties of CNTs, together with their high aspect ratio, miniature size and ability to be incorporated onto electronic devices, make them potentially useful in many applications including nanotechnology, electronics, optics and sensors. Here, I will mainly focus on the sensing applications of CNTs; especially carbon nanotube based chemical sensors and biosensors. In this chapter, the historical background, the synthesis methods of CNTs as well as their unique properties will be described. Based on those properties, various types of CNT sensors that have been developed will be introduced in the following paragraph. One drawback of SWNTs in gas sensing and biosensing applications is the lack of selectivity due to nonspecific binding. Biomolecules, such as DNA, are utilized to enhance the surface affinities of SWNTs to certain molecules. The interactions between DNA and CNTs as well as their sensing applications are introduced. Then the motivation and outlines of this thesis are introduced.

1.1 INTRODUCTION TO CARBON NANOTUBES

1.1.1 THE HISTORY OF CARBON NANOTUBES

Carbon Nanotubes was first discovered by Sumio Iijima by high resolution transmission electron microscopy in 1991, while he was studying the byproducts of fullerenes synthesized by arc discharge method. The so called multiwalled carbon nanotubes (MWNTs) were imaged as shown in Figure 1.1 [1]. Prior to that, the existence of carbon nanotubes (tubular fullerene) has been predicted by Smalley and Dresselhaus in 1990 and 1991, respectively [2, 3]. In 1993, Iijima and Ichihashi at NEC [4] and Bethune et. al. at IBM [5] simultaneously and independently reported SWNTs. These carbon nanotubes with a single atomic layer were synthesized in an arc discharge chamber as MWNTs but with a small piece of catalyst coevaporated with carbon. The observed diameter of SWNTs was about 1.2 nm. Following these pioneering discoveries, carbon nanotubes have been the leading research area in nanotechnology and significant amount of papers about carbon nanotubes were published.

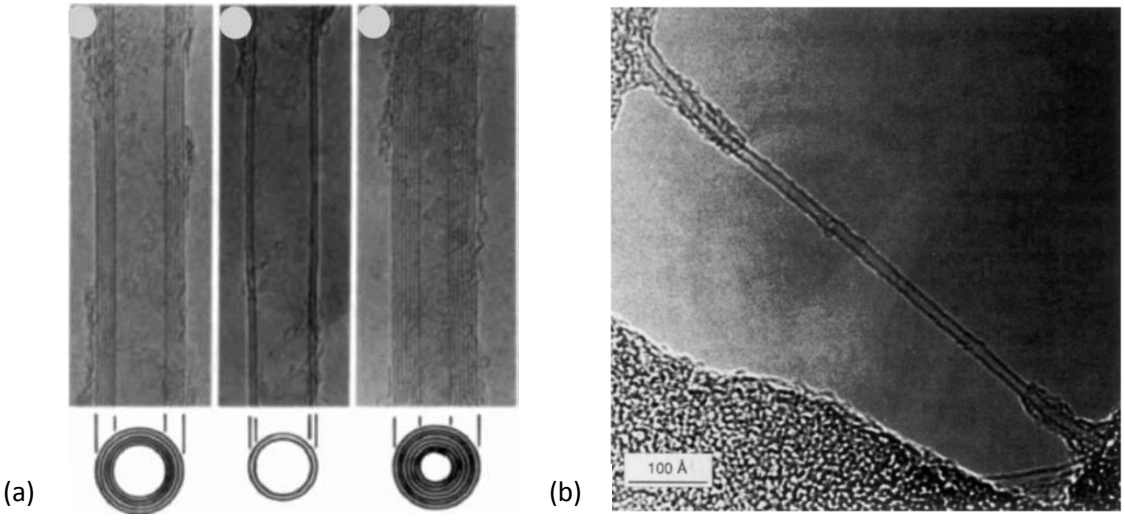

Fig. 1.1: (a) Transmission electron micrographs (TEM) of Multiwalled carbon nanotubes observed by Iijima in 1991[1]. (b) TEM image of one single-walled carbon nanotube [5].

1.1.2 GROWTH METHODS

Nowadays, MWNTs are prepared in large quantities by the chemical vapor deposition process. SWNTs can be prepared in reasonably high yields by Arc-discharge, Laser Ablation and Chemical Vapor Deposition. The first two methods require high temperature (close to the melting temperature of graphite, 3000 ºC - 4000 ºC) to generate carbon atoms evaporated from solid carbon sources. Experimental setup of these three growth methods can be illustrated in Figure 1.2 [6].

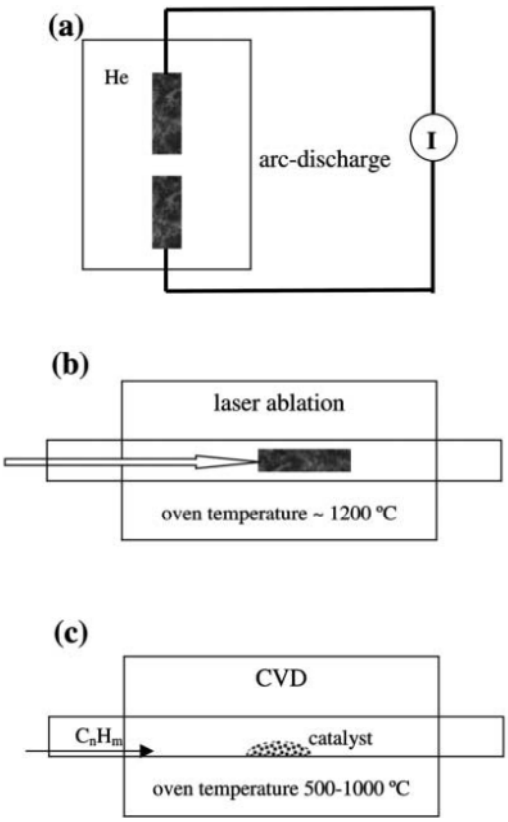

Fig. 1.2: Schematic illustration of the growth setup for carbon nanotubes. a) Arc-discharge. b) Laser ablation. c) Chemical vapor deposition [6].

In Arc-discharge, plasma of helium gas is generated by current passing through the carbon anode and cathode which evaporate carbon atoms. This method can fabricate high quality multi-walled carbon nanotubes as well as single-walled carbon nanotubes. The key parameters are the inert gas pressure inside the chamber and the arcing current [7]. Smalley and coworkers utilized laser ablation (laser oven) to grow

high quality SWNTs at 1-10 scale [8]. A carbon target containing 0.5 atomic percent of nickel and cobalt is placed in a tube-furnace oven heated to 1200 ºC. Intense laser pulses ablate carbon atoms from the target source. The grown nanotubes inside the chamber are carried by a flow of inert gas to a cold finger. Chemical Vapor Deposition (CVD) uses hydrocarbon gases as sources for carbon atoms and metal catalyst particles are used as the seeds to grow CNTs. The reaction temperature (500 ºC - 1000 ºC) is relatively lower compared to arc-discharge and laser ablation. However, the quality and structure of carbon nanotubes are not as good as those grown by other methods. The growth process of CVD involves heating a catalyst material to high temperature (typically 850 ºC) in a tube furnace and flowing a hydrocarbon gas through the tube reactor for some time. The grown nanotubes are collected after cooling the system to room temperature. The key parameters are the vapor pressure of hydrocarbons, the catalysts and growth temperature. The active catalytic species are typically transition metal nanoparticles [6]. In these growth methods, iron, cobalt and nickel are favored catalytic metals. However, other types of metal particles including copper and various noble metals can also produce SWNTs when their sizes become 1-3nm [9]. The schematic mode for CVD growth of SWNTs is shown in Figure 1.3.

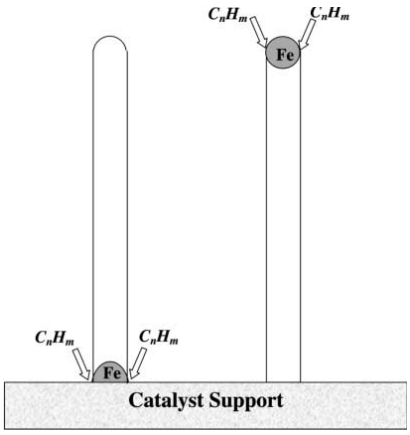

Fig. 1.3: Growth mode of chemical vapor deposition. Carbon atoms are precipitated from saturated metal nanoparticles and form tubular carbon solids in sp^2 structure [6].

1.1.3 STRUCTURE AND PROPERTIES

The interest on carbon nanotubes was triggered by their unique properties and potential applications in many areas. The fundamental properties of nanotubes are determined by their structures. A SWNT is made of a rolled up graphene sheet and the way that the graphene is rolled effect the properties of CNT significantly. The structure and properties (including electrical, optical, mechanical, chemical, thermal properties) of CNTs will be introduced in the following paragraph.

As illustrated in Figure 1.4a, SWNT is formed by rolling a graphene sheet into a cylinder along an lattice vector (m, n) in the graphene plane [10]. The m and n indices determine the diameter and chirality of nanotubes. The chiral angle $\theta = \tan^{-1}[\sqrt{3}(n/(2m + n))]$ separates carbon nanotubes into three classes: armchair ($n = m$, $\theta = 30^\circ$), zig-zag ($m = 0$, $n > 0$, $\theta = 0^\circ$), and chiral ($0 < |m| < n$, $0 < \theta < 30^\circ$) (Figure 1.4).

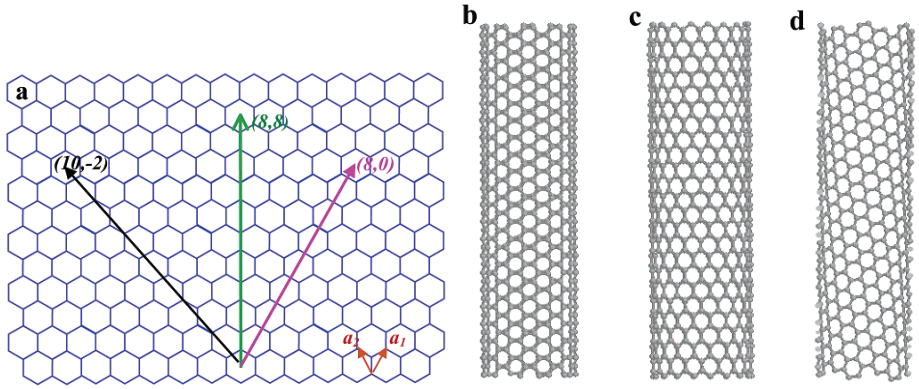

Fig. 1.4: (a) schematic illustration of hexagonal structure of graphene layer. Single walled carbon nanotube is folded by the sheet along lattice directions. (b) armchair structure formed by folding graphene sheet in (8,8), (c) zigzag folded in (8,0), (d) chiral folded in (10,-2) [10].

1.1.3.1 ELECTRIC PROPERTIES

The electrical properties of CNT and their interplay with mechanical and chemical properties have attracted lots of attention among researchers. SWNT can be metallic, semiconducting and semi-metallic wires depending on two structural parameters, chirality and diameter. Armchair carbon nanotubes are metallic (a degenerate semi-metal with zero band gap). While Zig-zag and chiral nanotubes can be semi-metallic if the band gap is finite ($n-m = 3N$, N is an integer) or semiconducting in all other cases. For

semiconducting nanotubes with the same chirality, the band gap is inversely proportional to the diameter. Thus each SWNT could exhibit distinct electrical properties. The energy gap of semiconducting nanotubes is approximately 0.5 eV [11]. SWNTs grown by CVD on supported catalyst are basically semiconducting in nature and roughly two-thirds of them are expected to be semiconducting [12], while the rest of them are metallic.

With the diameter of about 1 nm and high aspect ratio, SWNT is a one dimensional material which exhibits many unique electronic properties. Electrons in a 1D nanotube can only move forwards or backwards, so that there is no scattering of electrons in different directions. Backscattering and scattering from defect are the major causes of resistivity in CNTs. For metallic nanotubes, backscattering of electrons has been found to be almost absent. For high quality metallic carbon nanotubes with few defects, the resistance at low bias is mainly caused by acoustic phonons, which is a weak type of scattering [13]. Thus high quality metallic nanotubes are ballistic conductors at low bias (less than 200 meV) [14]. The electrons can travel several micrometers without collision at room temperature. In a conventional conductor, such as copper, the electrons can only travel for about 40 nm before scattering [15]. Semiconducting nanotubes can also exhibit ballistic conduction on the scale of several hundred nanometers [16].

Electrical properties of carbon nanotubes can undergo dramatic changes in the presence of trace amount of gases, mechanical deformations or variations in operating conditions such as temperature. The optical, mechanical, chemical and thermal properties of CNT and their correlation with electrical properties of CNT will be introduced next.

1.1.3.2 Optical Properties

High quality nanotubes, especially SWNTs, have direct band gap and well defined band and subband structure. These make individual SWNT or SWNT ropes ideal for photoluminescence and optoelectronic applications. Various optical instruments have been utilized to investigate the optical properties of carbon nanotubes. Rao and collaborators studied Raman scattering from vibrational modes of SWNT ropes with

laser excitation [17]. Numerous Raman peaks were observed and identified with the vibrational modes of armchair SWNTs. They found that different diameter tubes with different mode frequencies could be coupled with different frequencies to the laser field. Spectrofluorimetric measurements were used to differentiate semiconducting nanotubes by electronic adsorption and emission transitions [18]. Combining the fluorimetric spectra with resonance Raman measurements, the lattice structure (m, n) of carbon nanotubes can be detected therefore the tube diameter and chiral angle can be obtained. Optical spectroscopy is capable to determine the detailed composition of bulk SWNT samples [18]. Adsorption spectroscopy from the ultraviolet to the near infrared regions (UV-VIS-NIR) was utilized to investigate the electronic excitations of specific carbon nanotubes. The adsorption spectra were correlated with lattice structure (m, n) and interband transitions of specific tube types. The spectral features can be used to screen sample compositions during SWNT synthesis [19]. Hartschuh et. al. measured the electronic structure of individual SWNTs using single-molecular photoluminescence spectroscopy coupled with Raman scattering. They found that individual SWNT with identical structures have different emission energies and linewidths in fluorescence spectra which might be due to defects or difference in the local environment of carbon nanotubes. Photoluminescence was observed from individual SWNT incased in a cylindrical micelle by laser excitation. The characteristic luminescence lifetime was found to be less than 2 ns in the near infrared range and the quantum yield was estimated to be on the order of 10^{-3}. Thus this luminescence was classified as fluorescence which is spin-allowed emission from singlet excitation [20]. Photoconductivity of a single CNT incorporated on an ambipolar field-effect transistor (FET) has been observed upon infrared laser illumination [21]. The photocurrent depends on the wavelength and polarization of infrared laser. The photon energy which produces the maximum current agrees well with the second excitation state of the semiconducting nanotubes. In addition, the maximum current has been generated with light polarized along the nanotube axis. These indicate that the electron-hole pairs produced in SWNT are generated by the decay of electrons from the excitation state. On the other hand, polarized infrared optical emission has been observed from a SWNT ambipolar FET device under electrical bias [22]. The optical emission was generated from radiative recombination of electrons and

holes that were simultaneously injected into the nanotubes.

1.1.3.3 MECHANICAL PROPERTIES

Carbon nanotubes, which are essentially rolled up graphene sheets, exhibit remarkable mechanical properties. The tensile strength of nanotubes is higher than any other known materials [23]. Besides, nanotubes are extremely elastic and can reversibly bend to very large angles [24]. Unlike graphite which is brittle, some SWNTs exhibit an impressive elongation range (up to 50%). This ductile behavior is attributed to vacancy defects within nanotubes [16]. Mechanical properties of SWNTs and MWNTs are significantly different. The radial Young's modulus of MWNTs strongly decreases with increasing radius [25]. For nanotubes with 2 nm external radii, the Young's modulus is about 400 GPa. However, for nanotube with 4 nm external radii, the Young's modulus drops off to an asymptotic value with the magnitude lower than 30 GPa. Sensors based on mechanical properties or electromechanical properties of CNTs should use homogeneous nanotubes with the same type (SWNTs or MWNTs) and same radius.

Due to the large tensile strength of nanotubes, they have been widely investigated for target components of nanoscale fiber-reinforced composites for mechanical applications. They have either been dispersed individually or incorporated as filamentary bundles or ropes. Epoxy thin films with 0.1 wt % MWNTs showed a 20% increase in elastic modulus compared to net resin thin film [26]. CNT reinforced Aluminum composites exhibit an increase in relative microhardness [27]. It has been observed that nanotube composite carbon fibers increased its tensile strength by 90% and its modulus by 150%, after adding 5% SWNTs [28].

Due to potential application of CNTs in electromechanical devices, such as strain sensors, the effect of mechanical deformation on electrical properties of CNTs have been investigated. Researches in this area mainly used metallic CNTs because basically the conductance of metallic nanotubes changed when a deformation is applied. Tombler and colleagues investigated the effect of local probe manipulation on the electrical properties of CNTs [29]. An AFM tip was applied to bend a metallic SWNT suspended between two metal electrodes. The middle part of the SWNT was suspended over a trench etched into the SiO_2

surface. The AFM tip was located over the middle of suspended SWNT to apply a force to bend the nanotube. In the meantime, the conductance of the nanotube was recorded by the electrodes. The experimental setup and measured deflection and conductance of SWNT are illustrated in Figure 1.5. From the image, the conductance of nanotube decreased with increased bending and this electrical response to mechanical deformation was reversible and repeatable. This indicated that the change in conductance was purely due to mechanical deformation of the nanotube caused by the tip. In addition, the change in conductance increased with deformation angle. For small bending angle (< 5º), the conductance decreased slowly with bending angle; at higher bending angle (> 5º), the conductance decreased much faster with bending angle.

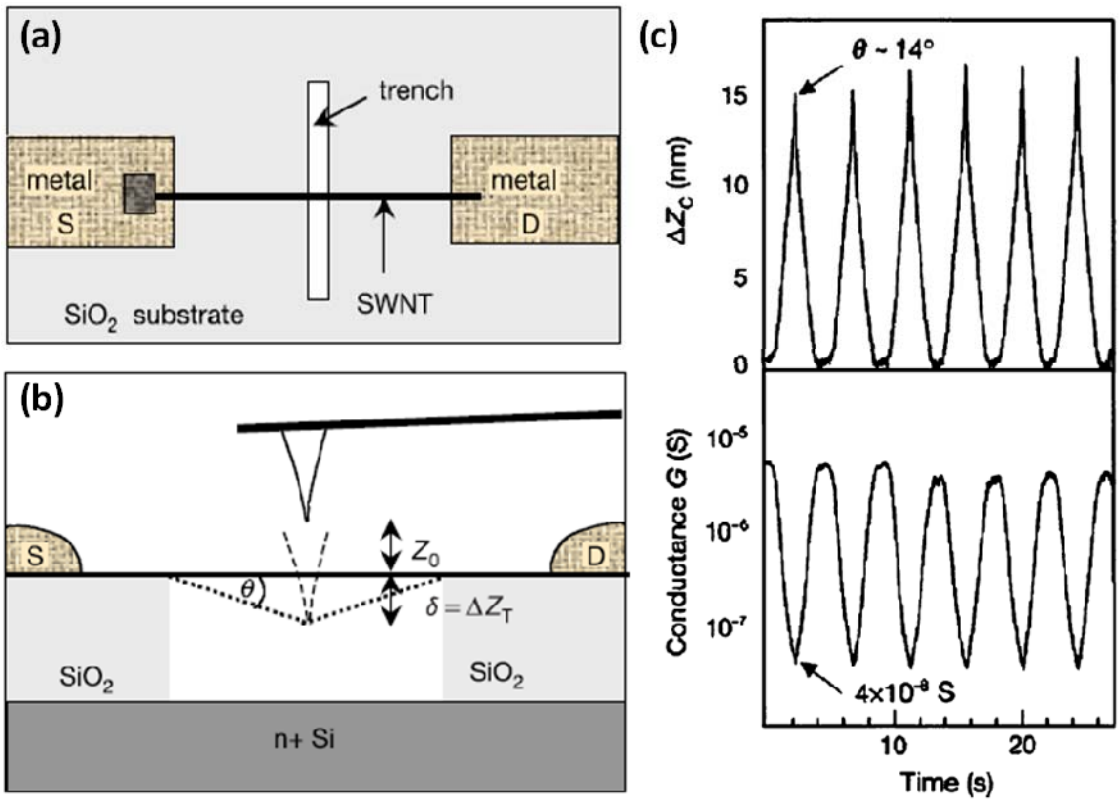

Fig. 1.5: Experimental setup for bending SWNT suspended between two electrodes by AFM tip. (a) Top view of the device. (b) Bottom view of the experiment. (c) Deflection of the cantilever and conductance of carbon nanotube during repeated cycles of bending the suspended SWNT [29].

Cao et. al. investigated the electromechanical properties of metallic, quasimetallic and semiconducting carbon nanotubes under stretching [30]. They found that small band-gap semiconducting (or quasimetallic) nanotubes exhibited the largest resistance change and piezoresistive gauge factors (600~1000) under axial strains, while metallic nanotubes showed the least but nonzero sensitivity to tensile stretching.

1.1.3.4 CHEMICAL PROPERTIES

High aspect ratio, large surface area and σ-π rehybridization make CNTs have great potential in chemical and biological sensing applications due to their high sensitivity to chemical and environmental conditions. Thus the study of chemical properties of nanotubes including surface reactivity, wetting, filling properties, adsorption, charge transfer and ionic chemistry (doping) has been of keen interest.

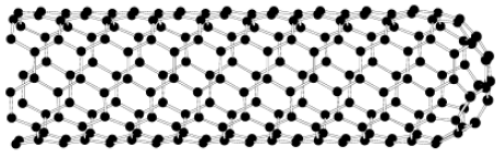

Fig. 1.6: Diagram of SWNT with end cap. The structure of end cap is a hemispherical fullerene.

Perfect SWNT without any surface functional groups is a one dimensional cylindrical aromatic macromolecule (Figure 1.6) and is chemically inert. However, there are curvature-induced pyramidalization and misalignment of the π-orbitals of the carbon atoms which induces a local strain [31-34]. Thus carbon nanotubes are expected to be more reactive than a flat graphene sheet. The nanotube end cap is more reactive than the sidewall due to the presence of pentagons and metallic catalysts sitting at the ends and its greater curvature. Many approaches have been developed to modified the ends of carbon nanotubes with various functional groups, while maintain their basic electronic structures. When sonicate CNTs in strong oxidizing agents, such as HNO_3 or H_2SO_4, the ends of nanotubes can be functionalized with carboxyl groups [35]. Sonicating nanotubes in organic solvents produces dangling bonds in the SWNTs which can undergo further chemical reactions [36].

Nanotubes are hydrophobic and extremely resistant to wetting in most aqueous solvents. They normally exist as ropes or bundles with 10-25 nm diameter and a few micrometers long. The SWNT ropes are entangled together and form a dense, complex network. Nitric acid treated SWNTs with the end caps oxidized to carboxylic acid and other weakly acidic functionalities can be dispersed in various amid-types of organic solvents with the help of ultrasonication. However, the nitric acid treatment will introduce defects on the nanotube surfaces [37]. A carbon nanotube provides a capillary force which is inversely proportional to the tube diameter. Therefore, wetting agents of CNTs are able to fill inside the nanotubes by capillary force. For nonwetting agents, the filling can be assisted by applying wetting agents such as HNO_3.

Enhanced molecular adsorption and charge transfer make nanotubes a unique sensing material for chemicals and biomolecules. It has been observed that various gases and vapors could adsorb on CNTs and change their conductance [38]. Theoretical calculations using first principle approaches have been conducted to analyze the adsorption of various gases [39]. The gas adsorption and charge transfer capability are depended on the sites and type of gases. Normally the gas molecules tend to adsorb on the interstitial in tube bundles, groove above the gap between two neighboring tubes, nanopore inside a tube and surface of single tube [40, 41]. The adsorption and charge transfer capability are found to follow a decreasing order:

Sites: Interstitial, groove, nanopore and surface

Gas: $C_8N_2O_2Cl_2$, O_2, C_6H_{12}, C_6H_6, NO_2, H_2O, NH_3, CH_4, CO_2, N_2, H_2, Ar

The calculated distance between the gas molecules and the nearest nanotubes after adsorption ranges from 0.193 nm for NO_2 and 0.332 nm for Ar. The adsorption energy ranges from 30.6kJ/mol for $C_8N_2O_2Cl_2$ to 1kJ/mol for Ar. The partial charge of gas molecules ranges from 0.212 for $C_8N_2O_2Cl_2$ to 0.01 for N_2 [39]. Among these gases, $C_8N_2O_2Cl_2$, O_2 and NO_2 are electron acceptors which attract negative charge from the nanotubes after being adsorbed. Thus the resistance of CNTs will decrease due to more charge carriers (holes) been created, while other gases are electron donors which compensate the holes in

nanotubes and increase the resistance of CNTs.

Boron and Nitrogen as substitutional dopants were used to make nanotubes p- and n- types. Adsorbed gas molecules can provide noncovalent doping to carbon nanotubes. For example, CNTs can be easily turned into p-type by oxygen or water adsorption, while n-type by C_6H_{12} adsorption. Intercalation of alkali metals with nanotubes is used to enhance their metallic conductivity. Experimental observation and theoretical calculations indicate that these intercalating agents mainly enter intertube spaces or defects on nanotubes for enhanced electrochemical capability for charge transfer and storage [42].

1.1.3.5 THERMAL PROPERTIES

Graphite and diamond exhibit extraordinary heat capacity and thermal conductivity, carbon nanotubes are expected to have similar thermal properties at room or higher temperature but different behavior at low temperature due to the effects of phonon quantization. For T > 100K, a SWNT, SWNT rope and MWNT all follow or are almost close to specific heat relation of graphite (the measured specific heat of CNTs is very close to that of graphite at T > 100). However, at low temperature, CNTs exhibit quantum confinement effects [39]. Hone et. al. measured the thermal conductivity of crystalline ropes of SWNTs from 350K to 8K [43]. The thermal conductivity decreased smoothly with decreasing temperature and linearly depended on temperature below 30K (phonon confinement). Their results indicated that the thermal conductivity of SWNTs was dominated by phonon at all temperature rather than electrons and the intertube coupling of SWNT bundles was weak. Thermal conductivity of MWNTs of a few tens nm diameter was measured and found to linearly depend on temperature from 10 ~300K [44]. The interwall coupling of tubules was rather weak compared to graphite. Thus, a MWNT can be treated as a few decoupled single walled tubules.

Thermal conductivity of nanotubes is one dimensional similar to their electrical conductivity. Thus, a broad range (200~6000 W/mK) of thermal conductivities have been observed by different researchers [43, 44]. The measured conductivity is highly dependent on sample quality and alignment. Thermal conductivity of an individual MWNT was measured to be 3000 W/mK [45]. It has been observed that the

thermal conductivity of SWNTs was diameter dependent. SWNTs with the modest diameters exhibit the minimum conductivity. For most of SWNTs except the smallest diameter nanotubes, the thermal conductivity is smaller than that of graphene [46].

Thermoelectric electric power is defined by TEP = $\Delta V/\Delta T$. Here V is the thermoelectric voltage and T is the temperature. When a bias is applied on nanotubes, the temperature gradient will build up along the tube axis via Joule heating [39]. TEP for a single metallic or semiconducting tube linearly depends on temperature with positive (negative) slope for p-doped (n-doped) nanotube. At room temperature, TEP for a semiconducting SWNT is 280 μV/K [43] for a MWNT is 80 μV/K [44]. The measured thermal electric properties vary significantly from sample to sample.

1.2 CARBON NANOTUBE BASED SENSORS

As mentioned in the previous sections, carbon nanotubes have remarkable mechanical properties and unique electronic properties as well as high thermal stability and excellent heat conductions. Carbon nanotubes have attracted much attention from researchers for applications in nanoelectronics, field emissions and sensors. The diameter of SWNT is about 1 nm, while the length is up to several micrometers. Nanotubes have high surface-to-volume ratio and aspect ratio. Electrical properties of CNTs are extremely sensitive to chemical, mechanical and physical environment. In this section, applications of CNTs in chemical, biological, flow, force, thermal and mass sensors will be discussed.

1.2.1 CHEMICAL SENSORS

Chemical sensors based on individual SWNT have been demonstrated for detecting NO_2 and NH_3 at room temperature [47]. The conductivity of semiconducting carbon nanotubes changed dramatically over several orders of magnitude upon exposure. The response of SWNT sensor was extremely fast (10 sec for NO_2 and 1~2 min for NH_3), while the recovery was slow at ambient environment. The conductance of nanotube increased by three orders of magnitude after 200 ppm NO_2 was introduced. After recovery from NO_2, the same SWNT device was exposed to 1% NH_3 flow, the conductance was observed to decrease

~100 folds. These responses of semiconducting SWNT were due to the charge transfer from the electron donating NH_3 or electron accepting NO_2 gas to p-type SWNT. Li et. al. developed a SWNT sensor on interdigitated electrodes and measured its response to NO_2 and nitrotoluene at room temperature [38]. They used a SWNT network rather than individual SWNT as the sensing element. The response was linear for concentrations of sub ppm to hundreds of ppm. The reported detection limit was 44 ppb for NO_2 and 262 ppb for nitrotoluene. The recovery time was shortened to several minutes by using ultraviolet light illumination to decrease the desorption-energy barrier. SWNTs were integrated on a circular disc resonator for gas sensing [48]. Before testing, SWNTs were degassed by heating in a high vacuum chamber. The dielectric constant of SWNTs changed in the presence of various types of gases. The measured resonant frequency shifted by both polar (NH_3 and CO) and nonpolar gases (He, Ar, N_2 and O_2). The reported sensitivity was about 100 ppm. The sensing characteristics of CNT sensors were summarized in table 1.1.

In order to develop SWNT sensors with high selectivity and sensitivity, polymer functionalization has been utilized on carbon nanotubes. Qi and collaborators differentiated NO_2 and NH_3 using SWNTs coated with different polymers [49]. Polyethyleneimine (PEI) coating affords n-type nanotube devices which detect NO_2 with the concentration as low as 1 ppb while is insensitive to NH_3. PEI functionalized n-type semiconducting devices specifically respond to strong electron acceptors. No change in conductance was observed when PEI-SWNT sensor was exposed to other molecules such as CO, CO_2, CH_4, H_2, O_2. Another polymer, Nafion (a polymeric perfluorinated sulfonic acid ionomer) was coated on SWNTs to block NO_2 and allow for selective sensing of NH_3. Nafion is a polymer with a Teflon backbone and sulfonic acid side groups and is well known to be perm-selective (selectively permeate to certain molecules) to –OH-containing molecules such as NH_3 which tends react with H_2O in the environment to form NH_4OH. Bekyarova et. al. covalently functionalized SWNTs with poly-(m-aminobenzene sulfonic acid) (PABS) and tested their response to NH_3 [50]. PABS coating improved the response of pure SWNTs twice upon exposure to NH_3. The sensor recovered in several minutes when exposed to nitrogen.

The detection limit is 5ppm. SWNT network electrochemically functionalized with polyaniline (PANi) was tested with NH_3 [51]. The change in resistance of PANi-SWNTs was 60 times higher than that of intrinsic SWNTs. The sensing response was reversible and reproducible. A detection limit of 50 ppb was obtained at room temperature. The sensing characteristics of polymer functionalized CNT sensors were summarized in table 1.2. In addition, some metal nanoparticles were utilized to decorate CNTs for gas sensing and their performances were collected in table 1.3. It is well known that metal oxide gas sensors have high sensitivity, fast response and short recovery time to various pollutant gases. However, they have to be operated at high temperature to achieve high sensitivity, normally from 400-600°C. Gas sensors based on metal oxide/CNT composites have been developed and exhibit improved sensing properties at room temperature. Gas sensing performances of metal oxide modified CNT sensors were summarized in table 1.4.

Table 1.1: Summary of gas sensing performances of CNT sensors (N/A means not available).

CNT s	Sensor configuration	Target analytes	Detection limit	Response time	Recovery time	Ref.
Semi-SWNT	FET	NO_2, NH_3	2ppm NO2; 0.1% NH_3	< 10min	1h (200°C)	[47]
SWNTs	Resistor	NO_2, Nitrotoluene	44 ppb NO_2; 262 ppb Nitrotoluene	10min	10min (UV)	[38]
SWNTs	Resistor	NH_3	5ppm	10min	20min (80°C)	[52]
SWNTs	Resistor	NH_3	5ppm	10min	10min (70°C)	[53]
MWNTs	Capacitor and resistor	NH_3	10ppm	2-3min	Several days (100°C in vacuum)	[54]
MWNTs	Resistor	NH_3	2500ppm	N/A	N/A	[55]
MWNTs	FET	NO_2	50ppm	500s	10min (10V bias potential)	[56]
MWNTs	Resistor	SO_2, HF	10ppm SO_2; 4ppm HF	N/A	N/A	[57]
MWNTs	Electrochemical Gas Sensor	Cl_2	100ppm	150s	150s	[58]
Aligned CNTs	Resistor	NO_2	10ppb	60min	60min (165°C	[59]
Aligned CNTs	Resistor	NO_2	10ppm	N/A	N/A	[60]
Aligned CNTs	Resistor	NO, NO_2	2ppm NO; 2ppm NO_2	N/A	20min (150°C and UV)	[61]
Aligned CNTs	Resistor	NH_3	~ 0.1%	N/A	N/A	[62]
Aligned CNTs	FET	N_2	50mTorr	N/A	N/A	[63]

Table 1.2: Summary of sensing performances of polymer functionalized CNT sensors (N/A means not available).

Polymer	CNTs	Sensor configuration	Targeted analytes	Detection limit	Response time	Recovery time	Ref.
PEI; Nafion	SWNTs	FET	NO_2, NH_3	100ppb NO_2;	1-2min	N/A	[49]
PABS	SWNTs	Resistor	NH_3	5ppm	1-2min	Several minutes in nitrogen	[50]
PANi	SWNTs	Resistor	NH_3	50ppb	10min	a few hours	[51]
PABS	SWNTs	Resistor	NO_2, NH_3, H_2O	20ppb NO_2; 100ppb NH_3	1-10min	Several hours	[64]
PPy	SWNTs	FET	NO_2	N/A	N/A	2h	[65]
PPy	Semi-SWNT	FET	NO_2, NH_3	100ppm NO_2; 5ppm NH_3	N/A	N/A	[66]
PDPA	MWNTs	Electro-chemical gas sensor	CO	0.01ppm	2s	3s	[67]
PMMA	MWNTs	Resistor	Dichloromethane; chloroform; acetone	N/A	2-5s	10s	[68]
Poly (3-methylthiophene)	MWNTs	Resistor	CH_2Cl_2; $CHCl_3$; CCl_4; CH_4	N/A	60s	30-45s	[69]
Polystyrene	MWNTs	Resistor	The good solvents of PS	N/A	< 4min	1min	[70]
PEG	MWNTs	Resistor	Chloroform	N/A	< 1s	N/A	[71]
POAS	Aligned-CNTs	Resistor	HCl	100ppm	N/A	N/A	[72]
Poly(vinyl acetate); Polyisoprene, etc.	Aligned-CNTs	Resistor	Ethanol; cyclohexane; tetrahydrofuran	N/A	< 2min	< 2min	[73]

Table 1.3: Summary of sensing performances of metal decorated CNT sensors (N/A means not available).

Metal	CNTs	Sensor configuration	Targeted analytes	Detection limit	Response time	Recovery time	Ref.
Pd	Semi-SWNTs	FET	H_2	< 40ppm	5-10s (half resistance change)	400s	[74]
Pd	SWNTs	Resistor	H_2	1000ppm	N/A	N/A	[75]
Pd	SWNTs	Resistor	H_2	100ppm	10min	20min	[76]
Pd	SWNTs	Resistor	H_2	100ppm	3-60s (36.8% resistance change)	5min	[77]
Pd	SWNTs	Resistor	H_2	10ppm	< 10min	< 30s	[78]
Pd	Aligned-CNTs	Resistor	H_2	100ppm	< 7min	N/A	[79]
Pd	SWNTs	Resistor	CH_4	6ppm	2-4min	N/A	[80]
Pd	MWNTs	Resistor	CH_4	2%	310s	176s	[81]
Pt	MWNTs	Resistor	H_2	N/A	10min	15min	[82]
Pd	MWNTs	Resistor	H_2	N/A	7min	7min	[83]
Pt	MWNTs	Resistor	H_2, NO_2, H_2O	N/A	10min	14min	[84]
Au	SWNTs	Resistor	NO_2, NH_3	< 120 ppb NH_3	150s	200s	[85]
Au, Pt	MWNTs	Resistor	NO_2, NH_3	100 ppb NO_2; 5ppm NH_3	N/A	N/A	[86]
Au, Ag	MWNTs	Resistor	NO_2	500 ppb NO_2	20min	N/A	[87]
Pt, Pd, Sn, Rh	SWNTs	FET	H_2, CH_4, CO, H_2S, NO_2, HCN, HCl	N/A	5min	N/A	[88]
Pd, Au	SWNTs	Resistor	Cl_2, acetone, benzene	5ppm	N/A	N/A	[89]

Table 1.4: Summary of sensing performances of metal oxide decorated CNT sensors (N/A means not available).

Metal oxide	CNTs	Sensor configuration	Targeted analytes	Detection limit	Response time	Recovery time	Ref.
SnO_2	SWNTs	Resistor	NO_2	N/A	9 min	1.5min	[90]
SnO_2	SWNTs	Resistor	H_2	300ppm	2-5s (200-250°C)	3-5s (200-250°C)	[91]
SnO_2	SWNTs	Resistor	NH_3	10ppm	100s	3.2min	[92]
SnO_2	MWNTs	Resistor	LPG; C_2H_5OH	10ppm	N/A	N/A	[93]
SnO_2	MWNTs	Resistor	C_2H_5OH	10ppm	1s (300°C)	10s (300°C)	[94]
SnO_2	MWNTs	Resistor	NO_2	100ppb	N/A	20min (150°C)	[95]
SnO_2	MWNTs	Resistor	NH_3	60ppm	< 5min	< 5min	[96]
SnO_2	MWNTs	Resistor	formaldehyde	0.03 ppm	100s (250°C)	90s (250°C)	[97]
WO_3	MWNTs	Resistor	NO_2; CO; NH_3	500 ppb NO_2; 10ppm CO; 10ppm NH_3	N/A	N/A	[98]
TiO_2	MWNTs	Resistor	Acetone; NH_3	N/A	10-40s (acetone)	10-300s (acetone)	[99]
TiO_2	CNTs	Resistor	O_2	10 ppm	5-8min (350-550°C)	20min (350°C)	[100]
SnO_2, TiO_2	MWNTs; SWNTs	Resistor	C_2H_5OH	100 ppm	< 10s (210-400°C)	< 10s (210-400°C)	[101]

1.2.2 BIOSENSORS

Biomolecules typically carry many ions and are expected to change the electronic properties of CNTs more dramatically than small molecules such as simple gases. Analytical applications of CNTs as biosensor have been partly reviewed by several researchers [102-104] Proteins can be directly attached on CNTs and the electrons can transfer between nanotubes and proteins. Immobilizing cytochrome C and hemoglobin have been reported [105, 106]. However, the interactions between proteins and carbon nanotubes are primarily due to nonspecific adsorption.

Proteins can specifically bind to sidewalls of carbon nanotubes by surface functionalization of nanotube. As mentioned before, in terms of covalent attachment, CNTs will be oxidized to have carboxyl groups which can couple with amino groups in proteins. Noncovalent bindings on SWNTs are mainly in two ways. One is using bifunctional molecules that exhibit π-π stacking on the sidewalls of carbon nanotubes. A pyrene moiety, commonly used for graphite functionality, is typically used for noncovalent functionalization of carbon nanotubes [107]. Li and coworkers utilized this mechanism to bind PSA antibody on SWNT-FET device for prostate-specific antigen detection [108]. The reported detecting limit was ca. 500 pg/ml, or 14 pm, at a signal to noise ratio of 2. The interaction was thought to be charge-transfer mechanism. Figure 1.7 is a schematic of this bifunctional molecular interaction incorporated for antibody antigen detection.

The other noncovalent approach used a polymer addition to immobilize protein on SWNTs [109, 110]. Dai and coworks modified carbon nanotubes by coadsorption of the surfactant Triton and poly (ethylene glycol). They tested the resistance changes to nonspecific binding while using a “director” for specific protein attachment [111].

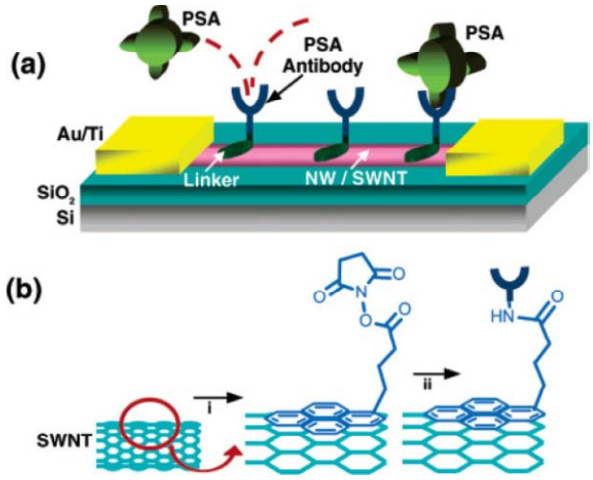

Fig. 1.7: (a) Schematic illustration of a nanosensor. Prostate-specific antigen antibodies (PSA-ABs) are anchored to the NW/SWNT surface and function as specific recognition groups for PSA binding. (b) Reaction sequence for the modification of the SWNT. i) Deposition of 1-pyrenebutanoic acid succinimidyl ester, ii) PSA–AB incubation [108].

Surface functionalized SWNT-FET sensors have been investigated for blood glucose monitoring. As other glucose sensors, electrochemical glucose detection is based on enzymatic glucose oxidation and subsequent hydrogen peroxide detection on the carbon nanotube electrodes [103, 112]. Dekke et. al. have fabricated a nanotube FET sensor decorated with glucose oxidase as a versatile glucose biosensor [113]. The redox enzyme glucose oxidase (GOx) that catalyzes the oxidation of *b*-D-glucose ($C_6H_{12}O_6$) to D-glucono-1,5-lactone ($C_6H_{10}O_6$) has been studied. The redox enzymes go through a catalytic reaction cycle, where groups in the enzyme temporarily change their charge state and conformational changes occur in the enzyme that can be detected by using CNT-FET devices [114].

In addition to pH sensitivity, GO_x-coated semiconducting SWNTs have been verified to have electrical response to glucose in liquid. Figure 1.8 shows real-time measurement of the conductance of a GOx-coated semiconducting SWNT in milli-Q water. The conductance barely changed after adding water on the device (red arrow in Figure 1.8). However, the conductance of the tube increased by about 10% when 0.1 M glucose in milli-Q water was added to the liquid (blue arrow). In inset (a) of Figure 1.8, a similar 10% conductance change was observed for another device, which had a lower conductance by a

factor of 10. Inset (b) of Figure 1.8 shows a measurement on a bare semiconducting SWNT. Glucose did not change the conductance of the bare SWNT, but did increase the device conductance after GOx was immobilized. These measurements clearly indicated that the GOx activity was responsible for the measured increase in conductance upon glucose addition, thus rendering such nanodevices as feasible enzymatic-activity sensors.

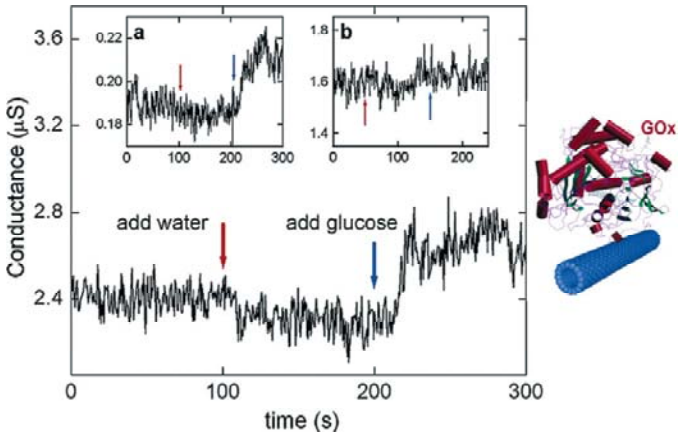

Fig. 1.8: Left: Real time electronic response of a CNTFET sensor to glucose (the substrate of GOx). The conductance of a semiconducting SWNT with immobilized GOx was measured as a function of time in 5 lL milli-Q water. The conductance of the GOx-coated SWNT was observed to increase upon addition of glucose to the liquid. Insets: (a) the same measurement on a second device, where the conductance was a factor of 10 lower. (b) The same measurement on a semiconducting SWNT without GOx. No conductance increase was observed in this case [113].

Another detection target for biosensors is DNA molecules. There are several groups have reported electrochemical detection of DNA hybridization by carbon nanotube modified electrode [112]. DNA is a nucleic acid which can wrap around SWNTs and form a helical structure. This mechanism was used to disperse SWNTs in water [114]. The interaction between DNA and SWNT is π-π stacking [113] so DNA can be absorbed nonspecifically on SWNT surface. The nucleic acid-base will attach on CNT surface and the hydrophilic sugar-phosphate backbone of DNA will point to the exterior. The hydrophilic end will help to dissolve SWNTs in water. Molecular model of this binding is shown in Figure 1.9.

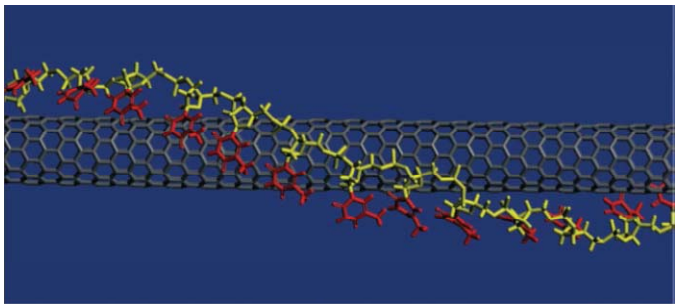

Fig. 1.9: DNA-SWCNT binding model. The red ends are bases which attach on carbon nanotube surface through π-π stacking, while the yellow ends are sugar phosphate backbones pointing exterior. DNA molecule either wraps on SWNT in helical fashion or is linearly adsorbed on a carbon nanotube [114].

Johnson and coworkers applied DNA decorated SWNT on FET device to detect various chemicals [115]. DNA molecules with different sequences were wrapped on SWNT and their responses were found to be different toward different detecting gases. The gases tested were methanol, trimethylamine (TMA), propionic acid (PA), dimethylmethylphosphonate (DMMP) and dinitrotoluene (DNT). Nanotube FET sensor has been applied for DNA detection. DNA hybridization was detected on the surface of the back gate of CNTFET [116]. 5'end-amino modified peptide nucleic acid (PNA) oligonucleotides were covalently bonded on to the Au surfaces of the back-gate. PNA works as DNA which can hybridize with complementary DNA or RNA sequences. When hybridization occurred at the gate of nanotube transistor, the negative charges from complementary DNA or RNA were induced on the gate. The conductance of SWNTs was changed through the gate insulators. This can be a PNA based biosensor. A micro flow chip made of PDMS can combine with this biosensor to detect DNA in liquid. DNA hybridization was detected by measuring the electrical characteristic and this DNA decorated SWNT-FET device provided real time, label free detection of the binding activities of biomolecules. Tang and collaborators reported DNA hybridization detected on gold electrodes instead of nanotube sidewalls [117]. The change in electrical conductance is due to the modulation of the energy alignment between SWNTs and the gold contact. The Schottky barrier modulation has a more significant role in DNA sensing. Their experimental setup and testing image is shown in Figure 1.10.

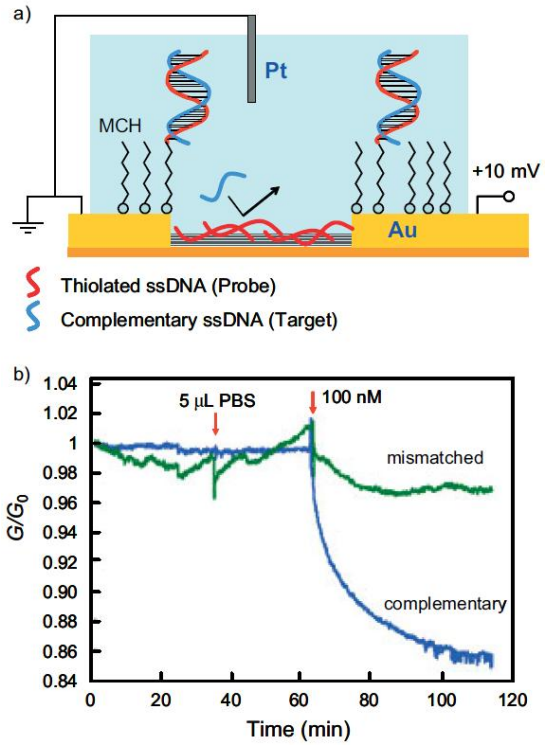

Fig. 1.10: (a) Schematic illustration of a CNT device during electrical measurement. Complementary ssDNA oligomers hybridize to thiolated ssDNA co-immobilized with mercaptohexanol (MCH) on the gold electrodes. (b) Real-time monitoring of 30 mer DNA hybridization in PBS, pH 7.4. Two liquid cells were used in parallel for simultaneous drop adding 5 lL of complementary and mismatched target oligo solution to 500 lL of buffer. The conductance of a nanotube device functionalized with thiolated ssDNA exhibits a selective response to the addition of complementary ssDNA [117].

Maehashi et. al. have fabricated a biosensor based on aptamer and antibody modified SWNT-FET devices [118]. They used this biosensor to detect immunoglubin E (IgE) in PBS buffer solution. Again the pH was controlled to be 7.4. They reported a detection limit of 250 pM. After comparing the electrical properties of aptamer and antibody modified CNT-FET devices, aptamer modified device was found to have a better performance. Aptamer as a synthetic oligonucleotide can be a promising sensing element for label-free protein biosensors. Debye length is the typical distance required for screening the surplus charge by the mobile carriers present in a material [119]. This distance is inverse proportional to square root of ionic length. If the attached molecule is placed a Debye length away from a carbon nanotube, the effect of this target molecule can't be sensed by the nanotube. The typical length of antibody is 10~15nm

which is larger than the length of aptamer. As IgE attaches on the sensing area, CNT decorated with aptamers should generate a more significant response [Figure 1.11].

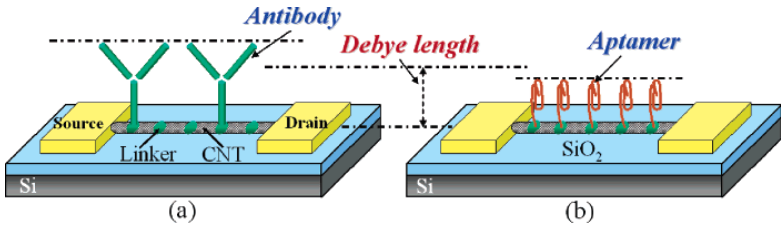

Fig. 1.11: Schematic representation of label-free protein biosensors based on CNT-FETs: (a) antibody-modified CNT-FET. (b) Aptamer modified CNT-FET [118].

1.2.3 FLOW SENSORS

Theoretical calculations conducted by Kral et. al. predicted that an electrical current can be generated in metallic carbon nanotubes immersed inside liquids flowing along them [120]. Fluids can wet and coat the surface of nanotube and form many layers around it. Momentum from the moving liquid can be transferred through the slipping layers to the nanotube momentum and then to the quasimomentum of its phonons and other elementary excitations. The resulting phonon wind will drag free carriers in the tube and induce an electric current or voltage along the direction of liquid flow [120]. Two years later, Ghosh et. al. developed a CNT based flow sensor which measured the flow by current/voltage induced in SWNT bundles [121]. The voltage produced by flow has a logarithmic velocity dependence over nearly six decades of velocity. This result didn't agree with the predicted relationship between electric current and liquid velocity which was linear [120]. The dominant mechanism responsible for this highly nonlinear response involved a direct forcing of the free charge carriers in the nanotubes by the fluctuating Coulombic field of the liquid flowing past the nanotubes. Besides, the ionic conductivity and the polarity of the liquid were found to have a great effect on the magnitude of the generated voltage. Saturation of the induced voltage was observed for flow velocity on the order of 10^{-5} m/s.

1.2.4 PRESSURE SENSORS

SWNT has been demonstrated as molecular pressure sensors [122]. Specific peaks of Raman spectrum of SWNTs shifted significantly under various molecular pressures produced by liquids on nanotubes. Immersing SWNT aggregates in liquids of various cohesive energy densities shifted the frequency of D* band (2610 cm^{-1} in air) in Raman spectrum to different magnitudes. This was due to the SWNTs deformed by the molecular forces generated from those liquids. In addition, the observed shift in Raman peaks was highly reversible. CNTs have great potential to be used in pressure sensing based on the shifts of Raman band. Fung et. al. fabricated a polymer-based MEMS pressure sensor based on the piezoresistive properties of MWNTs [123]. 300 μm thick Polymethylmethacrylate (PMMA) diaphragm was fabricated by SU-8 and was used as a flexible substrate for CNT pressure sensor (Figure 1.12). Parylene C was deposited on the top and followed by metal deposition and CNT assembly. The gap separation between Au electrodes ranged from 3μm to 10μm for Dielectrophoretic assembly (DEP). The deflection of this membrane due to the pressure change caused bending in the nanotubes. The change in resistance of MWNTs was then recorded. The maximum deflection at the center of the diaphragm was linearly proportional to the input pressure and the measured resistance of MWNTs almost linearly depended on the input pressure.

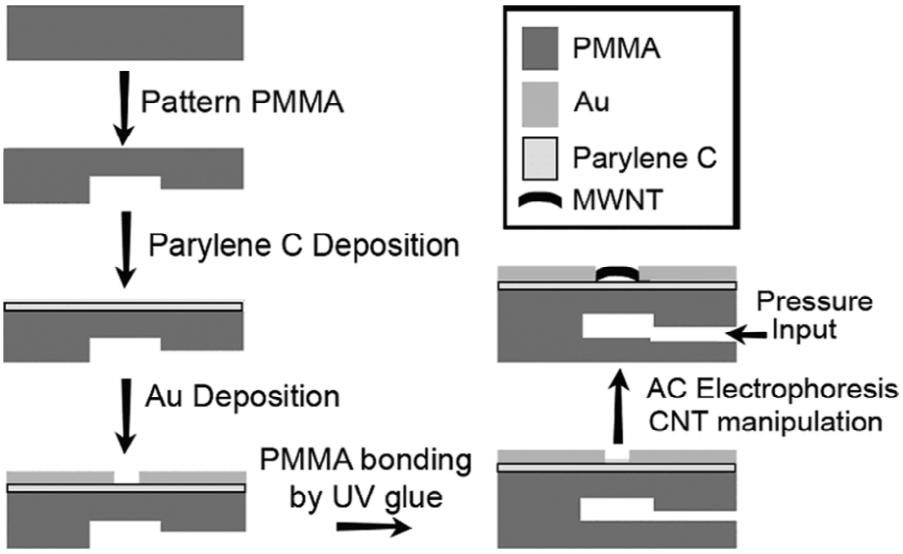

Fig. 1.12: Fabrication process of a MWNT-based MEMS device for pressure sensing [123].

1.2.5 THERMAL SENSORS

Wood et. al. observed that the Raman spectrum of CNTs shifted by variations in temperature [122]. The nanotubes were embedded and cooled in polycarbonate and the wave number of the *D** band of the SWNT increased with decreasing temperature as the tubes experience compression. This indicates the possibility of using CNT composite materials for temperature sensing. However, there are variations in sensing performance among different CNT devices because the types of CNTs embedded in the polymer matrices are not consistent. It is hard to control the chirality, diameter, length and number of nanotubes in the sensing devices. Furthermore, the dispersion and interconnectivity of the CNT network may also affect the sensing performance. Fung et. al. fabricated carbon nanotube thermal sensors on Si/SiO_2 substrates [124]. MWNT bundles were assembled by DEP between two Au electrodes and they claimed a 70% yield in placing the nanotubes. The two-terminal resistance of nanotube bundles under different temperatures was measured. They found that the resistance of CNTs decreased linearly with increasing temperature. However, after multiple thermal cycling, the resistance of MWNTs at room temperature decreased by 40% due to thermal annealing.

1.2.6 MASS SENSORS

Chiu and collaborators developed an atomic scaled mass sensor using doubly clamped suspended carbon nanotubes as nanomechanical resonators, in which their single electron transistor properties allows self-detection of the nanotube vibration [125]. A shift in resonant frequency of CNT was detected and used to determine the mass of nanotubes and the inertial mass of atoms adsorbed on nanotubes. The device was fabricated by first growing nanotubes from catalyst islands on a Si/SiO_2 substrate. The Pd/Au source/drain electrodes and the side gate were then deposited by electron beam lithography (EBL). A layer of PMMA was spun coated on the chip, and a window was opened over a segment of the nanotube using EBL. Next SiO_2 substrate below the CNT was etched to suspend the CNT within this window. The experiment temperature was set to 6K, at which single-electron properties can be observed from the CNT. This transistor was then integrated with testing circuitry and functioned as a nanotube resonator. The

vibration characteristics of this resonator were recorded while the device was exposed to an atomic or molecular beam. The experimental setup is illustrated in Figure 1.13 (inset). As Xe atoms landed on and got adsorbed on the surface of carbon nanotube, the resonance frequency shifted to lower frequency and got broadened. The amplitude also decreased slightly as shown in Figure 1.13. Since this experiment was conducted at a very low temperature, desorption did not occur and the resonant frequency remained stable when pumping out the sensing reservoir.

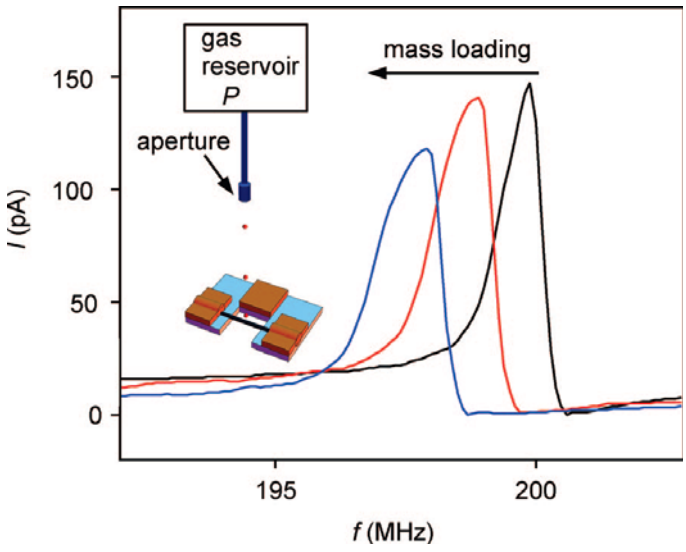

Fig. 1.13: Response of nanomechanical resonator under mass loading and the experimental setup. Main panel: mixing current *I* versus drive frequency *f* for a resonator device during mass loading by Xe. The black curve shows the initial resonance, the red curve shows the resonance after mass loading for ≈ 600 s, and the blue curve shows the resonance after mass loading for ≈ 1600 s. Inset: schematic diagram of the experimental setup for mass loading nanotube resonator devices [125].

Jensen et. al. built a mass spectrometer using a suspended individual double-walled carbon nanotube (DWNT) as a mechanical resonator and demonstrated atomic mass resolution at room temperature [126]. The reported mass sensitivity is down to 1.3 x10-25 kg·Hz-1/2 which is equivalent to 0.40 gold atom·Hz-1/2. Except having higher sensitivity to molecules, nanomechanical mass spectrometers do not require the potentially destructive ionization of the test sample. The mechanical resonance testing setup was schematically illustrated in Figure 1.14.

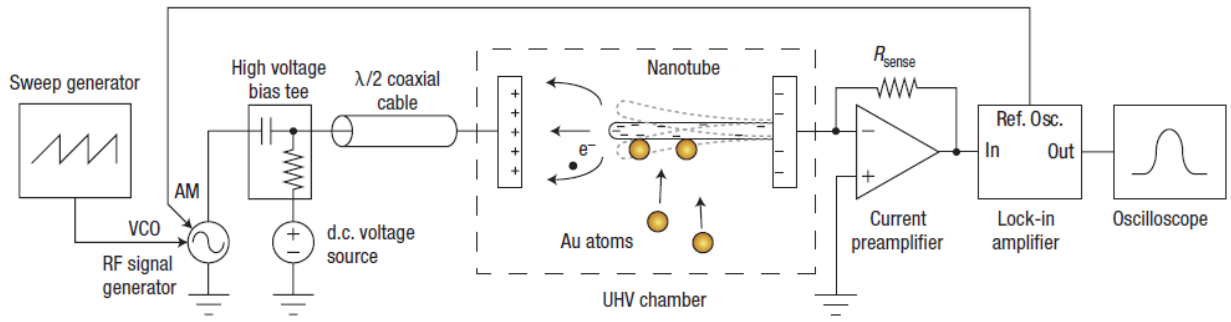

Fig. 1.14: Schematic of the mechanical resonance detection setup. The electrode opposite the nanotube is biased to induce a field emission current from the nanotube. An amplitude-modulated (AM), frequency-swept (using a voltage-controlled oscillator, VCO), radio-frequency (RF) signal is coupled to the nanotube, forcing it into resonance, and consequently modulating the field emission current. The modulated field emission current is recovered by a lock-in amplifier and the resonance peak is displayed on the oscilloscope or recorded by a computer [126].

1.3 FUNCTIONALIZATION OF CARBON NANOTUBES

Biomolecules, such as protein peptides and nucleic acids, functionalized CNTs have shown great potential for applications in bioengineering and nanotechnology. Fundamental understanding, manipulation and regulation of these biomolecules on nano materials and nano devices will lead to a new generation of integrated systems that combine the unique properties of nanomaterials (such as CNTs) with the specific recognition capabilities of biomolecules. In this section, the fundamentals of DNA, the interactions between DNA and CNTs and sensing applications of DNA-CNT devices will be introduced.

1.3.1 FUNDAMENTALS OF DNA AND RNA

DNA and RNA are the basic building block of all living organisms (except RNA virus). Genetic information is contain in DNA and used to construct other components of cells, such as protein and RNA molecules. The double-helix molecular structure of DNA was proposed by Watson and Crick in 1953 [127]. DNA is composed of two long polynucleotide chains that run in opposite directions and are twisted around each other right-handedly. Each strand of the double helix is a linear chain consisting of a phosphate-sugar backbone to which four different chemical groups or bases are attached: the purines, adenine (A) and guanine (G), and the pyrimidines, cytosine (C) and thymine (T). Each unit of a phosphate,

a sugar molecule and a base is called a nucleotide (Figure 1.15 B), and each nucleotide is approximately 0.34 nm long. The specific binding of two hydrogen bonds between adenine and thymine and three hydrogen bonds between cytosine and guanine can result in the joining of two complementary single-stranded (ss) DNA to form a double-stranded (ds) DNA. This complementarity (base-pairing; Figure 1.15 A) gives rise to informational redundancy and allows for chemical fidelity in replication [128].

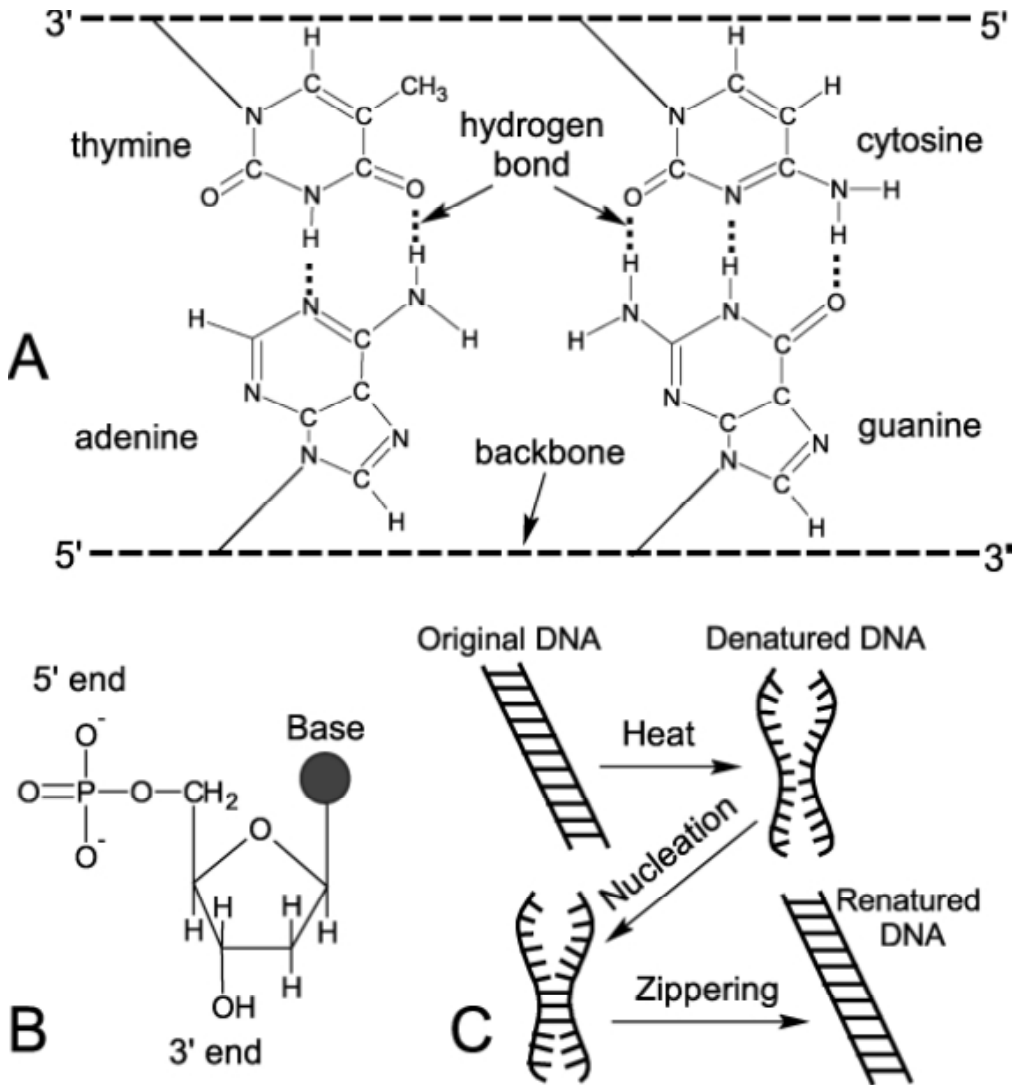

Fig. 1.15: (A) The four bases of DNA showing their complementary binding properties. (B) DNA nucleotide. (C) Schematic showing denaturing and hybridization of DNA [128].

Base pairing can be used to assemble new strands of DNA, allowing information transfer to offspring, and to assemble strands of ribonucleic acid (RNA), letting the DNA control which proteins are manufactured and when [129]. These functions are realized as well as controlled by gene regulatory proteins and other DNA-associated proteins through their interactions with DNA, which often result in DNA twisting, stretching, and bending. The joining of two ssDNA through hydrogen bonding to form a double-stranded DNA (dsDNA) is called hybridization (Figure 1.15 C). If a dsDNA is heated above a certain temperature, called the melting temperature (T_m), the two strands will separate into single strands. The melting temperature is a function of the ion concentration of the ambient and the guanine-cytosine (GC) content in the DNA sequence. When the temperature is reduced, the two strands will eventually come together by diffusion and re-hybridize or re-nature to form the double stranded structure. These properties of DNA can be utilized in the ordering and assembly of artificial structures if the structures can be attached to ssDNA.

The global structure (handedness, helical pitch, effective diameter, etc.) adopted by a dsDNA therefore depends on a large number of environmental parameters, such as the solvent, the ionic conditions, and the temperature [130]. The right-handed B-DNA (the canonical form of DNA in solution) has an atomic diameter of approximately 2.4 nm and a helical pitch of 10.4 bps per turn with a vertical base spacing of approximately 0.34 nm. The double helix is not perfectly symmetrical, but is instead characterized by a major groove which is 1.2 nm wide and a minor groove which is 0.6 nm wide. The various interactions that stabilize the B-form of DNA determine its rigidity. A dsDNA is not only stiffer than artificial polymers, but also much stiffer than many other natural polymers, such as ssDNA or RNA. Its persistence length, the distance over which the orientation of the molecule's axis remains correlated despite thermal agitation, equals 50 nm. In contrast, a ssDNA molecule can adopt to very abrupt shape changes over distances of a few bases, on the order of 1 nm. A few noncanonical forms, such as bulge of unpaired bases, cruciform in the presence of a palindromic sequence, and denaturation bubble, may locally exist in B-DNA. Other structure forms of DNA exist besides the B-form [130], such as the more

compact A-DNA, with a base-spacing of 0.26 nm, and left handed Z-DNA, with a pitch of 12 bps per turn. Under stretching or twisting, canonical B-DNA can transform into overstretched S-DNA or over wound P-DNA [131].

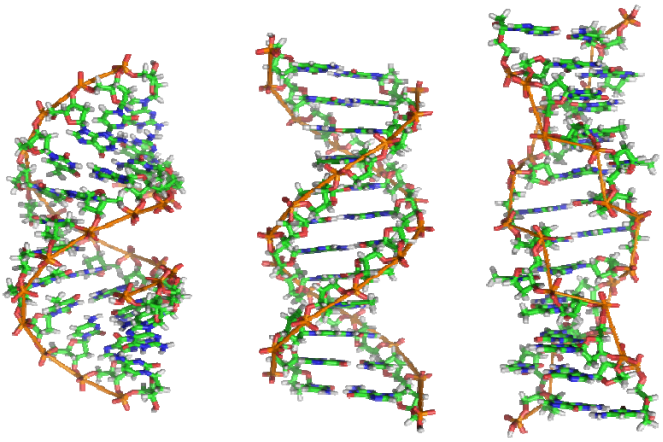

Fig. 1.16: From left to right, the structures of A-, B- and Z-DNA. The structure a DNA molecule depends on its environment. In aqueous environments, including the majority of DNA in a cell, B-DNA is the most common structure. The A-DNA structure dominates in dehydrated samples and is similar to the double-stranded RNA and DNA/RNA hybrids. Z-DNA is a rare structure found in DNA bound to certain proteins [132].

RNA (Ribonucleic acid) forms the genetic material in smaller organisms namely viruses. RNA is important in the production of proteins in living organisms. RNA can move around in the cells of living organisms and serves as a genetic messenger, passing the information stored in the cell's DNA from the nucleus to other parts of the cell [133]. In the process of protein synthesis, a universal function whereby mRNA molecules direct the assembly of proteins on ribosomes. This process uses transfer RNA (tRNA) molecules to deliver amino acids to the ribosome, where ribosomal RNA (rRNA) links amino acids together to form proteins [134]. The molecular structure of RNA with the molecular structure of DNA is shown in Fig. 1.17 for comparison [135]. Similar to DNA, RNA is made up of a long chain of components called nucleotides. Each nucleotide consists of a nucleobase, a ribose sugar, and a phosphate group. The chemical structure of RNA is very similar to that of DNA, but there are two differences between the RNA and DNA. First, RNA contains the sugar-ribose, while DNA contains the

slightly different sugar-deoxyribose (a type of ribose that lacks one oxygen atom). Second, RNA has the nucleobase uracil while DNA contains thymine. Unlike DNA, most RNA molecules are single-stranded and can adopt very complex three-dimensional structures, such as hairpin, loops, bulges and internal loops [136, 137].

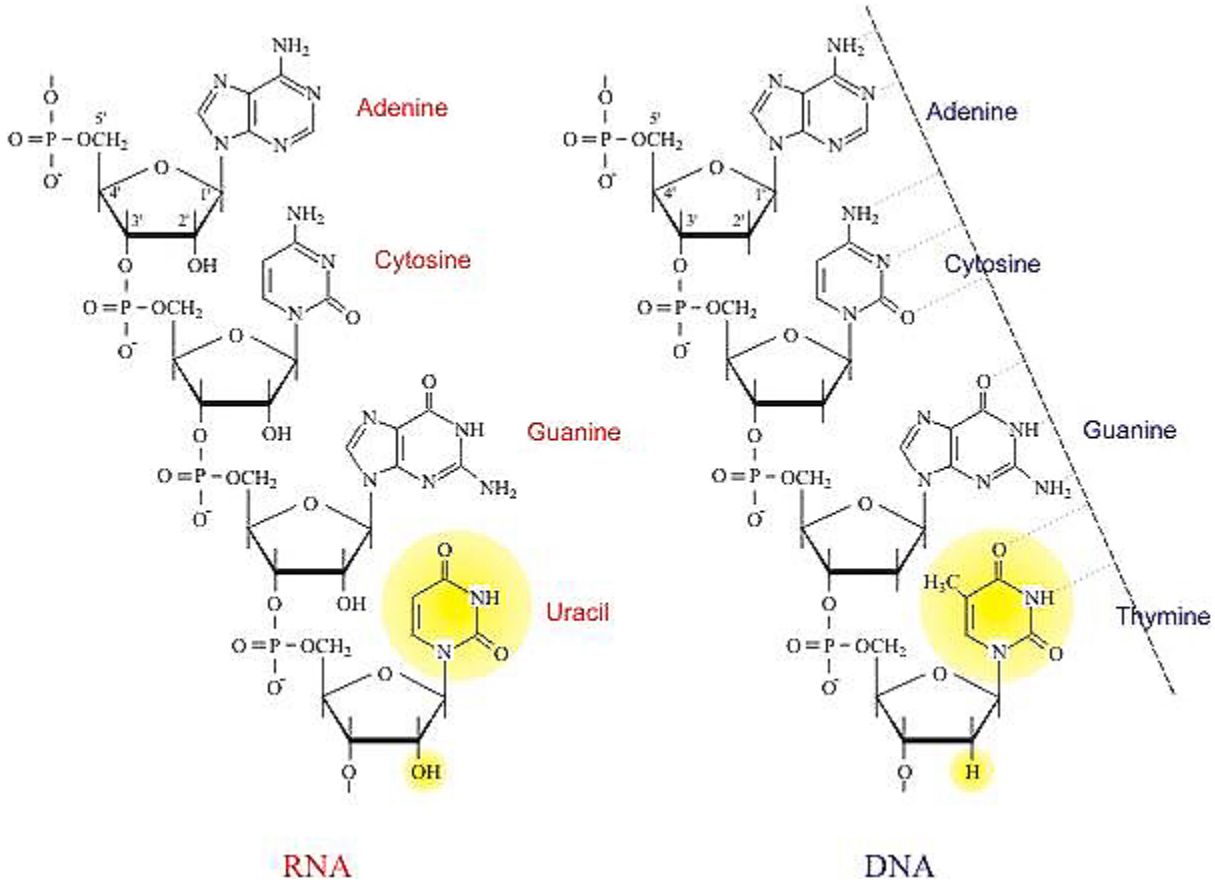

Fig. 1.17: Molecular structures of RNA and DNA nucleotides [135].

1.3.2 Interactions Between DNA and CNT

The interactions between ssDNA and CNTs have been investigated by molecular dynamic simulations. A nucleotide strand can self-assemble on nanotubes via the π-π stacking interactions between ssDNA and the surface of CNTs [138]. The presence of SWNTs in liquid induces the ssDNA to undergo a spontaneous conformational change and wrap around nanotubes into compact right- or left-handed helices within a few nanoseconds. This helical wrapping is driven by electrostatic and torsional

interactions within the sugar-phosphate backbone. As shown in Figure 1.18, the linear oligonucleotide in S1/S2 spontaneously wraps around the SWNT into right/left-handed helix. The helical wrapping does not occur uniformly over the entire length of the oligonucleotide. Actually, the 5'end of ssDNA remains stationary while the 3'end rapidly encircles the SWNT circumference. As a result, additional helical turns are generated at the 3'end, which then propagate toward the 5'end. The winding continues until ssDNA forms a compact helix about SWNT. Analysis of the structural and energetic changes indicates that electrostatic interactions within ssDNA backbone are mainly responsible for wrapping of the initial linear oligonucleotide into a helical structure [138].

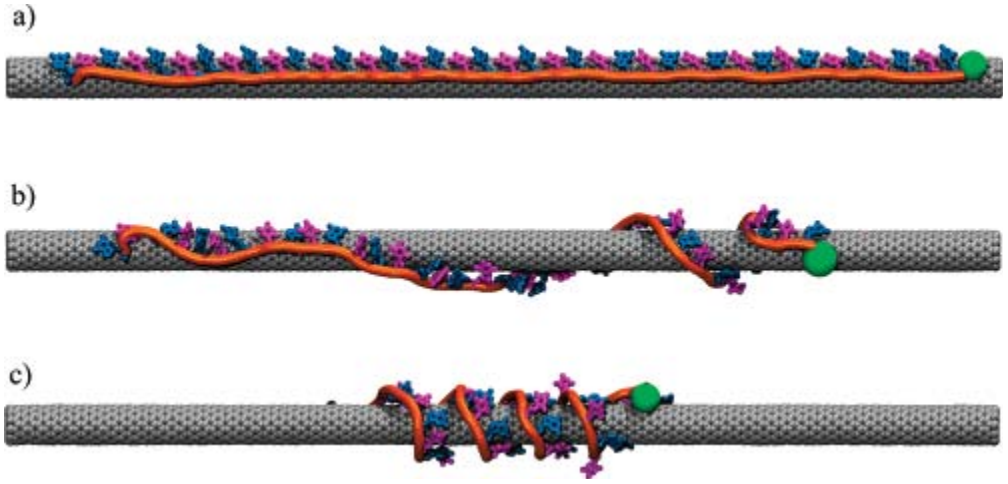

Fig. 1.18: Simulation of S1 displaying right-handed helical wrapping of (GT) 20 around SWNT. (a) Initial configuration. (b) Configuration after 2.2 ns. (c) Configuration after 7 ns. The green sphere marks the ssDNA 3' end. Similar results occur for S2, but with left-handed helical wrapping [138].

Molecular dynamic simulations conducted by Gao et. al. found that DNA could be encapsulated inside CNTs in a aqueous environment, when the tube diameter exceeded a certain critical value [139]. Both the Van Der Waals and hydrophobic forces play important roles in the binding process of DNA on nanotubes. Strong hydrogen-bond interactions among water molecules are known to produce hydrophobic forces that cause hydrophobic solutes (both CNT and DNA) to aggregate to reduce solvent-solute interface energy. Thus DNA will attach on the surface of nanotubes to minimize the interface energy. This hydrophobic effect alone is insufficient to encapsulate DNA inside nanotubes due to resistance from

water molecules inside the CNT. However, the carbon nanotube and oligonucleotide will also experience an attractive force due to van der Waals interaction between them when their separation is about 1 nm or smaller. This attractive interaction is found to play a dominant role in the DNA insertion process. The derived van der Waals energy between nanotube and DNA decreases rapidly when nucleotide entered nanotube. The simulated binding process of DNA on SWNT is presented in Figure 1.19.

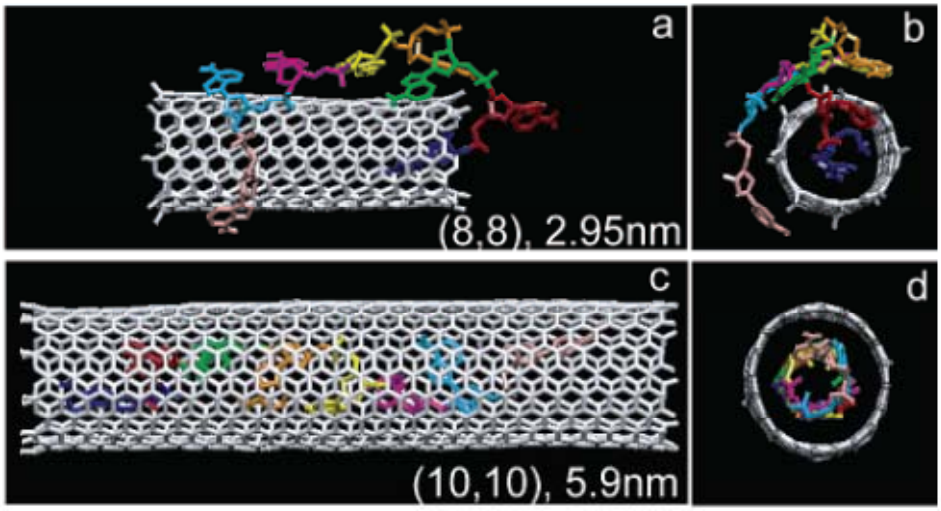

Fig. 1.19: Snapshots (sideview a, c and top view b, d) of oligonucleotide-nanotube system simulations after 2 ns. Water molecules are not shown [139].

Experimentally, interaction of nucleic acids with SWNT was studied by surface-enhanced infrared absorption spectroscopy [140]. The analysis of vibrational modes of a DNA-SWNT complex indicated that numerous structural changes in DNA could be interpreted as A-B conformation transition and as stabilization of DNA structure in some DNA fragments. The spectroscopic data was explained by the model of DNA interacting with SWNTs based on wrapping of nucleic acid molecules around CNTs [141]. In this model, the wrapping of the SWNTs by water-soluble polymers is a general phenomenon, driven largely by a thermodynamic force to eliminate the hydrophobic interface between the tubes and their aqueous medium. Optical detection of DNA conformation on SWNTs revealed that the secondary structure of DNA on nanotubes transformed from B to Z conformation when exposed to counter ions [142]. The SWNT band gap fluorescence exhibited a red shift which indicated the transition in

conformation. It has been observed that the energy shift in SWNT emission has a relative ion sensitivity of $Hg^{2+} > Co^{2+} > Ca^{2+} > Mg^{2+}$. The shift can also be observed via monitoring the SWNT photoadsorption bands. The emission energy returned to its initial value after the removal of the ions from the system, which indicated that the thermodynamic transition was completely reversible. The transition from B to Z conformation is shown in Figure 1.20.

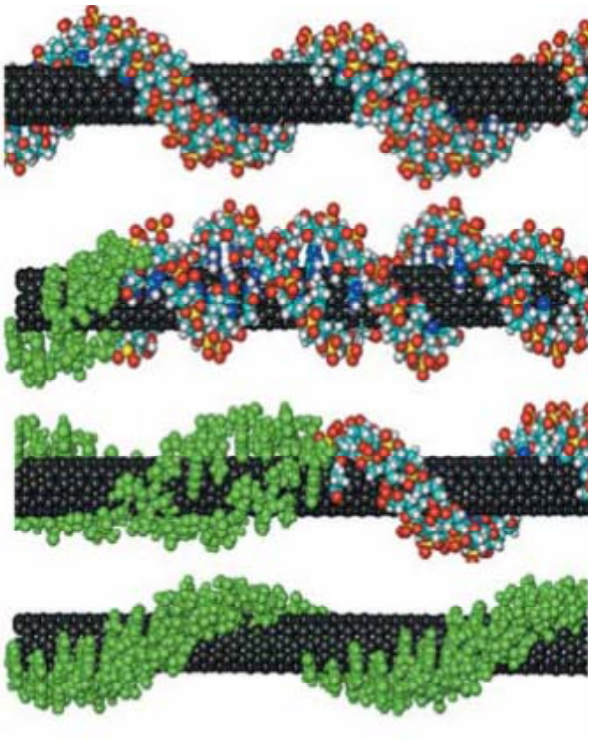

Fig. 1.20: Illustration of DNA undergoing a conformational transition from the B form (top) to the Z form (bottom) on a carbon nanotube.

1.3.2 CHEMICAL SENSING AND BIOSENSING USING DNA-CNT COMPLEXES

DNA functionalized CNTs have been developed for various sensing applications. The detecting analytes include gases or vapors, toxic ions or organics in liquid, DNA hybridization, glucose and virus [143-149]. ssDNA was decorated on SWNT field effect transistor (FET) and the change in conductance was measured upon exposure to gases and vapors [143]. Two types of DNA sequences were used: Seq1 (5’ GAG TCT GTG GAG GAG GTA GTC 3’) and Seq2 (5’ CTT CTG TCT TGA TGT TTG TCA AAC

3'). The response of ssDNA-SWNT sensors differ in sign and magnitude for different gases and different DNA sequences that used. The sensor can maintain the same response through at least 50 gas exposure cycles with no need of refreshing. This DNA-SWNT sensor was reusable and reliable. A schematic image of the sensing device and its response to methanol, TMA and PA are shown in Figure 1.21 and Figure 1.22.

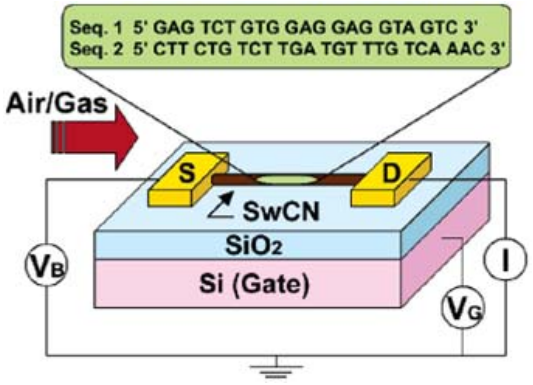

Fig. 1.21: Experimental setup for ssDNA functionalized SWNT FET sensor [143].

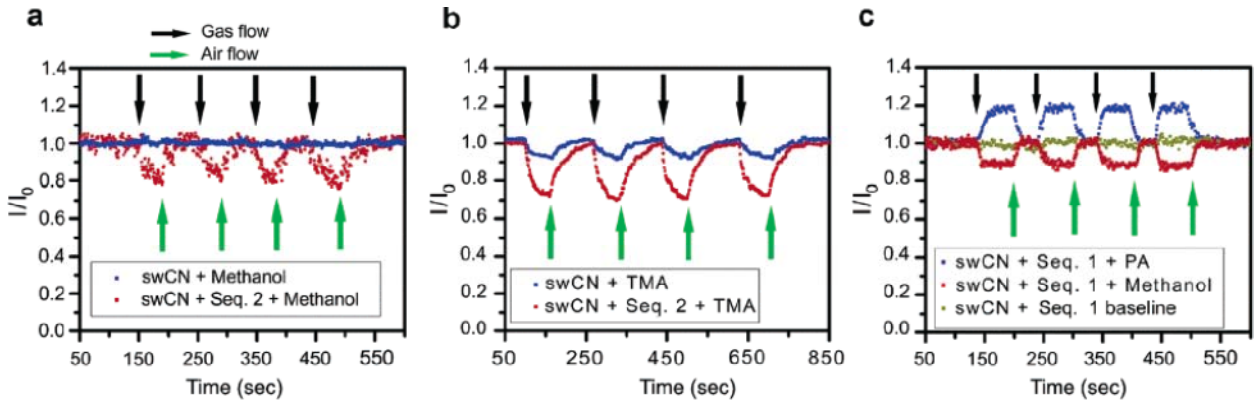

Fig. 1.22: Change in sensor current upon exposure to gas vapors. Currents are normalized to I_0, the value when exposed to air (no gas). (a) Bare SWNT-FETs do not respond to methanol vapor (blue curves). The same device coated with ss-DNA sequence 2 (Seq 2) shows clear responses to methanol (red curves). (b) A second bare device responds to TMA (blue points), but after application of Seq 2, its response tripled (red points). (c) The sensor response to propionic acid (blue curves) differs in sign and magnitude from the response to methanol (red points). Green data are the current baseline (no odor). V_B = 100 mV and V_G = 0 V for all data sets [143].

Oligonucleotides are used as versatile recognition sites for metal ions including Lead (II) and Mercury (II) ions [150]. A DNA duplex containing T-T mismatches showed high selectivity for Mercury ions (Hg^{2+}) against other metal ions due to the formation of T-Hg^{2+}-T base pairs. A T-rich ssDNA ((50-TTCTTTCTTCCCCTTGTTTGTT-FAM-30) was labeled with a fluorescein derivative 6-carboxyfluorescein (FAM) and noncovalently assembled on SWNTs for Hg^{2+} detection [144]. Before reacting with Hg^{2+}, the ssDNA wrapped around SWNTs and formed stable ssDNA/SWNT complexes. The fluorescent dye molecule was close to the surface of nanotube and thus quenched the intensity of fluorescence significantly. Upon addition of Hg^{2+}, the ssDNA formed a double helical structure with Hg^{2+} via T-Hg^{2+}-T base pairs, which dissociated from SWNTs and resulted in an increase in fluorescence emission compared to ssDNA-SWNT complexes. The change in fluorescence intensity was recorded by fluorescence spectroscopy. The sensing mechanism is illustrated in Figure 1.23 and the measured fluorescence intensities are compared in Figure 1.24.

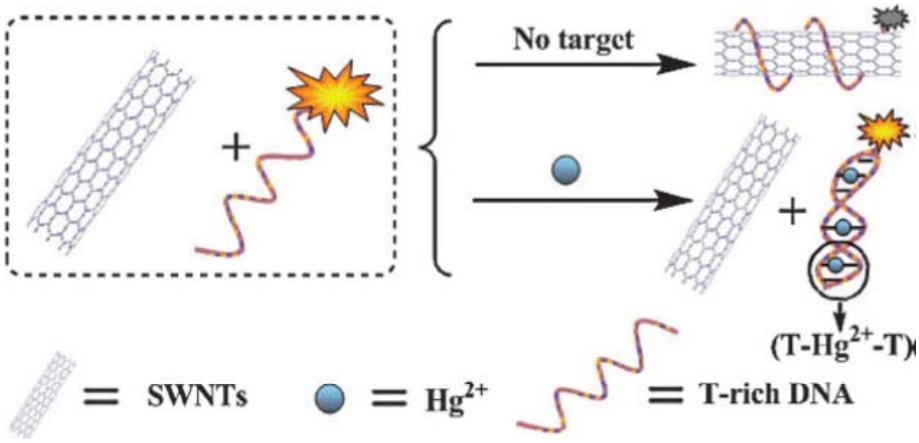

Fig. 1.23: Schematic description of fluorescence based sensing of Hg^{2+} using the complexes of SWNTs and T-rich DNA [144].

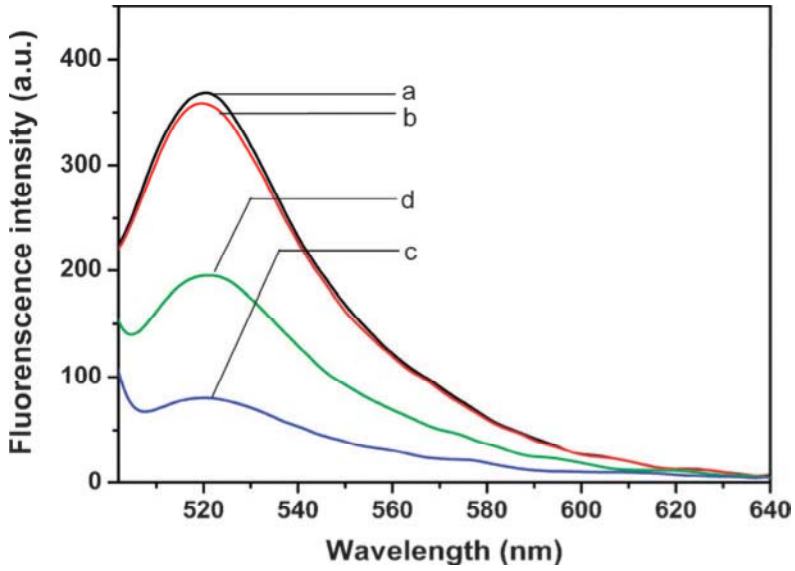

Fig. 1.24: Fluorescence emission spectra of ssDNA (100 nM) under different conditions: (a) ssDNA in tris-HCl; (b) ssDNA + 4.0 mM Hg^{2+}; (c) ssDNA + SWNTs; (d) ssDNA + SWNTs + 4.0 mM Hg^{2+}. λ_{ex} = 480 nm [144].

ssDNA was also immobilized on Double-walled carbon nanotubes (DWNTs) for electrical detection of DNA hybridization [145]. The DNA-DWNT device functioned as a chemiresistor and its drain current decreased by 40% after to DNA hybridization. The DWNT resistor immobilized with probe-DNA was highly selective to DNA with a complementary sequence. The response to target DNA was linearly proportional to concentration. Double-stranded DNA (dsDNA) SWNT hybrids were found to be optically sensitive to hydrogen peroxide and glucose in the presence of glucose oxidase enzyme. This redox reaction was conducted under pH conditions mimicking those in the human body. Near-infrared (NIR) spectra of dsDNA-SWNT suspension was red shifted by 20-30nm after reacting with hydrogen peroxide. Since hydrogen peroxide is the major product of the glucose oxidase-catalyzed glucose reaction, dsDNA-SWNT sensor can also detect glucose in the presence of glucose oxidase due to the generation of hydrogen peroxide from this reaction. The change in NIR intensity was found to linearly depend on the reaction time (the amount of hydrogen peroxide generated from the glucose oxidize reaction). ssDNA immobilized on MWNTs was used for label-free detection of influenza virus (type A) via DNA hybridization [149]. The DNA probe was attached onto the nanotube sensor by covalent bonding between

the amine and phosphate groups of the DNA sequence. The change in conductance of the MWNT device was measured to detect hybridization of target DNA with probe DNA. The detection limit was reported to be 0.5nM of the target DNA and the response time was about 4min.

1.4 MOTIVATION

The living environment of human beings is in a critical time when the air, land, water and wildlife resources of this planet are being decimated with astonishing speed [151-153]. Rapid industrialization, militarization and population growth throughout the world are not only destroying the quality of life but also the earth's capacity to support life [154]. The World Health Organization (WHO) estimates that about a quarter of the diseases facing mankind today occur due to prolonged exposure to environmental pollution [155]. Effectively monitoring of environmental pollutants has tremendous impact on human health and the ecosystem.

The air quality has been a major concern of United States Environmental Protection Agency (EPA). EPA's research and technical assistance on air quality monitoring are focused on several major areas that include: air quality, air toxics/pollutants, indoor air contaminants, air pollution sources, and air and climate change [156]. The most reliable, sensitive and selective instrument which has been widely utilized for detecting air pollutants is gas chromatography (GC)-mass spectrometry (MS). However, the GC-MS instrument is expensive, bulky and needs skilled operator which makes the equipment unable to be widely installed at any location and unable to monitor the air pollutants in a continuous manner. The water quality is essential for life and plays a vital role for the proper functioning of all living creatures. Water quality monitoring involves a series of observations, sample collection and analysis in a laboratory. Since water quality varies with time and location. The water quality evaluated by this strategy can only represent the quality of water at the specific location and in specific time of sampling. Besides, the current evaluation process is tedious and time consuming. Effectively and efficiently monitoring of air and water qualities requires the development of sensing systems which can be widely installed and mass produced

for in situ analysis and can accomplish the sampling, detection and analysis autonomously to eliminate human labor involved.

Nanomaterials, especially carbon nanotubes, exhibited many unique electrical, chemical and mechanical properties. SWNTs have been demonstrated by many researchers as the promising sensing elements due to their high sensitivity, fast response and miniature size. Since the conductance of SWNTs can be affected by various gases and vapors in air, tailoring the surface properties of SWNTs to attract specific gas or vapor is necessary to improve the selectivity of nanotube based sensors.

The major focus of this thesis is to provide a new approach to develop highly sensitive, low cost, miniature and autonomous sensing systems by functionalizing carbon nanotubes and integrating them with microdevices for real-time air quality and water quality monitoring. In order to achieve this goal, the SWNTs are assembled onto microelectrodes and function as a chemiresistor which will change its resistance when exposed to analytes. To improve the sensitivity and selectivity of SWNTs, DNA and RNA are decorated on nanotubes and their sensing characteristics to alcoholic vapors are investigated. In Chapter 2, eight different RNA sequences are functionalized on SWNT sensors and the responses of RNA-SWNT sensors to methanol and IPA are measured and analyzed. It has been observed by researchers that DNA functionalization can improve the response of SWNT sensor to some gases/vapors and the sensing response depend on the sequence of DNA oligomer. However, no one has analyzed the effect of DNA sequence length to the gas sensing characteristics of DNA-SWNT sensors. In Chapter 3, DNA with four different sequence lengths: 8, 16, 24 and 32 are designed and utilized to functionalize SWNTs. The effect of sequence length to the responses of DNA-SWNT sensors when exposed to methanol and IPA are obtained and analyzed. With sufficient fundamental studies of SWNTs functionalized with oligonucleotides, a nanosensor array composed of six different DNA-SWNT sensors are developed in Chapter 4. Sensor array is able to differentiate the target analyte from a mixed gases and vapors by providing a characteristic response pattern from all the sensors included in the sensor array. Thus the selectivity and reliability of sensor array for gas monitoring is much higher than a single sensing

unit. The fabricated six channeled sensor array is mounted on a PCB board for signal conditioning and wireless transmission. The measured responses from six sensors are displayed on a computer by graphical user interface. The wireless nanosensor array is tested with six different gases and vapors and the obtained results provide a deeper understanding of the sensing mechanism of DNA decorated SWNT sensors. In Chapter 5, a wireless sensing unit based on SWNTs integrated with complementary metal oxide semiconductor (CMOS) circuitry is developed for explosive and chemical warfare vapors detection. This SWNT nanosensor integrated with on chip op-amp circuitry is mounted on a PCB board with all the testing components and connected with wireless transmission board. This novel CMOS integrated SWNT nanosensor as a highly sensitive, highly compact, miniature and independent sensing system is tested with explosives and chemical warfare agent detection.

To develop a highly sensitive, autonomous and in situ microdevice for real-time monitoring of water quality, it is critical to integrate SWNT sensors with the microfluidic system which can separate and guide the liquid sample to the sensing area. In Chapter 6, two approaches to integrate microfluidic system with SWNT sensor are introduced. The microfluidic-SWNT sensor is tested with different pH buffer solutions and different concentrated TNT in water. Connecting with the signal processing and wireless transmission unit, the nanosensor integrated with microfluidic system is developed as an independent sensing unit with a small size which can be placed in rivers or lakes and can be easily installed on various water transportation systems.

In addition, the impact of natural disasters, such as hurricanes and earthquakes to the living environment is also highly concerned by the environmental protection agencies [157]. One direct impact is the damage to structures such as buildings, bridges, dams and the damages are often hidden within the structure, such as damaged joints embedded behind walls [158]. Developing structural health monitoring system can effectively detect the damages caused by natural disasters and monitor the long-term deterioration of structures due to the environment and human use which provides vital information on public safety. SWNT networks with unique piezoresistivity, remarkable tensile strength, high

stretchability and flexibility may find potential applications in large strain or crack monitoring in structures. In Chapter 7, a highly stretchable and flexible strain sensor made of SWNT network embedded in polymer thin films is reported. The electrical properties of SWNT thin film under different amount of strain are investigated. To prevent the conductance change of SWNTs due to the adsorption of gases and vapors in the testing environment, the nanotube sensor is encapsulated by another polymer film on the top. The effect of encapsulation to moisture exposure and tensile measurement are studied. The repeatability and reliability of this nanotube strain sensor are tested with 200 cycling measurements.

At the end of this thesis, I briefly summarize my work and present some future directions for further research.

CHAPTER 2

RNA FUNCTIONALIZED SWNT GAS SENSORS

Carbon nanotubes are potentially the sensing materials for environmental monitoring. However, due to the lack in selectivity and specificity, the surface properties of nanotubes need to be tailored for attracting specific molecules. In this chapter, single-stranded RNA (ss-RNA) decorated single-walled carbon nanotube (SWNT) sensors were fabricated and the base dependent gas sensing characteristics were investigated. SWNTs were placed onto Au microelectrodes by a low temperature and low cost Dielectrophoretic assembly process. Four homo ribonucleic acid (RNA) sequences and four repeated RNA sequences were coated on to SWNTs and the corresponding changes in resistance of SWNT nanosensor were explored. These RNA-SWNT devices function as Chemi-resistors where the resistance changes in response to vapors of methanol and IPA were measured. RNA decoration was found to improve the response of SWNTs to vapors of methanol and IPA significantly. The sensing response of homo RNA decorated SWNTs followed the trend: C > G > U > A for methanol and G > C > U > A for IPA. The sensing response of repeated base RNA coated SWNTs followed the trend: GU > AG > AC > CU for methanol and GU > AC > AG > CU for IPA. These dramatic differences in sensing characteristics

of RNA-SWNTs provide new insights both to the binding affinities of RNA oligomers onto SWNT sensors and to the formation of stable 3D structures by ss-RNAs on carbon nanotubes. These findings demonstrate a potential for controlling sensing specificity of RNA functionalized SWNT sensors for chemical and biological detection.

2.1 INTRODUCTION

Single-walled carbon nanotubes (SWNT) with their unique electrical, mechanical and chemical properties have attracted intense interest and have been utilized in many fields including nanoelectronics [159], field emitters [160] and sensors [161, 162]. As a one dimensional material, a SWNT is made of a rolled up graphene sheet. With a diameter of 1~2 nm, the SWNTs exhibit many unique properties, such as high aspect ratios, ballistic carrier transport [163], high mechanical strength and thermal stability [164]. These properties enable SWNTs to have superior performance in various applications including electronics and sensors. SWNT based sensors are extremely sensitive to slight electrostatic changes in their environment and have a fast response where conductance of an SWNT is observed to change in less than 2 sec upon exposure [165]. In addition, SWNT sensors have size advantage over traditional sensors. Furthermore, detecting analytes at the ppm levels can be achieved by nanotubes at room temperature, while most conventional semiconducting metal oxide gas sensors require high operating temperatures of about 200ºC-400ºC [166]. Hence, Single-walled carbon nanotubes (SWNTs) have been widely explored as active sensing elements for chemical and biomolecular detection [167-169].

Despite the high sensitivities observed from nanotube sensors, one drawback is their lack of selectivity. For instance, nonspecific binding from other gas vapors may result in erroneous readings. To develop nanosensors with specific selectivity, oligonucleotides - DNA and RNA were decorated on SWNTs to modify their surface properties to achieve affinities to specific analytes [143, 170]. Oligonucleotides can assemble on carbon nanotubes by non-covalent π-π stacking interactions. This is more desirable than covalent functionalization which breaks excessive C-C bonds in the nanotube lattice and tends to degrade its electronic properties [171]. Recent studies have shown that DNA/RNA

functionalized nanotube sensors have fast, specific and reproducible responses to various polar molecules [172].

A RNA nucleotide is composed of a ribose sugar, a phosphate and one of the four nitrogenous bases which could be adenine (A), cytosine (C), guanine (G) or uracil (U). One difference between RNA and DNA is that RNA contains ribose sugar while DNA contains deoxyribose sugar. Another difference is that DNA has a trymine (T) base while RNA has a U base. Despite slight differences in its molecular structure, RNA is more reactive compared to DNA and serves in many biological reactions as a catalyst and a mediator [173]. Besides, RNA is a versatile molecule that tends to fold and pair with itself to form diverse structures and conformations. These 3D structures that ss-RNA forms can be utilized as receptors for specific molecular recognition sites [174, 175]. For example, Lee et. al. selectively detected E. Coli using RNA aptamer functionalized SWNTs [176]. Due to the more reactive nature of RNA molecules and their ability to form 3D structures, RNA functionalized SWNT devices have unique sensing properties compared to DNA functionalized SWNT sensors. Exploring the sensing characteristics of RNA decorated SWNTs will advance the development of RNA-SWNT based chemical sensors and biosensors. The obtained knowledge will provide critical information to further explore the bonding affinities of different RNA sequences on SWNTs and the stable 3D structures of RNA nucleotides formed on SWNTs. Such understanding furthers our capability to design specific oligonucleotide sequences to achieve desired affinities and recognition sites for molecular detection.

In this study, to test the differences in sensing characteristics of RNA bases, four homo-RNA sequences (24A, 24U, 24G and 24C) were decorated on SWNTs for methanol and IPA sensing. Next, four repeated RNA sequences (24GU, 24AC, 24CU, 24AG) were coated on SWNTs and the RNA-SWNT sensors were tested against the same vapors. The objective was to obtain and evaluate the differences in gas sensing response for SWNT sensors decorated with four homo-RNA sequences and four repeated-RNA sequences (as shown in table 2.1).

2.2 EXPERIMENTAL PROCEDURE

2.2.1 NANOSENSOR FABRICATION

The fabrication process is shown in Figure 2.1. First, I deposited and patterned Cr/Au microelectrodes using photolithography followed by metal sputtering and a lift-off process on oxidized silicon wafers. Then, the SWNTs were placed between the two Au microelectrodes by a Dielectrophoretic (DEP) assembly process [177]. Commercial SWNTs from Brewer Science (with a diameter of 1~2nm and length of 2~5μm) were dispersed in DI water at a concentration of 0.004g/ml. A 2μl solution containing SWNTs were dispensed on to the microelectrodes. Then an AC signal with 3 V_{pp} and a frequency of 10 MHz was applied between the electrodes to assemble carbon nanotubes between them. SEM micrograph (Figure 2.2a) shows a close up of one of the microelectrode area with assembled SWNTs. After assembly, I-V measurements confirmed connectivity of the two electrodes and the two-terminal resistance is around 30KΩ.

2.2.2 PROCEDURE FOR RNA DECORATION

Eight RNA sequences were used to investigate the influence of decorating SWNT sensors with different RNA bases. A concentration of 100μM containing the corresponding RNA bases was next applied on to the assembled carbon nanotubes and incubated in a chamber under 100% humidity for 1 hour. RNA oligomers are known to self-assemble on SWNTs via π-π stacking. Afterwards, the excess RNA solution was removed by compressed air. The RNA molecules were decorated on SWNTs where they formed many small spheres that wrapped around the carbon nanotubes which are shown in Figure 2.2b. The pearl like structure of RNAs formed on nanotubes is consistent with previous observations made by AFM and single-molecule fluorescence microscope imaging [178-180]. As previously mentioned, single stranded RNA is more prone to self-hybridization and forms a 3D structure. We believe that these spheres are likely to be the folded single stranded RNA nucleotides.

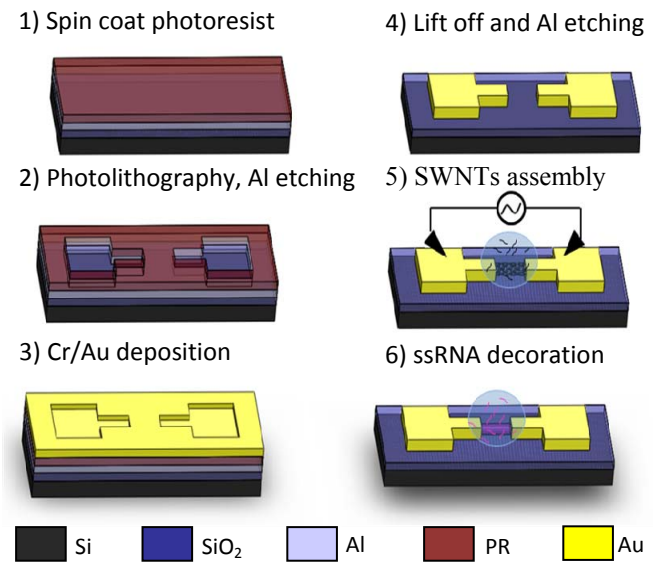

Fig. 2.1: Process flow for RNA decorated SWNT sensors assembled on Au microelectrodes.

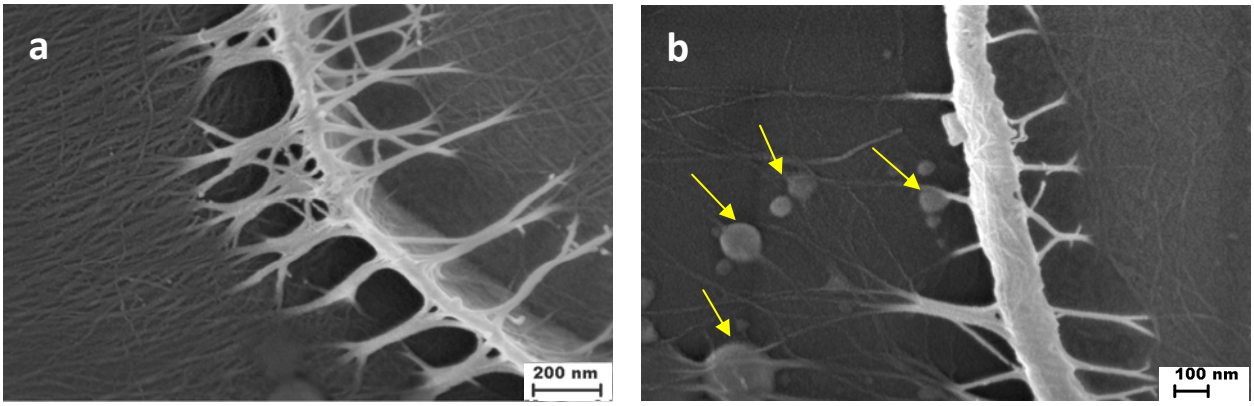

Fig. 2.2: (a) SEM micrograph of SWNT bundles assembled on Au electrodes; (b) SEM micrograph of SWNTs decorated with RNA. The yellow arrows indicate the 3D RNA structures formed on SWNTs.

2.3 RESULTS AND DISCUSSION

Gas sensing tests were performed on SWNT devices decorated with four homo and four repeated RNA sequences. The resistances of SWNT sensors and RNA-SWNT sensors were measured before, during and after exposure to methanol and IPA vapors. The changes in resistance of bare SWNTs and SWNTs functionalized with RNAs under exposure to methanol/IPA were calculated and summarized in table 2.1. The saturated vapor pressure of methanol at room temperature (23 ºC) is around 112 Torr and the

saturated vapor pressure of IPA at room temperature is around 38 Torr [181]. We found that the RNA decorated SWNTs showed an enhanced response to alcoholic vapors (methanol and IPA) than bare SWNTs. The graphene surface of SWNTs is known to be hydrophobic. Molecular dynamics simulations showed that the hydrophobic groups (the nitrogenous bases) of oligonucleotides tend to get attracted to and bond on to the surface of SWNTs, while the hydrophilic phosphate groups along the backbone of oligonucleotides do not bind to SWNTs [182]. Thus the exterior surfaces of RNA-SWNTs were covered by hydrophilic backbones of RNA. The presence of oligonucleotides has altered the surface properties of SWNTs from hydrophobic to hydrophilic. Accordingly, the polar molecules, such as methanol and IPA had a higher tendency to bind on to these functionalized nanotubes and change the resistance of SWNTs.

Table 2.1: Percentage change in resistance of RNA-SWNTs to methanol and IPA vapors.

Name	Sequences	Methanol (ΔR/R %)	IPA (ΔR/R %)
SWNT		15.5	11.4
RNA 24A	AAAAAAAAAAAAAAAAAAAAAA	18.0	16.2
RNA 24U	UUUUUUUUUUUUUUUUUUUUUU	26.8	28.1
RNA 24G	GGGGGGGGGGGGGGGGGGGGGG	56.0	40.7
RNA 24C	CCCCCCCCCCCCCCCCCCCCCC	78.1	35.8
RNA 24GU	GUGUGUGUGUGUGUGUGUGUGU	84.0	27.3
RNA 24 AC	ACACACACACACACACACACAC	35.8	16.1
RNA 24 CU	CUCUCUCUCUCUCUCUCUCUCU	19.2	12.8
RNA 24 AG	AGAGAGAGAGAGAGAGAGAGAG	51.5	14.2

The measured resistances of homo and repeated RNA-SWNT sensors when exposed to an air/methanol/air cycle were normalized and plotted in Figure 2.3 and Figure 2.4. The resistances of RNA functionalized SWNT sensors increased dramatically when exposed to methanol vapor (from 18% to 84%). It took a few minutes for methanol vapors to diffuse and adsorb on SWNT sensors. During this time, the resistance of the sensors has continuously increased and eventually reached a stable value in 2

mins. When the sensors were exposed to air, the adsorbed methanol molecules gradually desorbed from carbon nanotubes and the resistances of RNA-SWNT sensors returned to their initial values. These results indicate that the RNA coated SWNT sensors are reusable and robust.

Homo RNAs composed of different nitrogenous bases (such as 24A and 24C) on SWNTs showed a significantly different response to gas vapors (Figure 2.3). After exposure to methanol, the resistance of SWNTs decorated with RNA 24C increased by 78% and the resistance of SWNTs decorated with RNA 24A increased by 18%, where the RNA 24A only had a 3% improvement over the response from bare SWNTs. Repeated RNA sequences composed of two different bases (24GU and 24CU) also improved the response of SWNT sensors but in a different manner. The change in resistance for RNA 24GU functionalized SWNTs to methanol was 84% while the change in resistance for RNA 24CU-SWNTs was only 19% (Figure 2.4).

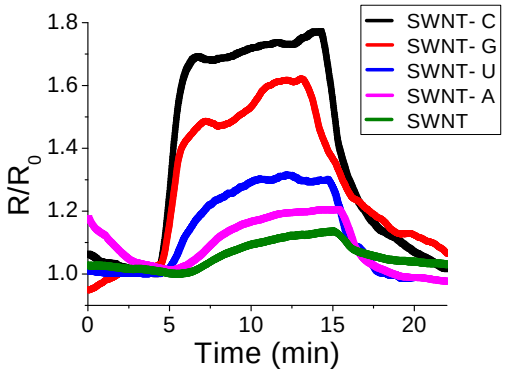

Fig. 2.3: The response of SWNT sensors decorated with homo-RNA sequence to methanol vapor [183].

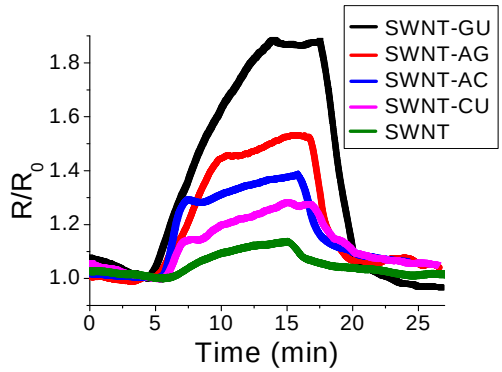

Fig. 2.4: The response of SWNT sensors decorated with repeated RNA sequence to methanol vapor [183].

It has been found that the response of homo RNA-SWNTs followed the trend: C > G > U > A for methanol and G > C > U > A for IPA (table 2.2). Thus, we believe that for SWNT sensors functionalized with RNA, the bases G and C play a key role in the sensing response. These trends were different than homo-DNA decorated SWNTs (G > A > C > T) which were reported by Khamis et al. [8]. RNAs composed of repeated bases followed the trend: GU > AG > AC > CU for methanol and GU > AC > AG > CU for IPA (table 2.2). This indicates that the response from repeated RNA bases do not simply equal to the sum of responses from homo bases. For example, homo base C plus homo base U should have a larger response to methanol than homo base G plus homo base A. However, the response of RNA 24AG to methanol (52%) was significantly higher than the response to RNA 24CU (19%).

The different responses of RNA-SWNTs to organic vapors are possibly due to a combination of effects. Among them four will be discussed. First, different responses could be due to the different binding affinities of RNA's nitrogenous bases with the SWNTs. Molecular dynamics simulations indicate that the hydrophobic nitrogenous bases of RNAs would be attracted to the hydrophobic surface of SWNTs [18]. RNA molecules composed of different base groups (A, U, G or C), the binding affinities between those bases and carbon nanotubes are different. We believe that the percent coverage of SWNT surfaces by RNAs played a vital role in gas sensing performance. Second, the different responses could also be attributed to the 3D structure of RNA sequences formed on nanotubes. As seen in the SEM images, multiple 3D pearl-like structures formed and wrapped around SWNTs after RNA decoration. The conformations of these 3D structures might affect the RNA-SWNT sensors' response to input analytes. Third, the nitrogenous bases of RNA attached on SWNTs had a chance to interact with the gas vapors (methanol and IPA) in addition to the interaction between the phosphate-sugar backbone of RNA and gas vapors. Further investigations are needed to confirm this possibility. Fourth, RNAs with various base compositions and sequences have a different stability in the ambient environment, as reported by Lesnik et. al. [184].

Table 2.2: Response order of different RNA decorated SWNTs upon exposure to methanol and IPA vapors.

	Homo RNA	Repeated RNA
Methanol	C > G > U > A	GU > AG > AC > CU
IPA	G > C > U > A	GU > AC > AG > CU

Four homo-RNA sequences and four repeated RNA sequences were coated on to SWNTs and their responses to various gas vapors were explored. RNA decoration improved the sensing response significantly when compared to the response obtained from bare SWNT sensors. The responses of RNA-SWNTs to methanol and IPA vapors were measured and found to be sequence dependent. This data will be included to vapor detection profile of RNA functionalized SWNT sensors. These results provide experimental data to understand the variations in SWNT sensing characteristics after decoration with different RNA bases. It also paves the way for exploring the mechanism behind sequence dependent gas sensing performance. With a better understanding of the sensing characteristics of oligonucleotide decorated SWNTs, specific oligomers with certain sequences and secondary structure could be designed and implemented to realize versatile nanosensing devices. These RNA sequences can be decorated on CNT sensor array and tested with other types of gases and vapors.

CHAPTER 3

DNA FUNCTIONALIZED SWNT GAS SENSORS-THE EFFECT OF DNA SEQUENCE LENGTH

DNA decoration has been found to improve the sensing response of SWNT sensors. However, on one has inspected the effect of sequence length to the sensing responses of DNA decorated nanotube sensors. This chapter reports the effect of sequence length on the sensing characteristics of DNA decorated single-walled carbon nanotube (SWNT) sensors. Four single-stranded poly-G oligomers with lengths of 8, 16, 24 and 32 were decorated onto SWNT sensors and the conductance of the nanosensors in response to methanol and IPA vapors were measured. Solution-based dielectrophoresis (DEP) process was used to assemble the SWNTs onto microelectrodes. DNA molecules with different sequence lengths were self-assembled onto the SWNTs via non-covalent π-π stacking interactions. The results show that the optimum DNA sequence length for sensing applications was 24 bases. Poly-G DNAs with various sequence lengths improved the response of SWNT nanosensors to vapors of methanol and IPA. The effect of sequence length dependent sensing performance is possibly due to the difference in binding affinities of nucleotides

onto SWNTs and the conformations that DNA molecules form on SWNTs. The measured responses of DNA-SWNT sensors to both gases were reversible and repeatable. We also observed that the DNA-SWNT sensors demonstrated an enhanced gas sensing response and also required a longer desorption time for the release of the adsorbed molecules, due to the adsorption of a larger amount of analytes. These findings will facilitate the development of DNA functionalized SWNT sensors for the detection of numerous chemicals and biomolecules.

3.1 INTRODUCTION

As described in Chapter 2, with these desirable properties, SWNTs are promising sensing elements for a wide variety of analytes of interest, from chemicals to biomolecules [102]. However, the sensitivity of nanotubes to many gases and vapors including oxygen and humidity in the environment is a concern for sensing applications. In order to achieve the desired specificity and selectivity of SWNTs to target analytes, several functionalization methods have been developed to modify the surface properties of nanotubes including coating them with a conducting polymer, metal nanoparticles or biomolecules, etc. Oligonucleotides (DNA and RNA) have previously been decorated on SWNTs to enhance their specificity and sensitivity. DNA decorated SWNTs have been demonstrated as chemical sensors that distinguished between various gases and vapors in air [143] and as biosensors to detect DNA hybridization in aqueous solutions [185]. Moreover, Zhao et. al. utilized the optical properties of DNA-SWNT hybrids to detect hydrogen peroxide and glucose in liquid which extended the applications of DNA-SWNT sensors into immunoassays [147]. DNA functionalized SWNTs have also been immobilized on Au electrodes as electrochemical DNA sensors with a detection limit down to 0.8 pM [186].

DNA is a long polymer made of repeated units, called nucleotides. As I mentioned in the introduction, a DNA nucleotide is composed of a deoxyribose sugar, a phosphate and one of the four nitrogenous bases which could be adenine (A), cytosine (C), guanine (G) or thymine (T). Single-stranded DNA (SsDNA) has been found to spontaneously wrap around carbon nanotubes and is reported to form various conformations on them. Several possible configurations, such as the double helix and the triple helix

structures have been proposed by Molecular dynamics simulations [187] and verified by experimental observations [188]. SsDNA binding to SWNTs occurs via π-π stacking interactions where the aromatic structures in oligomers' bases bind to the aromatic structures on SWNTs. Such non-covalent binding of DNA preserve the electronic integrity of SWNT's high conductance [171]. DNA decoration of SWNT sensors was previously reported where the DNA coating was found to enhance the sensitivity of the sensors. The DNA-SWNT sensors also displayed a reversible and reproducible response to numerous chemical vapors, and their responses were found to be highly sequence dependent [143]. While these results showed that the decoration of ssDNA improved the specificity and magnitude of the sensing response of bare SWNTs, detailed understanding of sequence dependent sensing mechanisms still needs further investigation. Khamis et al. previously reported that the gas sensing response of homo-oligomer ssDNA-decorated SWNTs to chemical vapors including methanol are in the following order: G > A > C > T [172]. Molecular dynamics simulations found that the binding affinities between homo DNAs and the SWNTs follow a comparable trend which is G > A > T > C, suggesting that the nature of ssDNA-SWNT binding plays a vital role in both the specificity and the sensitivity of the sensors.

In order to design an oligonucleotide that has the maximum binding affinity onto SWNTs and thus gives rise to the maximum response, the sequence length of DNA should also be considered. In this chapter, we investigate the sequence length dependent sensing characteristics of DNA on SWNTs and report the optimum sequence length that can bind on SWNTs for gas sensing applications.

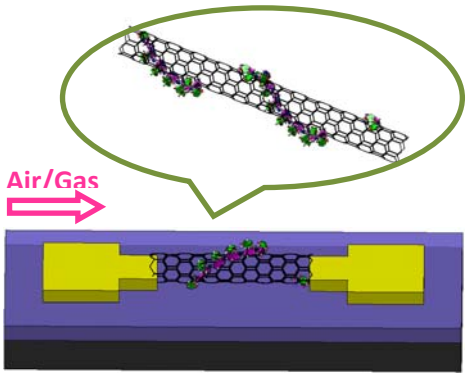

Fig. 3.1: Gas sensing device composed of ssDNA decorated SWNTs assembled on Au electrodes.

3.2 EXPERIMENTAL PROCEDURE

3.2.1 NANOSENSOR FABRICATION

The device fabrication procedure is similar to the process described in Figure 2.1. First, I deposited a thin (0.5 μm) insulating oxide on 3" silicon wafers using thermal oxidation. In this process, I utilized a high yield lift-off process which used a 0.3 μm Aluminum layer as the sacrificial layer. Hence, I next deposited the sacrificial Aluminum layer by a magnetron sputter deposition system (Perkin Elmer 2400 Sputter). Then, microelectrodes with 3 μm spacing were fabricated by photolithography followed by sputtering a Cr/Au (20 nm/150 nm) layer (MRC 8667 Sputtering). SWNTs were then placed between microelectrodes by a solution based dielectrophoretic (DEP) assembly process. DEP assembly is a low temperature, low cost and efficient method for carbon nanotube placement in an aqueous environment [177]. Commercially available SWNTs (diameter: 1~2 nm; length: 2~5 μm) were dispersed in DI water with a concentration of 0.004g/ml. Next, 2 μl of this SWNT suspension was placed on top of the microelectrodes with a pipette. An AC signal of 3 V_{pp} at a frequency of 10 MHz was applied for 30 secs between the microelectrodes. The DEP assembly not only connected the electrodes with SWNTs, but also provided some alignment to the assembled nanotubes. SEM image (Figure 3.2) shows the successful assembly of SWNTs on microelectrodes.

3.2.2 PROCEDURE FOR DNA DECORATION

It was reported that the decoration of CNTs with Poly-G DNA oligomers enhances the response of the nanosensors to methanol vapors in a significant manner [172]. Thus in this paper, we investigated poly-G DNA with sequence lengths of 8, 16, 24 and 32.

DNA 8 G:	GGGGGGGG
DNA 16 G:	GGGGGGGGGGGGGGGG
DNA 24 G:	GGGGGGGGGGGGGGGGGGGGGGGG
DNA 32 G:	GGGGGGGGGGGGGGGGGGGGGGGGGGGGGGGG

DNA is known to self-assemble on SWNTs by noncovalent π-π stacking interactions. 5 μl ss-DNA solution with a concentration of 100 μM was applied onto the carbon nanotubes and incubated in a chamber with 100% humidity for 1 hour. After that process, the excess DNA solution was removed by blow drying the sample with compressed air. A schematic image of DNA assembled on SWNTs is illustrated in Figure 3.1. The response of DNA poly-G decorated SWNTs to alcoholic vapors (methanol and IPA) were measured by a multimeter at room temperature and displayed by LABVIEW program.

3.3 RESULTS AND DISCUSSION

3.3.1 DNA FUNCTIONALIZED SWNTS

One of the main advantages of DEP assembly over other nanomaterial assembly methods is the alignment provided by the electric fields during assembly. As shown in Figure 3.2, the SWNT bundles were aligned in a parallel manner between the two microelectrodes. After the DNA molecules were coated on to the surface of SWNTs, we found that SEM imaging was not sensitive enough to resolve the increase in the thickness of the SWNTs bundles. It has been reported by Staii et. al. that ssDNA forms a ~1nm thin layer on SWNTs [143]. In addition, we observed the presence of tiny white dots randomly dispersed between SWNT bundles, which were likely caused by the aggregation of DNA molecules settling on SWNTs. The observed DNA aggregates were consistent with the AFM measurements reported by Strano et al. where DNA was adsorbed on SWNTs in a nonuniform manner [189].

The I-V measurements from the SWNT nanosensors assembled in between two microelectrodes before and after DNA decoration were plotted in Figure 3.3. After DNA attachment onto the SWNT surface, the current in the SWNT sensor decreased which indicated that the DNA decoration resulted in an increase in the two-terminal resistance of SWNTs. The increase in resistance after DNA decoration is consistent with the results reported by several other groups [145, 185, 190]. One possible reason for the reduction in conductivity could be that the electrons of the DNA bases act as a dopant for the semiconducting carbon nanotubes [185]. In other reports, the change in resistance after DNA decoration was attributed to the

modulation of the metal-nanotube contact resistance due to molecular absorption [117, 191]. Further study is required to investigate the charge transport characteristics of DNA-SWNT composites.

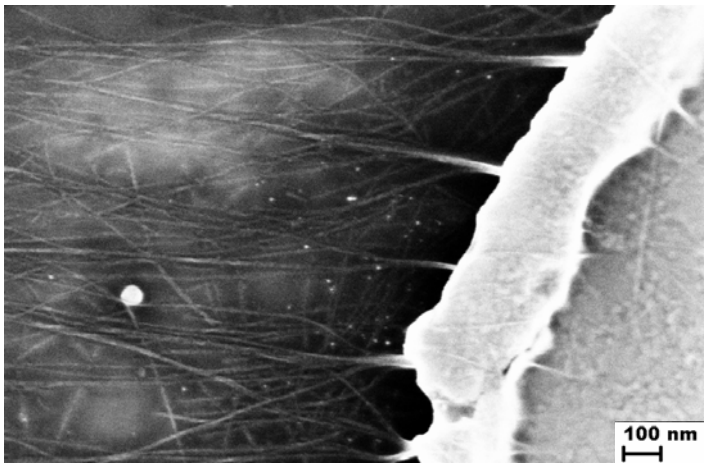

Fig. 3.2: SEM micrograph of SWNTs with DNA 8G assembled on Au electrodes. The white dots are aggregated DNA molecules.

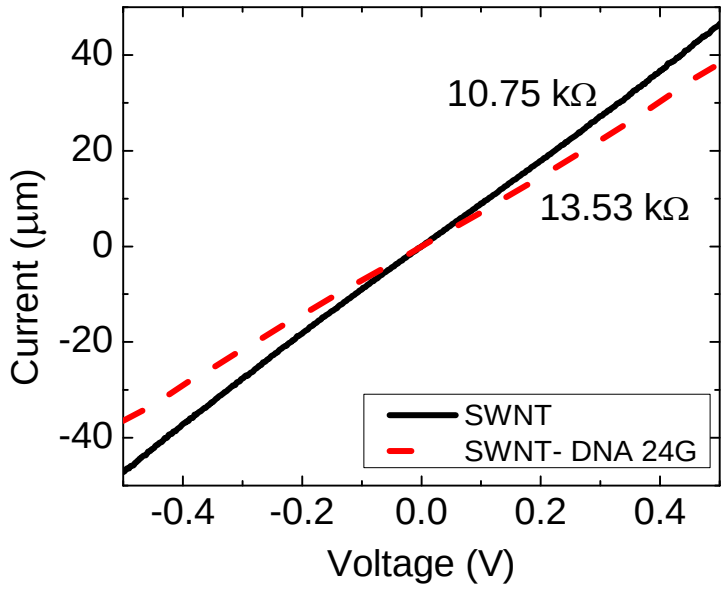

Fig. 3.3: I-V characteristics of SWNTs assembled on micro electrodes before and after decorating DNA 24G.

3.3.2 SENSING RESPONSE OF DNA-SWNTS TO ALCOHOLIC VAPORS

The sensing characteristics of SWNT sensors decorated with DNA nucleotides of different sequence lengths were next investigated. The resistance of bare SWNTs and DNA decorated SWNTs were recorded before, during and after exposure to methanol and IPA vapors. The saturated vapor pressure of methanol at room temperature (23 ºC) is around 112 Torr and the saturated vapor pressure of IPA at room temperature is around 38 Torr [181]. Figure 3.4 and Figure 3.5 show the normalized resistances of DNA-SWNT devices under exposure to methanol and IPA vapors, respectively. Figure 3.4 shows that SWNTs coated with DNA 24 G and DNA 16G have significantly higher responses than SWNTs coated with DNA 8G and DNA 32G. Figure 3.5 displays that the SWNT sensors functionalized with DNA 24G showed a higher response to IPA vapors compared to ones functionalized with other poly-G oligomers. Under exposure to methanol vapor, bare SWNTs were found to have an increase in resistance of about 15.5%. The decoration of DNA 8G and DNA 32G barely improved the response of SWNT devices to methanol as seen in Figure 3.4. The resistance of DNA 8G-SWNTs were increased by 18.55% (an improvement in the response of nanosensors by 3%) and the resistance of DNA 32G-SWNTs were increased by 22.8% (an improvement in the response of nanosensors by 7%) after exposure to methanol. However, after coating SWNTs with DNA 24G, the change in resistance when exposed to methanol was 45.8%, which resulted in an improvement in the response of bare SWNT sensors (15.5%) by about 300%.

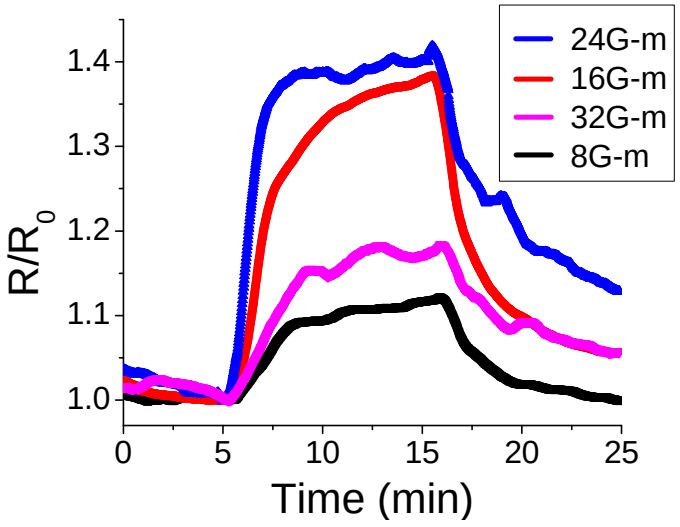

Fig. 3.4: Normalized resistance of DNA decorated SWNTs upon exposure to methanol vapor. CNTs were decorated with DNA poly-G with sequence lengths of 8, 16, 24 and 32.

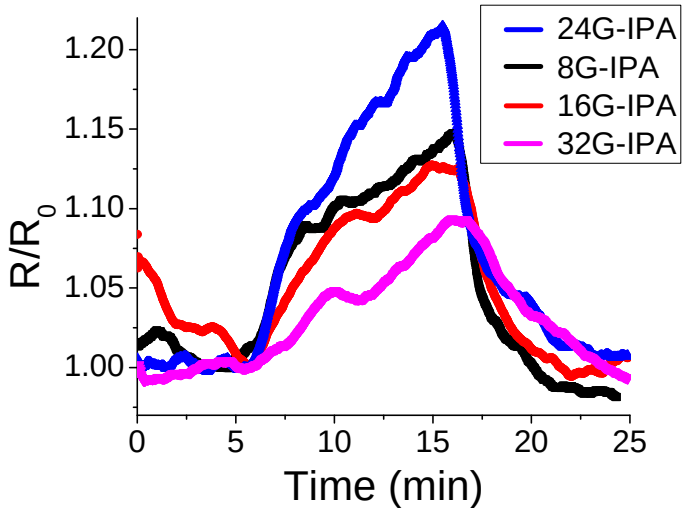

Fig. 3.5: Normalized resistance of DNA decorated SWNTs upon exposure to IPA vapor. DNA poly-G with sequence lengths of 8, 16, 24 and 32 was used.

The average resistance changes in bare and DNA functionalized SWNT sensors when exposed to methanol and IPA vapors were calculated and plotted in Figure 3.6. These results indicate that DNA poly-

G with a sequence length of 24 produced the maximum response to vapors of methanol and IPA. The decoration of SWNTs with poly-G ssDNA improved the sensitivity of bare SWNT sensors where the magnitude of the sensing response was also dependent on the length of the DNA sequence used. A possible reason for the DNA based sensitivity enhancement of SWNT sensors to polar molecules could be that the DNA altered the surface property of SWNTs from hydrophobic to hydrophilic. Molecular Dynamics simulation results reported by Zhao et al. suggested that the hydrophobic groups (the nitrogenous bases) of oligonucleotides tend to bind on to the surface of SWNTs, while the hydrophilic phosphate groups along the backbone of oligonucleotides do not bind to SWNTs [182]. Thus after coating ssDNA molecules onto the carbon nanotubes, the outer periphery of the DNA-SWNTs will be covered by the hydrophilic backbones of DNA which tends to further attract polar molecules including methanol and IPA. Hence the surface coverage of SWNTs by DNA oligomers plays a vital role in the sensing performance of the SWNT sensors. From these results, it is very likely that the DNAs with different sequence lengths have different binding affinities on to the surface of carbon nanotubes, thereby resulting in different gas sensing response. Sequence length of 24 might be the optimum length to wrap around nanotubes and provide a better coverage on the sidewalls.

Another possible reason for the sequence length dependent sensing response could be due to the 3D structures that ssDNA forms on SWNTs. We observed white dots on carbon nanotubes as shown in Figure 3.2. This indicates that the DNA molecules could aggregate and form stable conformations on carbon nanotubes. Surface enhanced infrared absorption (SEIRA) study on DNA-SWNT complex showed that numerous structural changes in DNA were connected with the appearance of new sugar and base conformations and changes in phosphate vibrations, which was likely interpreted as A–B conformation transition and stabilization of structure in some DNA fragments [140]. It is very likely that DNAs with different sequence lengths form different conformations on SWNTs in order to reach a stabilized state.

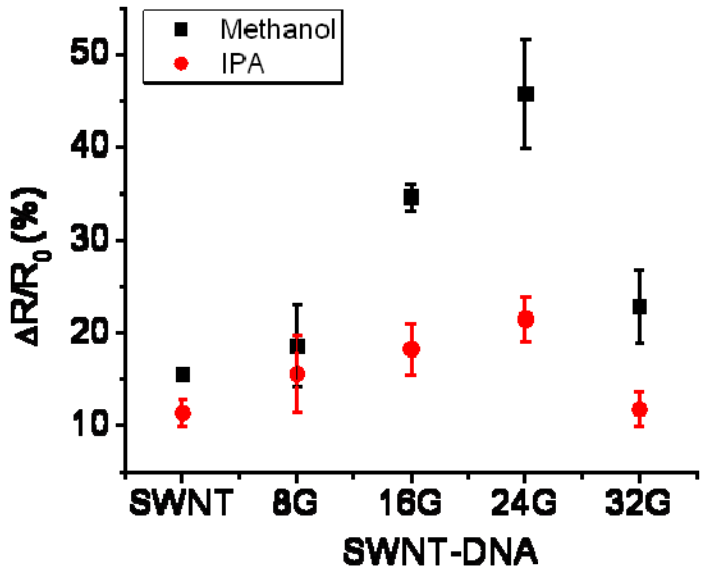

Fig. 3.6: Change in resistance of DNA-SWNT sensors upon exposure to methanol and IPA vapors. Sensing response of SWNTs decorated with DNA G of various sequence lengths was compared [192].

Figure 3.7 shows three methanol/IPA gas sensing cycles from bare and poly-G decorated SWNT sensors. The response of the bare and DNA functionalized SWNT sensors were reversible and repeatable to methanol and IPA vapors. We also found that the specific sequence length of the DNA molecules that gave rise to an enhanced response also increased the refresh time of the sensors. The enhancement in sensor response resulted in a larger number of gas molecules to be absorbed on the sensor surface which also took a longer time to desorb under ambient conditions. The average desorption times of DNA-SWNT sensors and bare SWNT sensors to methanol and IPA were measured and plotted in Figure 3.8. Both the desorption data and the sensor response curves show a similar trend where the maximum response is observed for a DNA sequence length of 24. Our results suggest that larger gas sensing response stems from larger amount of analyte adsorption and therefore results in a longer desorption time.

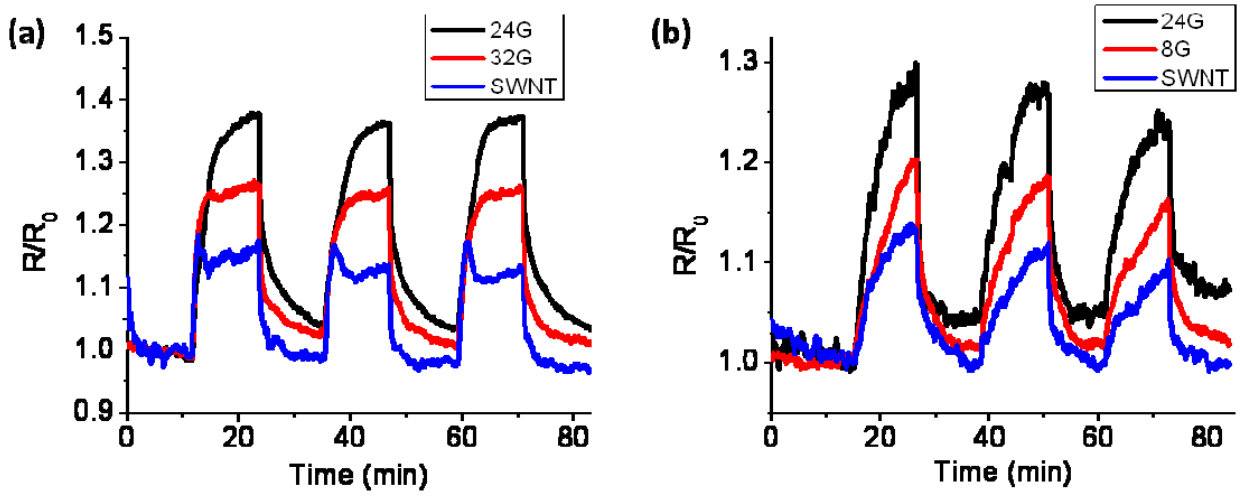

Fig. 3.7: (a) Multiple sensing measurements using DNA 24G and DNA 32G decorated SWNTs and bare SWNTs to methanol vapor. (b) Multiple sensing measurements using DNA 24G and DNA 8G decorated SWNTs and bare SWNTs to IPA vapor.

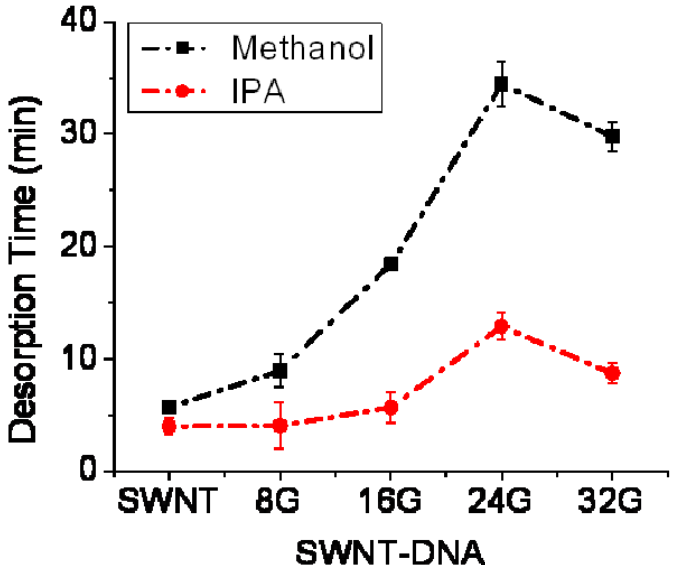

Fig. 3.8: Desorption time of DNA-SWNT sensors in ambient environment after exposure to with methanol and IPA vapors.

In this chapter, I demonstrated that the length of the ssDNA sequence that is functionalized on SWNTs impacts the gas sensing response of SWNT sensors. I found that the decoration of 24 bases of poly-G ssDNA molecules on SWNTs sensors resulted in the largest resistance change when the devices were

exposed to methanol and IPA vapors. Four different sequence lengths were tested and the gas sensing response of poly-G ssDNA-SWNTs were found to vary with the changes in the lengths of the DNA sequences. It is possible that both the binding affinity of DNA on SWNTs and the stable conformation of DNA formed on SWNTs are sequence length dependent. Thus the sensing characteristics of DNA-SWNTs depend on the sequence length of the functionalized oligomers. These results provide further insight into the interactions between ssDNA and SWNTs and will facilitate the design of oligomers with desired sensing properties for novel nanosensors.

CHAPTER 4

WIRELESS SENSOR ARRAY BASED ON DNA DECORATED SWNTS FOR GAS MONITORING

The response of nanosensor to the target analyte is susceptible to many gases and vapors including oxygen and moisture which are abundant in the ambient environment. In order to differentiate a type of gas or vapor in a mixture of various compounds, sensor arrays which are commonly called electronic nose have been proposed by researchers. The sensor arrays achieve selectivity by providing a characteristic signature for an analyte from the responses of several different sensors included in the sensor array. It has been demonstrated in the previous chapters that oligonucleotides (RNA and DNA) can increase the responses of nanotubes to alcoholic vapors and the responses of DNA-SWNTs are reversible, repeatable and sequence dependent. In this chapter, ssDNA of different sequences were used to functionalize the nanotubes assembled on microelectrodes to alter the surface affinities of nanotubes to analytes. To reduce the undesirable responses of SWNTs to interfering analytes, a wireless sensor array composed of six nanosensors functionalized with different ssDNAs were developed. The resistances of six SWNT sensors

were measured simultaneously during exposure to gases. The responses of different DNA decorated SWNTs and bare SWNTs to toxic organics were wireless transmitted and displayed by a GUI interface. Development of this wireless sensor array enabled selective, sensitive and real-time monitoring of hazardous gases and vapors from a distance.

4.1 INTRODUCTION

Sensor array is trying to mimic the mammalian olfactory system by collecting the responses of many different sensors simultaneously and obtaining the characteristic signature of a certain analyte by artificial computational programs, such as pattern recognition [193]. To date, many types of sensor arrays have been developed and demonstrated for reliable detection and identification of volatile organic compounds (VOCs) and other gases [89, 194-200]. The modalities of sensor array can be thin films of conducting polymers [201], surface acoustic wave sensors [202], semiconducting metal oxides [203], micromechanical cantilevers [204] and colorimetric sensor array composed of chemically responsive dyes [205]. Miniaturization of sensing elements is important for the design of high-density sensor arrays with relatively small spatial footprints. Recently, electronic devices utilizing nanomaterials including nanocomposites [206], nanowires [207] and carbon nanotubes [208] have been shown to function as extremely sensitive and small chemical sensors. Integration of these sensor elements into a complex sensor array may bring about electronic noses as complex as the mammalian olfactory system.

Carbon nanotube based sensor array has been achieved by decorating different metal nanoparticles onto SWNTs [88]. The differences in catalytic activity of 18 catalytic metals evaporated on nanotube transistors, for detection of H_2, CH_4, CO, and H_2S gases were observed. Furthermore, a sensor array was fabricated by site-selective electroplating of Pd, Pt, Rh, and Au metals on isolated SWNT networks located on a single chip. The resulting electronic sensor array, which was comprised of several functional SWNT network sensors, was exposed to three combustible gases, H_2, CO, and H_2S and two toxic gases, NH_3 and NO_2. Electronic responses of all sensor elements were recorded and the sensor array data was analyzed using pattern-recognition analysis tools. Carbon nanotubes were dispersed into five different

insulating polymer matrices to form conductive polymer nanocomposites which were utilized in five different sensors for gas detection [209]. The nanocomposites based sensor array was tested with nine organic solvent vapors (isopropanol, tetrahydrofuran, dichloromethane, n-heptane, cyclohexane, methanol, ethanol, water and toluene) and the responses of sensor array to different vapors were separated by principle component analysis which was demonstrated to be an excellent pattern recognition tool. Lu and collaborators combined the metal decorated SWNT sensors and polymer coated SWNT sensors into a sensor array with 32 sensing elements [89]. This sensor array was exposed to NO_2, HCN, HCl, Cl_2, acetone and benzene in ppm concentration levels. The obtained data was normalized and autoscaled for eliminating concentration and background noise, and ignoring outliers. The post processed array data was then subjected to a principal component analysis, a pattern recognition technique, for gas and vapor discrimination. Carbon nanotubes coated acoustic and optical sensors were combined into a sensor array and utilized for volatile organic compound detection [210]. The nanotube networks were dip coated onto quartz crystal microbalance resonators and standard silica optical fiber sensors with LB multilayered material of cadmium arachidate pre-deposited onto the sensor surface as the linker. Response from each sensor to six different volatile vapors were analyzed and processed by pattern recognition including principle component analysis and artificial neural networks.

In this chapter, DNAs with different sequences were decorated onto SWNT sensors for gas monitoring applications. The CNT microsensors were further placed on a PCB board with signal conditioning and connected with a wireless transmitter. This wireless nano-sensor array module is networked and scalable, consumes very little power, programmable, capable of fast data acquisition, reliable over a long term operation, low cost and requires minimum maintenance. A wireless sensing platform (Waspmote) is used for this project, which is suitable for environmental monitoring, fire & flood detection and logistics. The platform includes a range of radio ZigBee modules with a choice of protocol versions, radio frequency and range as well as a module for GPRS which can connect a sensor network to the outside world. The wireless transmitted signals from six sensors were recorded displayed on by GUI

on a computer for further analysis. This DNA functionalized SWNT sensor array were tested with six types of gases and vapors, at room temperature.

4.2 EXPERIMENTAL PROCESS

4.2.1 FABRICATION OF THE SWNT SENSOR ARRAY

The process of making SWNT sensors have been described in Chapter 2. DNAs with the following sequences were utilized to functionalize SWNTs:

DNA 24 G:	GGGGGGGGGGGGGGGGGGGGGGGG
DNA 32 G:	GGGGGGGGGGGGGGGGGGGGGGGGGGGGGGGG
DNA 1	GTGTGTGTGTGTGTGTGTGTGTGT
DNA 2	Amine-GACCTGTTCAAGGACCTGTTCAAG-Amine
DNA 3	AAAAAAAAAAAAAAAAAAAAAAAA
DNA 4	Amine-AAAAAAAAAAAAAAAAAAAAAAAA-Amine

4.2.2 WIRELESS TESTING BOARD

A functional block diagram of the wireless nanosensor array is shown in Figure 4.1 which was developed with a modular design concept. The modular design approach provided a flexible and versatile platform to address the needs for a wide variety of applications. For example, depending on the sensors to be deployed, the signal conditioning block can be re-programmed or replaced. This allows for a variety of different sensors to be used with the wireless sensing node. Similarly, the radio link may be exchanged as required for a given applications' wireless range and the need for bidirectional communications. The use of flash memory allows the remote nodes to acquire data on command from a base station, or by an event sensed by one or more inputs to the node. Figure 4.2 shows the actual system developed with this modular concept.

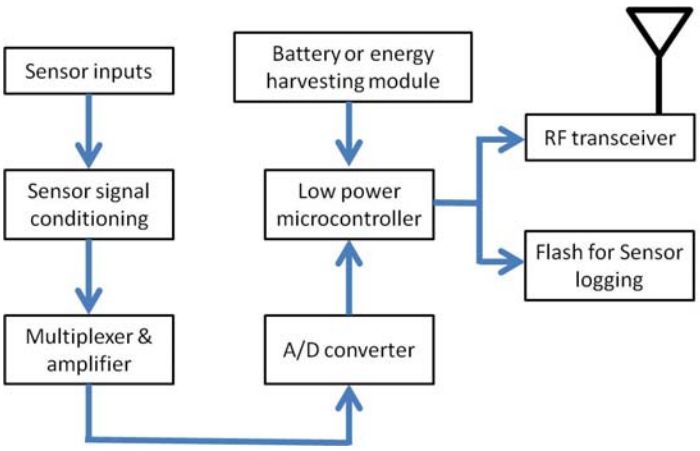

Fig. 4.1: The wireless sensor node functional block diagram for the wireless sensor node.

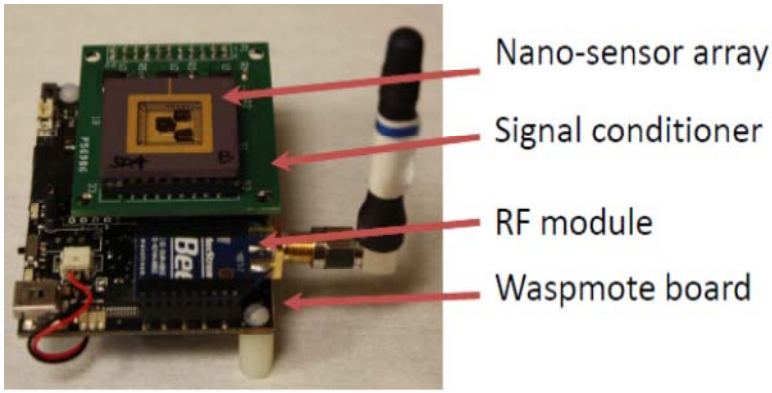

Fig. 4.2: A photograph of the wireless nanosensor array system.

4.3 RESULTS AND DISCUSSION

4.3.1 DNA DECORATED SWNTS ASSEMBLY

During the DEP process, the SWNTs in the aqueous solution will be aligned by the applied electrical field between the two electrodes [211]. Figure 4.3a shows that the SWNT bundles were successfully assembled on microelectrodes and aligned almost parallel to the electrodes. After ssDNA decoration, it was observed that some tiny white dots were randomly dispersed in CNT bundles, which were believed to be aggregated ssDNA molecules (Figure 4.3b). Aggregation of ssDNA on SWNTs was previously

reported by Jeng et. al. using AFM imaging [189]. This indicated that ssDNA molecules were attached on SWNTs in a nonuniform manner.

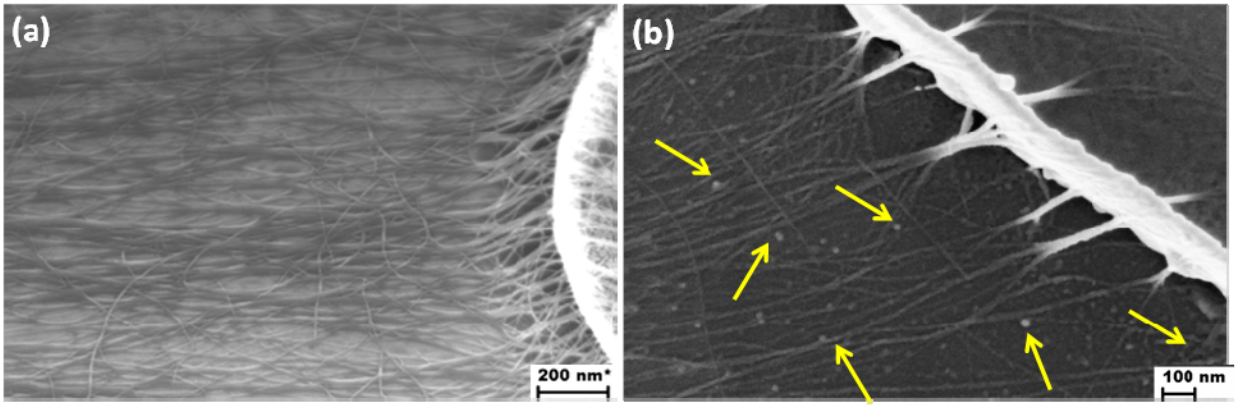

Fig. 4.3. (a) SEM micrograph of SWNTs assembled on an Au microelectrode (b) SEM micrograph of ssDNA functionalized SWNTs assembled on the microelectrode. The white dots were aggregated ssDNA nucleotides.

4.3.2 Remote Sensing with Nanosensors

To obtain data in a wireless manner, a graphic user interface (GUI) program was developed to control the application using a PC with LabWindows/CVI. As shown in Figure 4.4, the application obtained the data from Waspmote gateway through a USB port which received the data from the nanosensor array node wirelessly. Acquired data was real-time monitored, plotted and stored for further analysis. Figure 4.5 shows the GUI interface for this application.

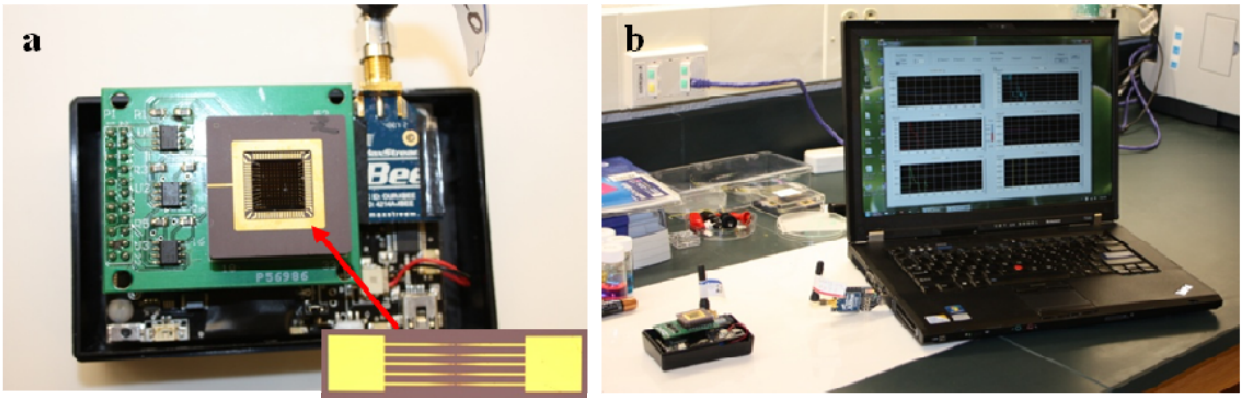

Fig. 4.4: Photograph of six channel sensing array made by SWNTs assembled on Au microelectrodes. (a) Photograph of nanosensor array connected with the testing board and the wireless transmission board.

(b) The measured output voltage was transmitted wirelessly to a computer and the resistances of nanotubes were calculated.

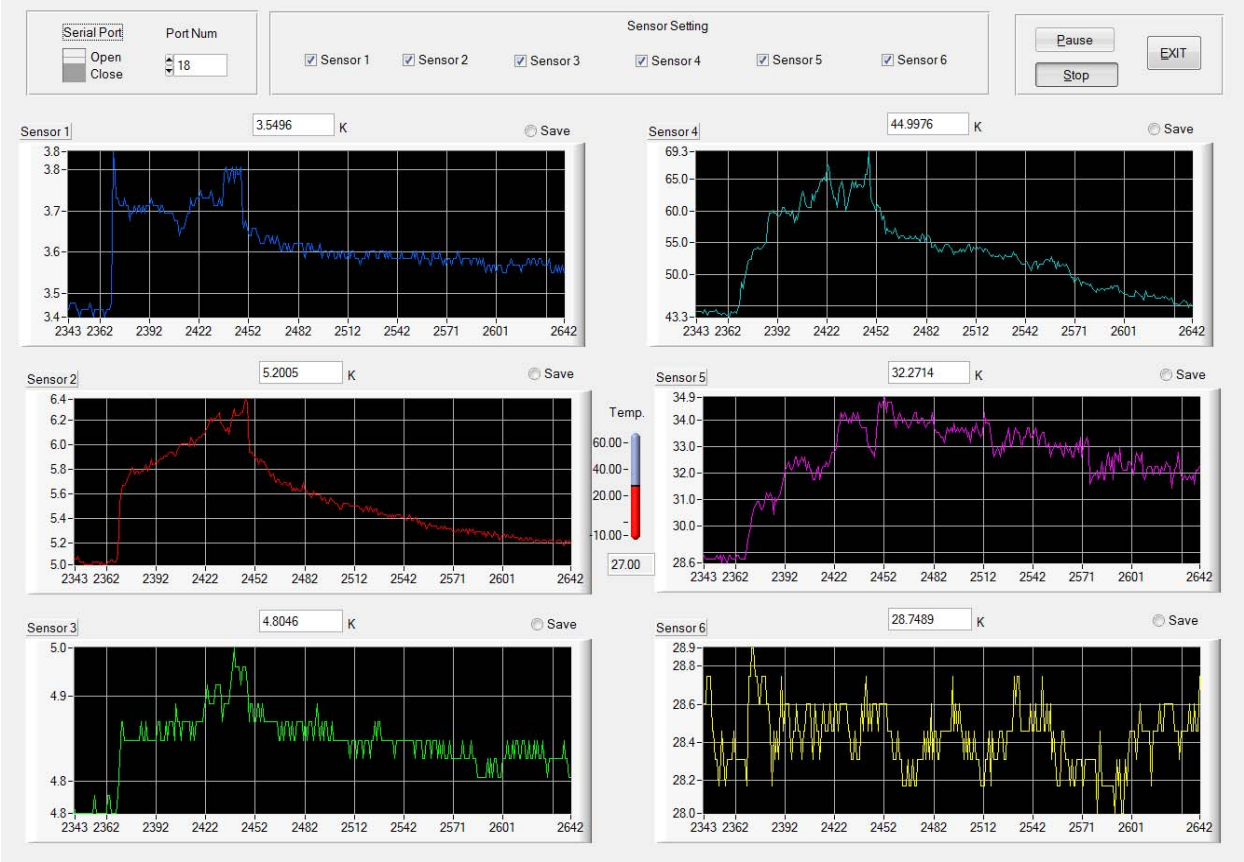

Fig. 4.5: GUI interface for the wireless nanosensor arrays.

The Waspmote main board contains a built-in accelerometer and when combined with the GPS module, the device can be used to measure speed, direction and location of vehicles or containers. The platform has outstanding power management allowing it to be deployed in remote locations and adverse conditions; an optional solar panel can allow almost indefinite operation.

4.3.3 GAS SENSING MEASUREMENTS

The six channel nanotube sensor array was utilized to detect methanol vapor at room temperature. DNA 24G and DNA 32G sequences were used to decorate two SWNT sensors, respectively. The sensing elements of the left two SWNT sensors were reserved for the bare SWNTs. The SWNT nanosensor array was next mounted onto a testing board with a signal processing unit and a wireless transmitter and functioned as an autonomous unit for gas monitoring. The wireless sensor array was tested in a sealed chamber and the vapors were carried into the chamber by nitrogen or compressed air. The testing setup was illustrated in Appendix C. The resistances of six SWNT sensors were recorded simultaneously and displayed by GUI on a computer (Figure 4.5). The nanosensor array was exposed to air, methanol vapor and air consecutively for three times. The normalized resistances of the six sensors when exposed to air/methanol vapors were collected and plotted in Figure 4.6. The SWNT sensors had a rapid and significant response to methanol vapor and after being exposed to air gradually recovered their initial values. In addition, the sensing characteristics of the SWNT sensors were reversible and repeatable. Decorating the CNT sensors with DNA 24G sequence improved their response by 300%, while decoration of DNA 32G sequence improved the response of SWNTs by 200%. For SWNT sensors functionalized with the same DNA sequence, the changes in resistance of the two SWNT sensors to methanol vapor were about the same. Hence, the sensing characteristics of DNA decorated SWNTs were confirmed independently by two channels under the same experimental conditions. The changes in resistances of DNA 24G-SWNT, DNA 32G-SWNT and bare SWNT sensors upon exposure to methanol are plotted in Figure 4.7.

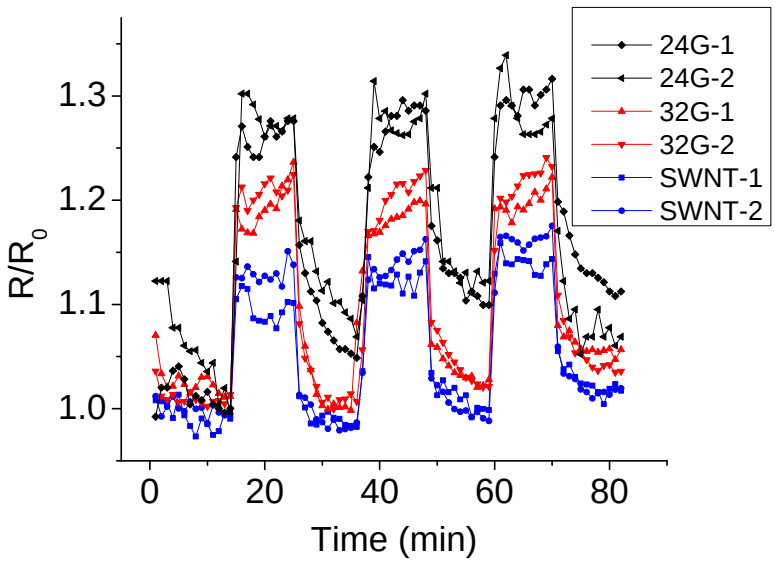

Fig. 4.6: Normalized resistances of SWNT nanosensors functionalized with DNA 24G, DNA 32G sequences and bare SWNT nanosensors when exposed to methanol vapors (three cycles are shown).

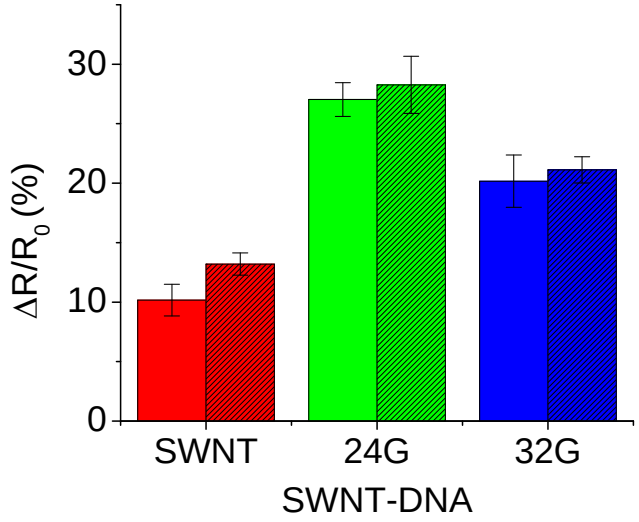

Fig. 4.7: The changes in resistance of SWNT nanosensors functionalized with DNA 24G, DNA 32G sequences and bare SWNT sensors upon exposure to methanol vapor.

The wireless nanosensor array was then utilized to detect various vapors with different chemical properties to explore the sensing mechanism of DNA decorated SWNT sensors. The molecular structures of testing analytes are illustrated in Figure 4.8. Here, methanol, water and acetonitrile are polar molecules and are hydrophilic. Benzene is a nonpolar organic molecule and has very limited solubility in water

(hydrophobic). Hydrogen sulfide and DMS are polar molecules but they are hydrophobic. Water, methanol, acetonitrile, benzene and dimethyl sulfide (DMS) vapors evaporated from the solutions in a petridish placed in a sealed chamber at room temperature. Since DMS is extremely volatile, DPG was utilized to dilute the DMS solution (5 µl DMS dissolved in 35 ml DPG solution). Since nanotubes do not respond to DPG, the change in resistance will be caused by DMS. The equilibrium vapor pressures of water, methanol, acetonitrile, benzene and DMS at 20 ^{0}C are 18.66, 97.66, 70, 71 and 0.076 torr, respectively. Hydrogen sulfide was generated from the reaction between FeS and H_2SO_4. The vapor pressure inside the sealed chamber after complete reaction is estimated to be 0.027 torr. DNA 1, DNA 2, DNA 3 and DNA 4 were decorated on SWNT sensors and their responses to these vapors were measured and displayed on GUI interface.

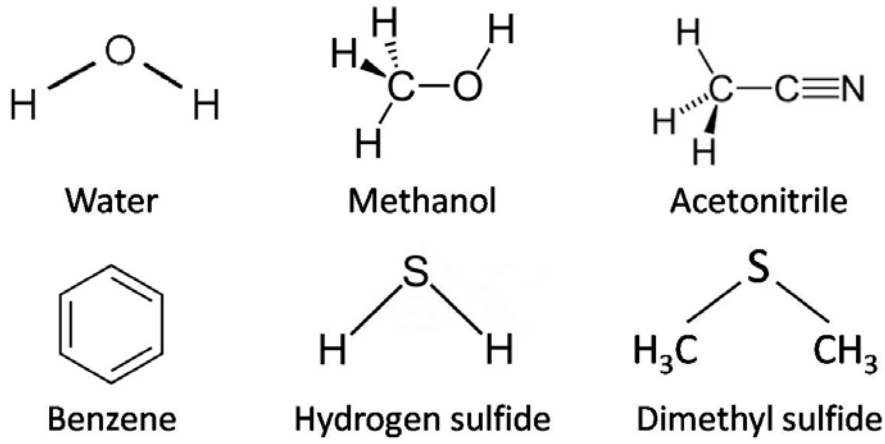

Fig. 4.8: The molecular structures of water, methanol, acetonitrile, benzene, hydrogen sulfide and dimethyl sulfide.

For each chemical, the response of DNA-SWNT sensor was confirmed using five different nanosensors decorated with the same DNA sequence. The average changes in resistance of DNA-SWNT sensor array after exposure to the chemical vapors for 10 minutes are organized in table 5.1 and plotted in Figure 4.9 for comparison. For methanol and water which are polar molecules and have similar structures, the responses of DNA-SWNT sensor array have the same trend (the red and pink curves in Figure 4.9). However, since methanol is more volatile and has a higher vapor pressure at room temperature, the

changes in resistance of the DNA-SWNT array in response to methanol (the red curve in Figure 4.9) is higher than the changes in resistance of nanosensor array when exposed to water (the pink curve). The trend in the response of the nanosensor array to acetonitrile vapor was also similar to that of methanol vapor which was expected since acetonitrile was also a polar molecule and hydrophilic. But the changes in resistance of nanosensor array after exposure to acetonitrile were much smaller compared to the changes in resistance for methanol. This was possibly due to the nitrile group (C≡N) being not as hydrophilic as the hydroxyl group (O-H), thus the affinity of DNA to acetonitrile was not as strong as the affinity of DNA to methanol. As shown in Figure 4.9, DNA decorated nanosensor array barely responded to benzene and DMS (the black and green curve). As mentioned before, benzene and DMS are hydrophobic molecules which do not tend to adsorb on the DNA decorated SWNTs. Especially for benzene, DNA decorated SWNT sensors exhibited even smaller responses compared to bare SWNT sensors. For hydrogen sulfide, the response pattern was found to be different from all other vapors. The resistance of SWNT sensor decorated with DNA 1 decreased significantly when exposed to hydrogen sulfide gas. However, the resistances of bare SWNT sensor and SWNT sensors decorated with DNA 2, DNA 3 and DNA 4 all slightly increased when exposed to hydrogen sulfide gas. This unique response of DNA 1 decorated SWNT sensor to hydrogen sulfide could be used to differentiate hydrogen sulfide from other vapors.

Table 4.1: Responses of DNA-SWNT sensor array to the gases/vapors of benzene, methanol, acetonitrile, water, dimethyl sulfide and hydrogen sulfide at room temperature.

	SWNT	SWNT-DNA 1	SWNT-DNA 2	SWNT-DNA 3	SWNT-DNA 4
Benzene	7.1 ± 2.7	6.7 ± 2.8	6.79 ± 3.1	6.64 ± 3.0	5.21 ± 0.7
Methanol	14.9 ± 5.0	24.0 ± 3.1	17.72 ± 1.9	23.09 ± 1.2	31.10 ± 5.2
Acetonitrile	10.2 ± 2.9	13.2 ± 3.6	10.09 ± 4.0	9.85 ± 1.0	10.50 ± 2.6
Water	6.4 ± 2.8	17.1 ± 1.4	8.44 ± 2.5	10.09 ± 2.9	8.48 ± 2.5
Dimethyl sulfide	4.3 ± 0.9	7.2 ± 1.6	6.18 ± 1.4	4.91 ± 1.9	5.35 ± 1.6
Hydrogen sulfide	6.8 ± 1.6	-8.2 ± 0.7	7.61 ± 1.2	9.26 ± 4.3	7.90 ± 1.5

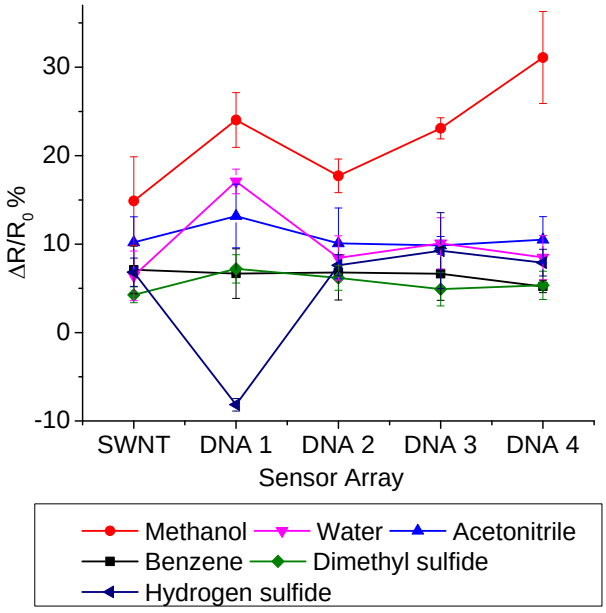

Fig. 4.9: The changes in resistance of DNA decorated SWNT sensor array under exposure to methanol, water, acetonitrile, benzene, dimethyl sulfide and hydrogen sulfide vapors.

In conclusion, a wireless nanosensor array using ssDNA decorated SWNTs was designed and fabricated. The SWNT sensors displayed reversible and repeatable changes in their response during exposure to methanol vapors. The results indicate that the nanosensor array can find use in real-time, highly sensitive and rapid monitoring of gases/vapors. The nanosensor array decorated with four different DNA sequences were tested with six types of vapors with different properties. The results indicated that DNA increased the affinity of SWNTs to hydrophilic molecules which was due to the surface properties of SWNTs being altered from hydrophobic to hydrophilic by the DNA decoration. In addition, DNA 1 decorated SWNT sensor exhibited different behavior (decrease in its resistance) compared to other type of SWNT sensors when exposed to hydrogen sulfide gas. This showed a great potential to distinguish hydrogen sulfide gas from other vapors by DNA 1 decorated SWNT sensor. Measuring the responses from six different DNA functionalized SWNT sensors simultaneously and analyzing the response pattern will allow one to selectively detect various gases and vapors. This sensing unit provides an attractive platform for various kinds of nanosensor arrays for chemical and bimolecular detection.

CHAPTER 5

CARBON NANOTUBE SENSING SYSTEM FOR ENVIRONMENTAL MONITORING

The detection of concealed explosives and chemical warfare agents is an urgent need to protect the safety of people and cities around the world. This requires the development of highly sensitive, portable and stand-off sensors. Here, I present a wireless sensing unit based on single-walled carbon nanotubes (SWNTs) integrated with complementary metal oxide semiconductor (CMOS) circuitry, which can effectively detect trace explosives and chemical agents. The response of SWNT sensors to Dinitrotoluene (DNT) (a byproduct of TNT) and Dimethyl methylphosphonate (DMMP) (an analog of nerve agent sarin) vapors were improved dramatically after decoration with single stranded-DNA (ss-DNA). The response of carbon nanotube sensors to DNT and DMMP vapors were reversible and repeatable. The nanosensors integrated on a CMOS chip were tested with DMMP (DNT) vapors with concentrations varying from 1.57 to 130.49 ppm (9.41 to 45.73 ppm) and the corresponding change in resistance of the SWNT sensor varied from 7.5% to 27.5% (6.53% to 22.76%). The detected signal was processed by off-chip components on a circuitry board and was transmitted wirelessly to a computer. This versatile sensing

system provides a promising platform to detect explosives and chemical agents at a trace level in a wireless manner and stand-off distance.

5.1 INTRODUCTION

DNT is well known as a precursor of trinitrotoluene (TNT) and is considered to be a toxic material, while DMMP is a chemical weapon conventions schedule 2 chemical used in the synthesis of nerve agent sarin. Detecting trace amount of these chemicals will provide an early warning for terrorist attacks. The major challenge in detecting explosives and chemical agents is that their vapor pressures are extremely low at room temperature. Vapor pressure of TNT is 4.8×10^{-6} torr at 20 ºC [212] and that of DMMP is less than 0.1 torr at room temperature [2]. The most common techniques for the detection of explosives and chemical warfare agents at a trace level include gas chromatography (GC) [213], mass spectrometry (MS) [214] and ion mobility spectrometry (IMS) [215]. The inspection and identification procedures typically include collecting vapors or particles from the chemicals and analyzing them in a laboratory with large sensing systems. However, direct sampling of chemical agents and explosives is likely to be lethal if conducted under an uncontrolled environment. In addition, these testing equipments are bulky, expensive and require long procedures and skilled operators. Thus, these equipments are only deployed at a few specific locations, such as the airport and government buildings. In order to effectively prevent threats of explosives and chemical agents, a highly sensitive, miniature, autonomous and low cost sensing system which can be mass produced and widely installed in any hidden locations is urgently needed.

SWNT, as a quasi-1D material, is composed of a rolled-up graphene sheet with a single atomic layer. The SWNTs can be used as the sensing materials, because their electrical properties are extremely sensitive to the adsorption of molecules on their surfaces and they have very fast response. The detection of gases and organic vapors down to ppb levels using carbon nanotubes has been reported [38, 216]. The response time of SWNT sensors to 1% hydrogen gas was found to be around 1.5s [165]. In addition, SWNT sensors exhibit high sensitivity at room temperature, whereas most conventional metal oxide thin film gas sensors require high operating temperatures (200ºC-400ºC) to maintain their sensitivity [14].

Thin films of zinc oxide are shown to detect 1 ppm ammonia gas at a working temperature of 350 ºC whereas they did not have any response at room temperature [217]. Due to these attractive properties, SWNT sensors are excellent candidates for detecting explosives and chemical warfare agents at trace levels. Several carbon nanotube based sensors have been developed and applied for the detection of explosives [218, 219] and chemical warfare agents [220-222]. Moreover, most of these sensors require off chip components to detect the variations in the signals which makes them bulky, complicated and not portable.

Here, I present a novel CMOS integrated SWNT nanosensor as a highly sensitive, highly compact and miniature sensing system for the detection of explosives and chemical warfare agents (Figure 5.1). The nanosensor is composed of ssDNA functionalized SWNTs integrated with custom designed operational amplifiers on a CMOS chip. Building nanotube sensors directly on CMOS circuitry provides a single chip solution and eliminates the need for long parasitic lines and numerous wire bonds. Decorating ssDNA with select sequence onto SWNT sensors increased their response by three times. The DNA-SWNT sensors on a CMOS chip were next mounted on a Printed Circuit Board with signal processing and wireless transmission components to realize an independent, autonomous and portable sensing system for ubiquitous detection of explosives and chemical warfare agents from a distance. This sensing system was shown to detect various concentrations of DNT and DMMP vapors at room temperature.

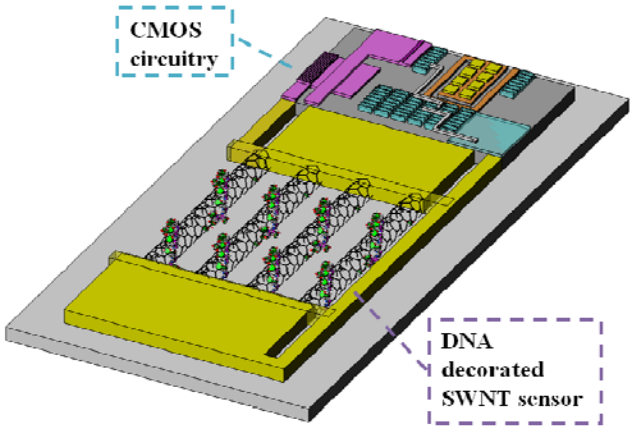

Fig. 5.1: Schematic illustration of DNA-SWNT sensor integrated with CMOS circuitry.

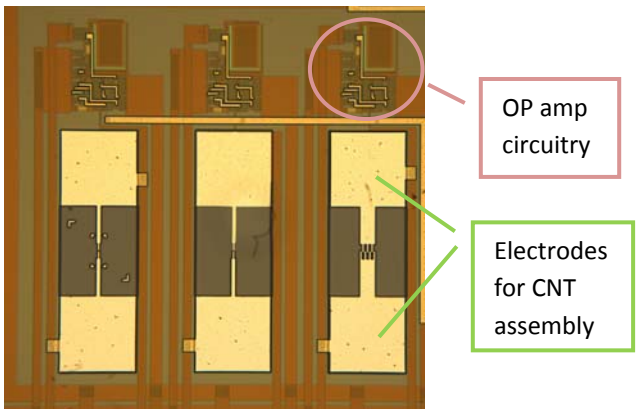

Fig. 5.2: Optical photograph of the CMOS chip.

5.2 FABRICATION PROCESS

5.2.1 POST CMOS PROCESS

CMOS chips with custom designed microelectrodes were fabricated by AMI semiconductor through the MOSIS (0.5 µm process). The photograph of the microelectrodes connected with op amp circuitry is shown in Figure 5.2. Electrodes with and without connecting to operational amplifiers on the CMOS chip were designed to demonstrate CMOS integration. The gap was kept at a minimum distance (0.5 µm) to reduce the voltage (< 5 volts) for DEP assembly which allowed direct integration of SWNTs onto the CMOS amplifiers without damaging the circuit.

Double zincation process has been used to remove aluminum oxide, deposit zinc and prevented the underlying aluminum from getting reoxidized before performing the assembly process. This low cost wet chemical process, called electroless plating, is capable of depositing a uniform and conformal layer onto microelectrodes with various shapes and geometries [220].

5.2.2 DIELECTROPHORETIC (DEP) ASSEMBLY

SWNTs were assembled onto CMOS chips by a room temperature, solution based DEP process. A commercial SWNT (diameter: 1~2nm; length: 2~5µm) solution was diluted with DI water to form a 0.004

g/ml suspension. 2µl of this SWNT suspension was dispensed on to the Zn coated electrodes and an AC signal of 5 V_{pp} at 10 MHz was next applied to the electrodes for 1 minute. The excess SWNT solution was dried with compressed air. The resistances of assembled SWNTs were around 30 KΩ.

5.2.3 DNA FUNCTIONALIZATION

Ss-DNA nucleotide (Invitrogen) with the following sequence has been reported to improve the response of SWNTs to DMMP and DNT vapors dramatically [143] and was utilized to functionalize SWNTs in this work:

DNA: GAG TCT GTG GAG GAG GTA GTC

The DNA powder was diluted in DI water to create a solution of 100 µM. 5µl of this DNA solution was applied on to the SWNTs assembled between the microelectrodes on the CMOS chip for 1h in a chamber with saturated humidity.

5.3 RESULTS AND DISCUSSIONS

5.3.1 SWNT NANOSENSOR ASSEMBLED ON A CMOS CHIP

SEM micrographs in Figure 5.3 show that the SWNTs were successfully assembled between the microelectrodes on a CMOS die. They formed suspended bridges and each of these bridges was comprised of several SWNT bundles. The amount of SWNTs assembled between the electrodes was found to depend on the applied voltage, frequency and time. After DEP assembly, the CNT connections between the microelectrodes were confirmed by SEM imaging and I-V measurements.

Next, DNA was decorated on to the SWNTs. We have found that following DNA decoration, the two-terminal resistance of the carbon nanotubes increased which was consistent with what had been reported by other groups [145, 185]. Since SWNTs are p-type semiconductors in the ambient environment and DNA is a negatively charged molecule, the increase in resistance might due to the holes inside the nanotubes being partially compensated by the charges on DNA molecules.

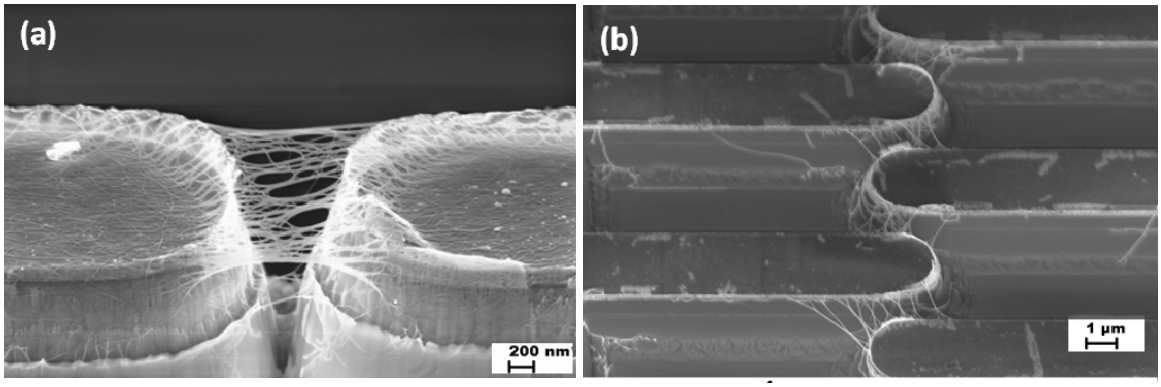

Fig. 5.3: SEM images of SWNTs assembled between (a) single finger and (b) multi-finger microelectrodes on a CMOS chip.

5.3.2 DMMP DETECTION

We utilized the DNA functionalized SWNT nanosensor on a CMOS chip to detect DMMP vapors with various concentrations (1.57, 14.21, 49.61, 72.05 and 130.49 ppm). Different concentrations of DMMP vapors were generated by diluting the DMMP solutions with the dipropylene glycol (DPG) solution. Prior to using DPG as the diluting solution, the response of bare SWNT and DNA-SWNT nanosensors to pure DPG vapor was tested and no significant response was observed. Thus, we believe that the change in resistance of nanotubes is purely caused by the DMMP vapors.

The change in resistance of bare SWNT and DNA-SWNT nanosensors on a CMOS chip during exposure to DMMP vapors and air were plotted versus time in Figure 5.4. The resistance of SWNTs assembled on multi-finger electrodes was measured during exposure to DMMP vapors and refreshed in ambient environment. The exposure time was 40 minutes for DMMP vapors and 20 minutes for air. Upon exposure to a DMMP vapor with a concentration of 1.57 ppm, the resistance of nanotube sensor increased instantly and dramatically, and then reached a stable value within a few minutes. Since DMMP is a non-volatile chemical, it took about 10 minutes for DMMP molecules to evaporate from the solution and aggregate on carbon nanotubes. For the bare SWNT sensor, the change in resistance ($\Delta R/R_0$) was found to be 2.5% when exposed to 1.57 ppm DMMP vapor. For ssDNA functionalized SWNT sensor, the change in resistance was 7.5% which showed a 3 times increase compared to a bare SWNT sensor. We

observed that DNA decoration enhanced the surface affinity of SWNTs to DMMP vapors dramatically (by three times).

After DMMP exposure, the nanosensor was refreshed by exposure to air where the resistance of the SWNTs recovered fairly quickly as shown in Figure 5.4. We also noticed that full desorption of DMMP from the SWNT sensors in the ambient environment may take up to 40 minutes. However, this can be expedited by heating the sample in a 40 ºC oven.

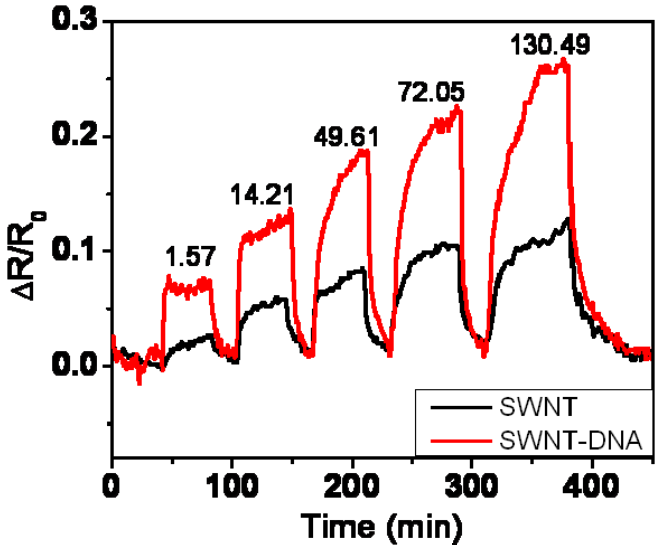

Fig. 5.4: The change in resistance ($\Delta R/R_0$) of bare and DNA functionalized SWNT sensors to different concentrations of DMMP vapors (1.57, 14.21, 49.61, 72.05, 130.49 ppm) vs. time. The experiment was conducted with SWNT nanosensors assembled on multi-fingered electrodes on a CMOS chip.

The change in resistance of bare SWNT sensor and DNA-SWNT sensor vs. the concentration of DMMP vapors was plotted in Figure 5.5. The response of the bare SWNT and DNA-SWNT sensors was increased as the concentration of DMMP vapors was increased. Following the increase in the concentration of DMMP vapors from 1.57 ppm to 130.49 ppm, the change in resistance of a bare SWNT sensor was found to increase from 2.5% to 11.6%, whereas the change in resistance of DNA-SWNT sensor was observed to increase from 7.5% to 27.5%. Due to the electrical noise of the SWNT sensor

[223-225], the detection limit of bare SWNTs is about 1ppm. We believe that after DNA decoration, the sensitivity of the SWNT sensors can be lowered to ppb level.

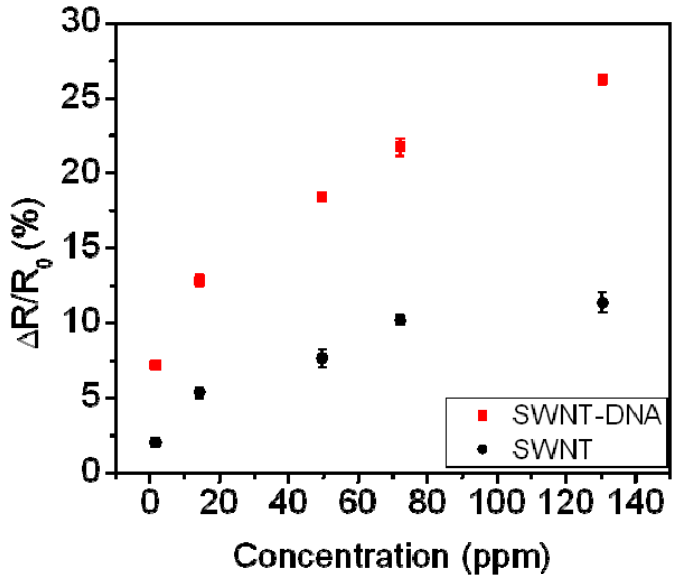

Fig. 5.5: The measured change in resistance of SWNT sensors (black dots) and DNA-SWNT sensors (red dots) vs. concentration of DMMP vapors.

A series of measurements consisted of exposing the bare SWNT and DNA-SWNT sensors to 150 ppm DMMP vapor followed by a refresh cycle in air were conducted and a typical response from 2 cycles is shown in Figure 5.6. The resistance of the SWNT sensors increased by the same amount when exposed to 150 ppm of DMMP vapor and returned to their initial values after removing the vapor source as the adsorbed vapor molecules dissociated in air. Thus, the response of both bare and DNA decorated SWNT sensors was reversible and repeatable. This experiment was repeated five times with three different samples to confirm the measurements.

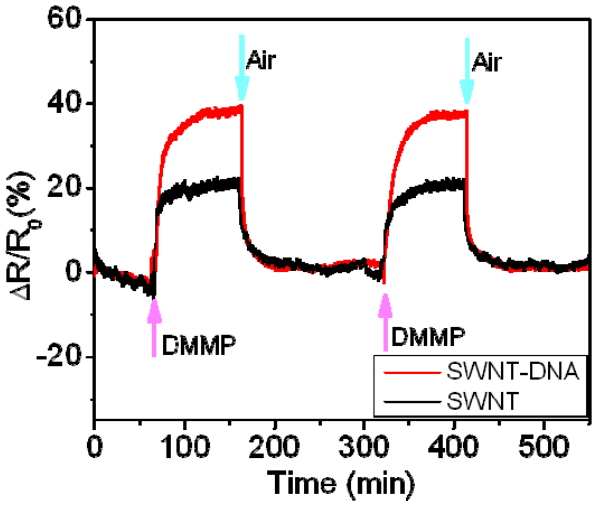

Fig. 5.6: The change in resistance ($\Delta R/R_0$) of SWNT and DNA-SWNT sensors assembled on multi-finger electrodes when exposed to 150 ppm DMMP vapors.

5.3.3 DNT DETECTION

DNT, a byproduct of TNT can be used as the signature product of TNT. DNA decorated SWNT sensors integrated on multi-finger electrodes were next used to detect DNT vapor at a concentration of 46 ppm. Here, the DNT vapor was also generated from a DNT solution using DPG as the solvent. Bare SWNTs have insignificant response to DNT vapor (< 5%). The resistance of DNA decorated SWNT sensor after exposure to DNT vapor was measured directly from the electrodes and plotted versus time in Figure 5.7. The resistance of the DNA-nanotube sensor was stable in air and started to increase after exposure to DNT vapor. Since the vapor pressure of DNT is very low (less than 1 torr) at room temperature and the partial pressure of DNT became even lower after mixing with DPG, it took about 20 minutes for DNT molecules to evaporate from the solution and aggregate onto the DNA decorated nanotubes. Accordingly, the resistance of DNA-SWNT sensor continued to increase for several minutes and finally reached a stable value. The change in resistance of DNA-SWNT sensor to 46 ppm DNT vapor was around 28%.

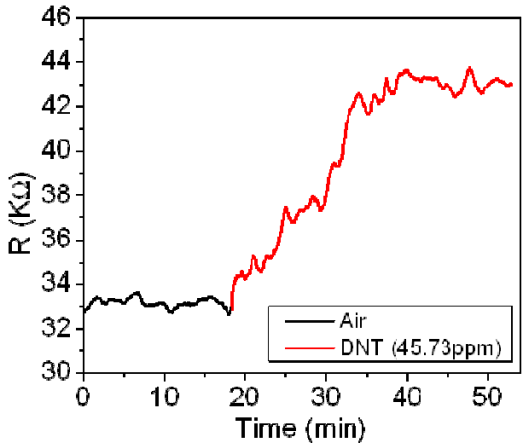

Fig. 5.7: The response of DNA decorated SWNT sensor to 46 ppm DNT vapor.

So far, all the data were acquired by directly measuring the resistance of SWNTs from the microelectrodes on the CMOS chip. Next, we measured the response of nanosensors to DNT vapors via on chip op-amp circuits to demonstrate the integration and performed the measurements on a PCB board with signal acquisition and wireless transmission units (Figure 5.8). The SWNT sensors were connected in the feedback path of the custom designed operational amplifier on the CMOS chip in an inverting configuration where the gain was defined as the ratio between the resistance of nanotubes and the resistance of external resistor. By monitoring the gain of the amplifier and using an external resistor with a known value (20 KΩ), we were able to calculate the resistance of the SWNT sensor during exposure to chemical vapors.

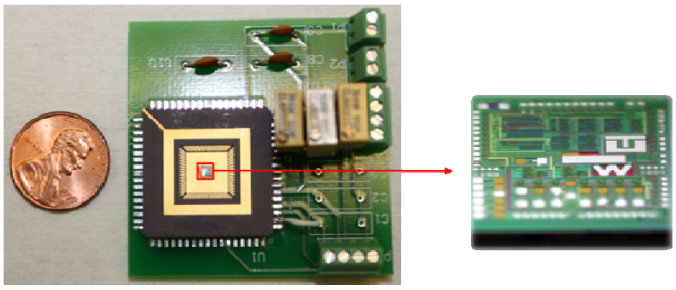

Fig. 5.8: Photograph of the CMOS chip containing SWNT nanosensors mounted on a PCB board with components for signal processing.

The nanosensor connected to an operational amplifier on the CMOS chip was first exposed to air and then exposed to DNT vapor (with a concentration of 46 ppm). The stabilized output voltages of the op-amplifier after exposure to air and DNT vapor for 20 minutes were plotted with the input voltage in Figure 5.9. The output voltage corresponding to air is shown by the blue curve and the output voltage of the amplifier after exposure to DNT vapor is shown by the red curve, respectively. The change in resistance calculated from the measured gain of amplifier after exposure to DNT vapor (46 ppm) was about 23%.

The DNA wrapped SWNT sensor on multi-finger electrodes connected to the op-amp circuitry on the CMOS chip was then exposed to five different concentrations of DNT vapors: 9 ppm, 19 ppm, 28 ppm, 37 ppm and 46 ppm. The Input and output voltages of the amplifiers after exposure to different concentrations of DNT vapors were then measured and plotted in Figure 5.10a. Here we changed the concentration of DNT vapors from 9 ppm to 46 ppm and found that the gain of the amplifier increased from 1.68 to 1.93. Using the measured gain of the operational amplifier, we calculated the change in resistance of the DNA-SWNT sensor in response to DNT vapors and plotted the results in Figure 5.10b. The resistance of the DNA-SWNT sensor increased dramatically after the sensor was exposed to 9.41 ppm of DNT vapor and kept increasing as the concentration of DNT vapor was increased. It was observed that the change in resistance of nanosensors was almost linear with the concentration of DNT vapors ranged from 0 to 40 ppm.

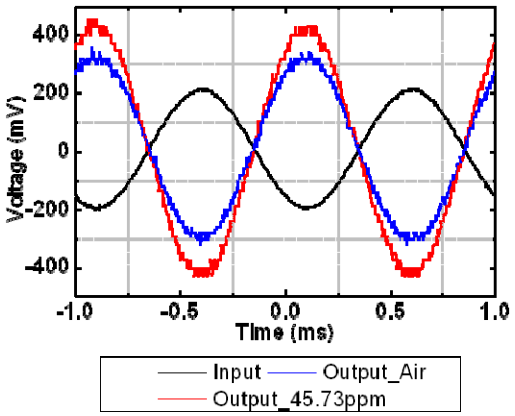

Fig. 5.9: The measured input and output voltages of CMOS op-amp with SWNT as the feedback resistor measured before and after exposure to 46 ppm DNT vapor.

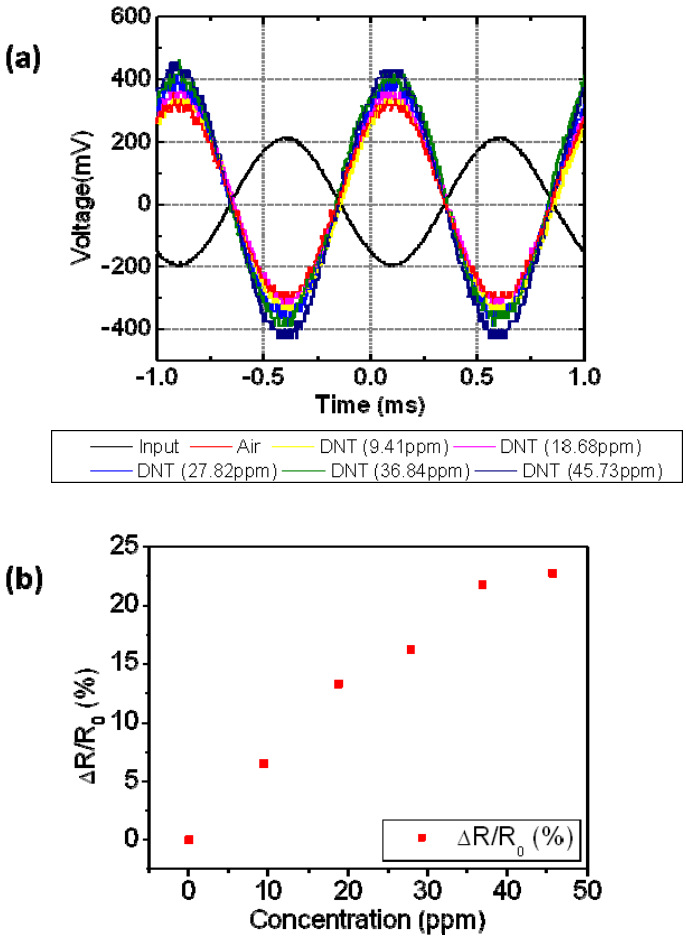

Fig. 5.10: (a) Measured output voltages of the on-chip amplifier with SWNT sensor assembled in the feedback path when the concentration of DNT vapor was changed from 0 to 45.73 ppm. (b) The relative change in the resistance ($\Delta R/R_0$) of an SWNT sensor corresponding to DNT vapors with concentrations of 0, 9.41, 18.68, 27.82, 36.84 and 45.73 ppm was plotted (red dots).

After testing with DNT vapors, the SWNT sensor was exposed to air at room temperature. We observed that the sensor recovered to its initial value after 2 hours, which indicated that the DNT molecules were completely desorbed from the surface of the carbon nanotubes. Repeated cycling data showed that the sensing response was reversible and repeatable. We measured this five times with three different samples (data not shown) and found that the sensing results were consistent. We also found that full desorption of DNT vapors from the SWNT sensors was achievable in 20 minutes by heating the tested sample in a 40°C oven.

5.3.4 SIGNAL PROCESSING AND WIRELESS TRANSMISSION

The signal acquisition and wireless transmission process for nanosensors are schematically illustrated in Figure 5.11. The CMOS chip with SWNT sensors was mounted onto a PCB board with signal conditioning, A/D converter, micro controller and connected to a wireless transmission board.

The CMOS chip mounted on a PCB board is shown in Figure 5.8 and the corresponding readout circuitry was schematically illustrated in Figure 5.12a. The gain of the amplifier is set by the ratio of the resistance of the SWNTs to the external reference resistor and can be obtained from the measured output voltage, using equation 4-1. Thus, the change in environmental conditions resulted in a change in the resistance of the SWNTs which was calculated by the measured gain of the operational amplifier.

$$Gain = -R_{SWNT} / R_{External} = -V_{out} / V_{in} \quad (4\text{-}1)$$

The wireless transmission was conducted using the ZigBee protocol (with a frequency of 2.4 GHz) which is a low-cost, low-power and wireless mesh network standard (Figure 5.12b). Its lower cost allows the technology to be widely deployed in wireless control and monitoring applications; its low power-usage allows a longer life with smaller batteries; and its mesh networking option provides high reliability and extended range.

A RF receiver module was directly connected to a PC through a USB port and enabled us to obtain data continuously from the transmission module. Acquired data were real-time monitored, plotted and

stored for further analysis by a Graphic User Interface (GUI) developed in LabWindows/CVI (Figure 5.12c). This platform enabled on-chip communications between the CMOS chip and the computer and enabled the implementation of a compact and portable CMOS integrated nanosensor.

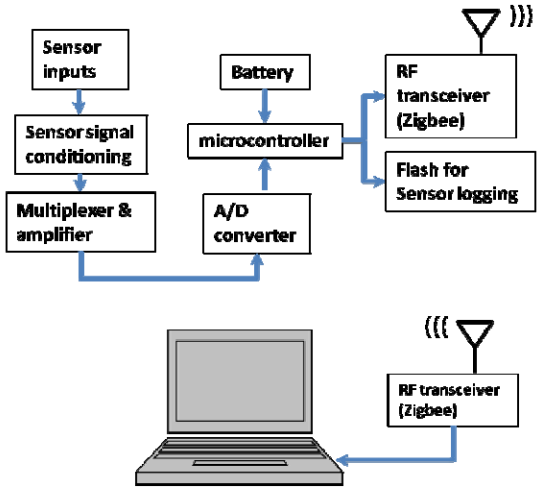

Fig. 5.11: Schematic illustration of the signal acquisition and wireless transmission process for nanosensors.

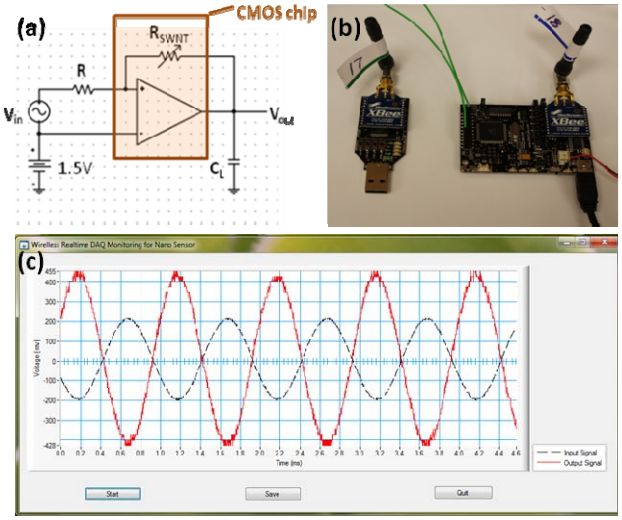

Fig. 5.12: (a) The readout circuitry for the SWNT sensors integrated on a CMOS chip. (b) Photograph of the ZigBee wireless transmitter and receiver. (c) Screen capture of the input and output voltages displayed on GUI interface.

I demonstrated a CMOS integrated, miniature, portable and stand-off nanosensing system for explosive and chemical agent monitoring. DNA decoration improved the response of SWNTs to DMMP vapors by 300%. The nanosensors (bare and DNA decorated) were integrated with custom designed operational amplifiers realized using a CMOS foundry process. The response of SWNT sensors measured directly from the microelectrodes agreed with the response taken from the custom designed op-amp circuitry on the CMOS chip. The resistance of the DNA-SWNT sensors measured from the electrodes on CMOS chip increased by 28% and the gain of the amplifier measured from the output voltage increased by 23% after exposure to 46 ppm of DNT vapors. The change in resistance of nanotubes or the gain of amplifier was proportional to the concentration of the input analytes. The nanosensors on CMOS chip were mounted on a PCB board with all the components for signal processing. The detected signal was transmitted wirelessly to a computer and displayed by a GUI interface. Our results illustrate the possibility of using biological molecules decorated onto SWNTs integrated on a compact conventional printed circuitry board for wireless detection of explosives and chemical warfare agents. With suitable functionalizations of SWNTs, this wireless CMOS integrated sensing platform has a great potential to be extended for the detection of other gases and vapors.

CHAPTER 6

INTEGRATION OF CNT SENSORS ONTO A MICROFLUIDIC CHIP FOR WATER QUALITY MONITORING

Water pollution has a tremendous impact on the ecosystem and human health. It is critical to real-time monitor the water quality, especially the pH, toxic chemicals and excess nutrients in aquatic environments in a low cost manner. Here I introduce a highly sensitive, fast response and miniature sensing device composed of SWNT nanosensors integrated inside a microfluidic chip. This sensing device was mounted on a circuitry board with signal processing and wireless transmission capabilities which was aimed to realize a remotely controlled sensor for real-time water quality monitoring. Two novel and efficient approaches were developed to integrate nanotube sensors with the microfluidic chip. First, SWNTs can be assembled in solution by Dielectrophoretic (DEP) process through the microfluidic system after bonding the chip with microfluidic chip. Second, the SWNTs can be assembled on microelectrodes and then protected by a parylene mask during plasma treatment before bonding the microfluidic channel. The SWNT sensors were characterized with different pH buffer solutions and showed a linear response as the

pH values changed from 5 to 8. In addition, the sensing system was demonstrated for detecting toxic organics. The resistance of the SWNTs was increased from 60 KΩ to 105 KΩ when the concentration of Trinitrotoluene (TNT) in water was increased from 1 to 100 ppm. This nanosensor incorporated within the microfluidic chip is a versatile platform and can be utilized to detect various chemicals or biomolecules with low concentrations in aqueous solutions.

6.1 INTRODUCTION

Perturbations in water have significant impact to human health and the ecological equilibrium. Environmental pollutions, such as increased nutrients, industrial wastes, toxicants and algal bloom outbreaks can lead to mass mortalities in fish, seabirds and may cause potential human illnesses. Traditional water quality evaluation is conducted by on-site sampling or data collection followed by transport to a laboratory for testing. This procedure is costly, time consuming and requires skilled operators. Besides, the testing results can only represent the water quality at specific time and location of sampling. Water quality needs to be monitored in a fast, inexpensive and efficient manner. Adequately figuring out the factors which influence water quality requires real-time water evaluation and data acquisition. Recent developments have a trend toward continuous data collection by in situ detectors [226]. In this chapter, I report an in situ sensing system composed of SWNT sensor integrated with microfluidic system and a circuitry board with signal processing and wireless transmission capabilities for real time water quality monitoring.

Carbon nanotubes with high aspect ratio, large surface area and unique electrical properties have great potential in chemical and biological sensing applications [57, 227]. Nanotube based sensors exhibit fast response (less than 5 seconds in response to pH buffers [228]), high sensitivity (down to 20 ppb in response to DMMP in water [229]) and miniature size. As a one dimensional nanomaterial composed of single atomic layer, SWNTs are extremely sensitive to chemical and environmental conditions and the conductance of SWNTs will change dramatically when exposed to a low concentration of ions and

molecules in a liquid. Various SWNT sensors have been developed and utilized for liquid analysis, including pH value [228], heavy metal ions [230], toxic organics [229], bacteria [231] and virus [232].

Microfluidics as an emerging technology is being intensively applied in chemical, biological and medical analysis. It offers numerous attractive features such as the abilities to use small amount of samples or reagents; carry out sample separations and detections with high resolution and sensitivity; lead to significant reduction in cost per analysis; replace the batch analysis into continuous flow analysis; and has small footprints for the analytical devices [233]. Especially, in bioanalysis, microfluidic systems are able to manipulate and examine samples containing a single cell or single molecule [234]. With specific design, newer capabilities have been achieved by the microfluidic systems in the control of the droplet volume, chemical concentrations within the droplet and sorting of droplets based on flow pattern [235]. Integration of microfluidic systems with a SWNT sensor will enable the development of a lab-on-a-chip device which performs water quality monitoring that is normally done in a lab manually with bulky equipments. With suitable design, the microfluidic system is able to filter and separate various components in a liquid sample and then guide them into multiple nanosensors for analysis.

To develop a highly sensitive, autonomous and in situ microdevice for real-time monitoring of water quality, the integration of the microfluidic system with the nanosensor is the most critical and challenging step. Permanent bonding of the microfluidic channel onto microdevices on the silicon substrate includes an oxygen plasma treatment and a thermal treatment. However, the plasma treatment on SWNTs will damage the nanotubes immobilized on the microelectrodes. Qiang and colleagues integrated a SWNT device with a microfluidic channel by covering the SWNTs with a continuous metal layer which protected the nanotubes underneath during exposure to oxygen plasma. After bonding the SWNT device with the microfluidic channel made of polydimethylsiloxane (PDMS), an etching solution was introduced through the channel to open a gap in the middle of the metal layer, so that the SWNTs inside the microfluidic channel can be exposed and utilized for sensing applications [236]. However, this integration process will introduce contamination to SWNTs from the etching solution and the substances generated

by chemical reactions. Bourlon and colleagues fabricated a flow and ionic sensor using a nanotube transistor covered with a PDMS channel without the oxygen plasma treatment [237], in this work, the microfluidic channel did sealed properly on the devices which would hence result in leakage of solutions during testing.

I developed two simple, high yield and effective processes to integrate SWNT sensors with microfluidic chip. A schematic illustration of the nanotube-microfluidic sensor is presented in Figure 6.1. The integrated nanosensing unit was further mounted on a custom-designed circuitry board with signal processing and connected to a wireless transmission board. The detection of two important water quality indicators (pH and toxic organic chemicals) was demonstrated by the sensing system.

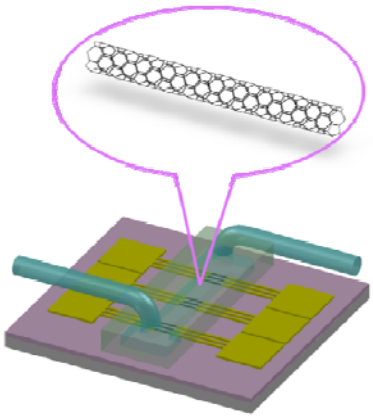

Fig. 6.1: The schematic illustration of the lab-on-a-chip nanosensor for water quality monitoring.

6.2 FABRICATION PROCEDURE

Microelectrodes composed of 20 nm Cr and 150 nm Au layers were fabricated by photolithography and metal deposition on an oxidized silicon wafer (Figure 6.2a). PDMS slab embossed with a microfluidic channel was cast using SU-8 replica molding which was created by photolithography [238]. Then two approaches were developed to permanently seal the SWNT sensor with microfluidic chip. The first approach is schematic illustrated in Figure 6.2. The microdevice with Au electrodes and the

microfluidic channel were exposed to oxygen plasma for 30 seconds and then placed them in contact for the bonding process conducted on a hot plate at a temperature of 150 ^{0}C for 15 min (Figure 6.2b). Two holes were punched with a syringe needle on the microfluidic chip. After inserting the tygon tubes (Small Parts, Inc.) to the holes, the commercial SWNT (diameter: 1-2 nm and length: 2-5 μm) solution (from Brewer Science) with a concentration of 40 mg/L was injected to the microfluidic channel by a syringe and covered the tip of the electrodes. An AC field of 5 V_{pp} and 300 kHz was applied between the two electrodes for 1 min and the SWNTs were assembled between Au electrodes by a low temperature, solution based DEP process inside the microfluidic channel (Figure 6.2c). After assembly, the remaining SWNT solution inside the microchannel was removed by injecting air into the channel. Carbon nanotubes were immobilized on Au electrodes by Van der Waals forces (Figure 6.2d). I-V measurement was conducted to confirm the assembly of SWNTs through the microfluidic system by DEP process (the resistance is around 10 kΩ~20 kΩ).

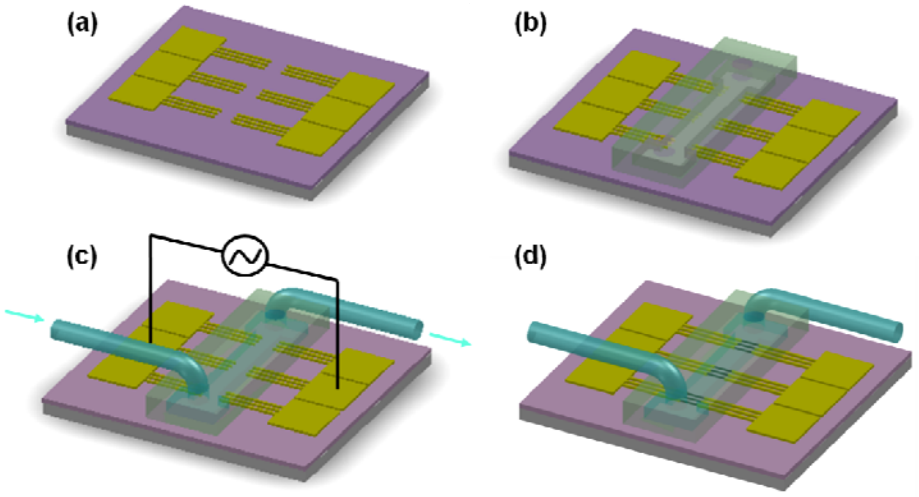

Fig. 6.2: Fabrication process for integrating SWNT sensors inside a microfluidic channel. a) Au microelectrodes fabricated by photolithography on SiO_2 substrate. b) Microfluidic channel was bonded onto the Si chip. c) The illustration of the DEP process for CNT assembly conducted inside microfluidic channel. SWNT solution was carried to the Au electrode by the microfluidic channel and an AC electric field was applied on outside Au pads to driven the assembly of nanotubes. d) The fabricated SWNT nanosensors integrated with the microfluidic chip.

In the second approach, the nanotubes were first assembled between the microelectrodes by the DEP process. The assembled SWNTs were then protected by 10 μm thick parylene mask (fabricated according to Selvarasah et. al. [239]) during the oxygen plasma treatment. The SEM images of SWNTs assembled on microelectrodes before and after the plasma treatment under parylene mask were compared in Figure 6.3a and 6.3b, respectively. Carbon nanotubes were attached onto the microelectrodes (the bottom circular shaped pad) and stretched to the SiO_2 substrate (the top area). They formed suspended bridges between the electrode and the substrate and each of these bridges was comprised of several SWNT bundles (Figure 6.3a). No damage was observed on SWNTs after plasma treatment in Figure 6.3b which indicated that the assembled SWNTs remained intact during oxygen plasma treatment with the protection of 10 μm parylene mask. After removing the shadow mask, the SWNT sensors were bonded with a microfluidic channel on a 150 ^{0}C hot plate for 15 min. I-V characteristics of SWNTs were obtained and shown in Figure 6.4. We found that the resistance of SWNTs decreased from 14KΩ to 11KΩ after bonding with the microfluidic channel on a 150 ^{0}C hot plate. This was possibly due to the contact resistance between assembled SWNTs and metal electrodes being reduced by the thermal treatment [240].

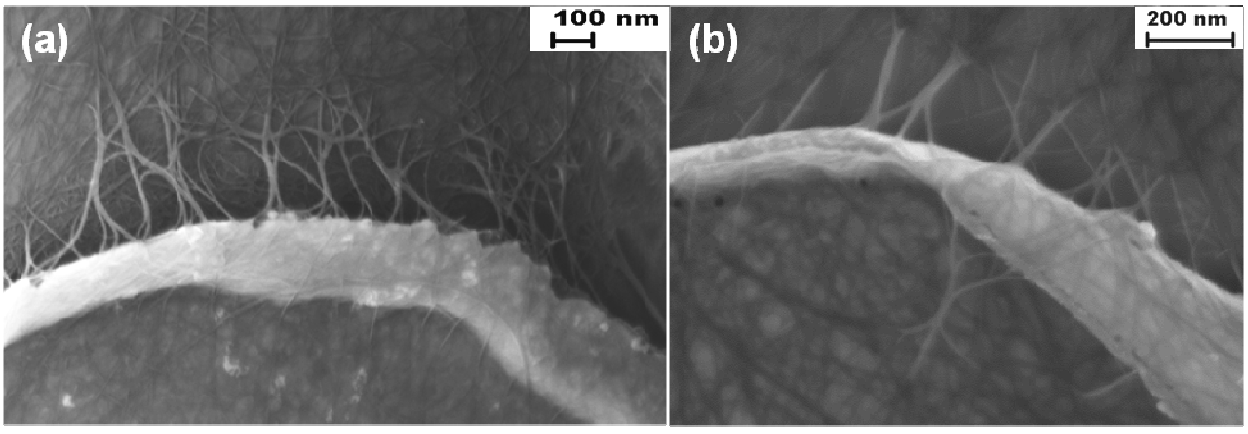

Fig. 6.3: SEM micrograph of SWNTs assembled on Au microelectrodes. (a) Nanotube bundles immobilized on the electrodes after DEP assembly. (b) SWNTs on electrodes after exposure to the oxygen plasma covered with parylene shadow mask. The coverage of the SWNTs with a parylene layer successfully protected nanotubes from being damaged by the plasma treatment.

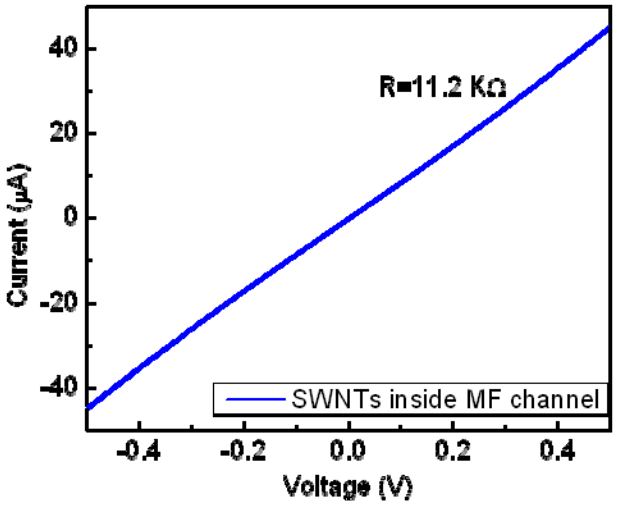

Fig. 6.4: I-V characteristics of the SWNT sensor integrated inside a microfluidic channel.

The fabricated device was next wire bonded onto a ceramic chip holder. As shown in Figure 6.5a, SWNT sensor integrated with the microfluidic chip was mounted on a circuitry board by the chip holder for signal conditioning (the corresponding circuitry was schematically shown in Figure 6.5c). The change in resistance of the nanosensor caused by the analytes in liquid was converted and transmitted by the change in output voltage, where the resistance of carbon nanotubes (R_{SWNT}) was related to the output voltage by equation 6-1 and R_{SWNT} can be calculated by equation 6-2:

$$\frac{R_{SWNT}}{R_{SWNT}+R}=\frac{V_{out}}{V_{cc}} \tag{6-1}$$

$$R_{SWNT}=R\times\frac{V_{out}}{V_{cc}-V_{out}} \tag{6-2}$$

Where, R_{SWNT} is the resistance of the SWNT sensor; R is an external reference resistor (10 KΩ); V_{out} is the output voltage and V_{cc} is the voltage of the power supply.

A wireless sensing platform (Waspmote) was used to acquire the output voltage and wirelessly transmitted the data to a remote receiver which was directly connected to a computer as shown in Figure 6.5b.

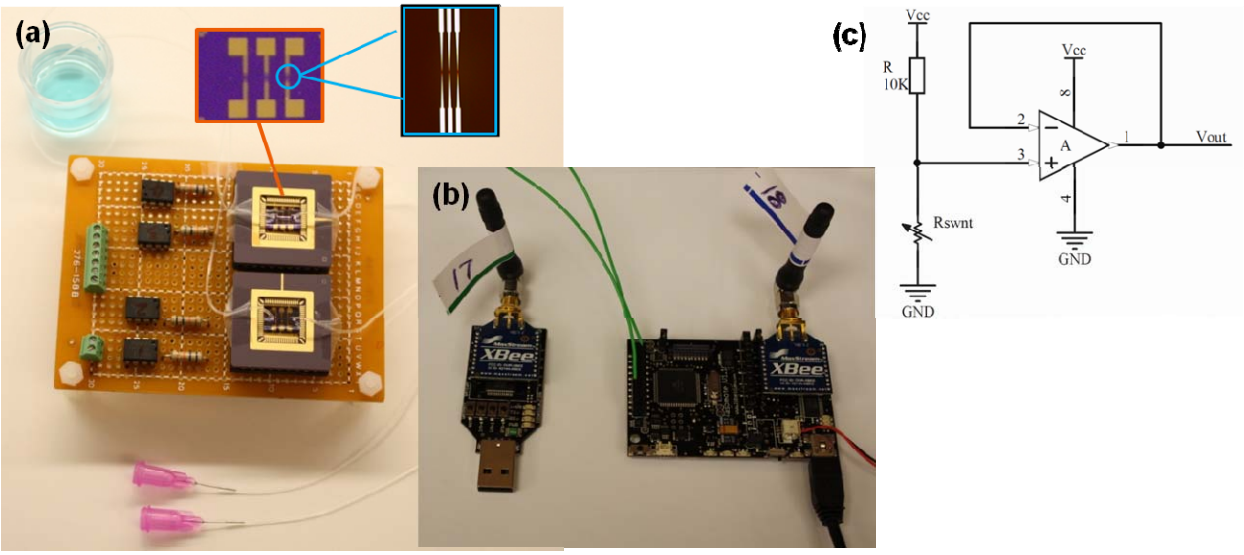

Fig. 6.5: Photographs of (a) the testing board and (b) the wireless transmission system. (c) Schematic illustration of the testing circuitry for the SWNT sensor. The insert in (a) illustrated the pattern of the chip and the structure of Au electrodes.

6.3 RESULTS AND DISCUSSION

6.3.1 REAL-TIME PH MONITORING IN WATER

The fabricated nanosensor system was utilized for pH detection in water. PH value in rivers and lakes may be changed by many human activities including automobile exhaust (related to acid rain), accidental spills, agricultural runoff and sewer overflows. Young fish and insect larvae are sensitive to a low pH (acidic environment) and extreme values of pH can be lethal to most organisms. Monitoring pH value in water is critical to preserve the aquatic life. The expected pH range in rivers is between 6.5 and 9.0 [241]. PH buffers with the values of 5, 6, 7 and 8 were prepared and calibrated by a commercial pH meter (Hach, company). Only the effect of ions/molecules within the Debye-length can be sensed by SWNTs. Debye length is simply defined as the typical distance required by surrounding charged molecules to be

sensed by charge carriers inside carbon nanotubes and is inversely proportional to the square root of ionic strength (I) in liquid [242]. In water, Debye length is ~$0.32I^{-1/2}$ nm. In order to keep the same Debye length of SWNTs inside the pH buffer solutions, the ionic strengths of the pH buffer solutions were controlled to be 100mM.

The output voltage of the nanosensor system during pH testing was recorded in a computer wirelessly and converted back into the resistance of nanotubes using equation 6-2. In Figure 6.6, the resistance of SWNTs was plotted versus time when the testing liquid was changed from pure DI water to an increasing range of pH solutions and from a decreasing range of pH solutions to pure DI water. The resistance of SWNT sensor increased from 50.26 kΩ to 61.54 kΩ when the pH values inside the microfluidic channel increased from 5 to 8. Besides, the forward measurement (pH values from 5 to 8) exhibited an opposite trend compared to the backward measurement (pH values from 8 to 5) which indicated that the response of SWNT to pH solution was reversible and repeatable. After testing with each pH solution, the SWNT sensor was rinsed with DI water thoroughly and dried with compressed air. The resistance of washed SWNTs in the dry state basically returned to their initial value after each pH test, which implied that the SWNT sensor was able to maintain its stability during liquid sensing. Moreover, the changes in resistance of the SWNT sensor during exposure to different pH buffers were calculated and plotted in Figure 6.7. The response of the nanotube sensor is almost linearly proportional to the pH value of the solution inside the microfluidic channel.

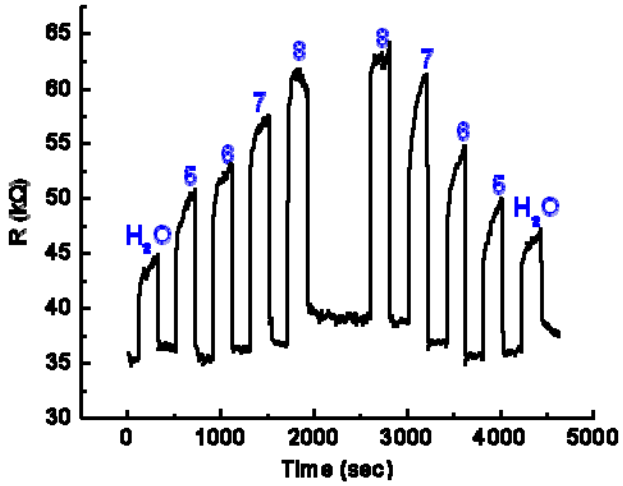

Fig. 6.6: The resistance of SWNTs after exposure to water and different pH buffers. The sensor was rinsed with DI water and dried with air before introducing each pH solution. The resistance dropped back to the initial value after rinsing and drying which meant that the nanotubes were stable during pH sensing.

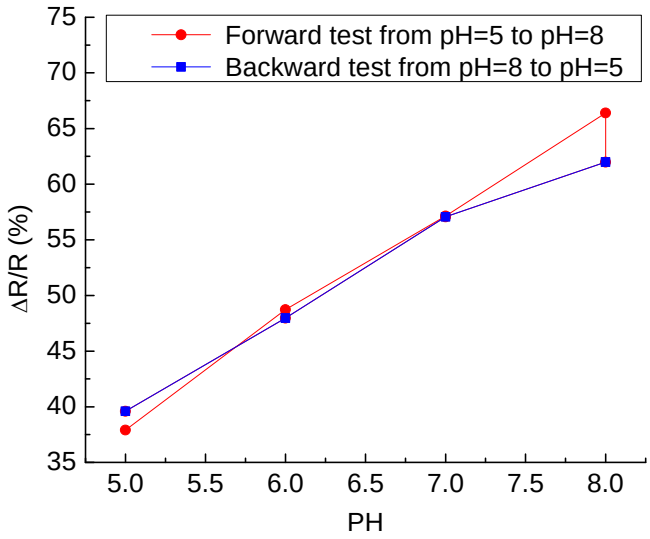

Fig. 6.7: Percentage change in resistance of the carbon nanotube sensor measured in pH buffer solutions ranged from 5 to 8 and from 8 to 5. The forward testing (from pH=5 to pH=8) is plotted with red round dots and the backward testing (from pH=8 to pH=5) is plotted with blue square dots.

Using the microfluidic system, the SWNT sensor was utilized for real-time liquid monitoring in a continuous flow. The resistance of the SWNT sensor was recorded against time when the solution inside the microfluidic channel was changed to different pH buffers. As shown in Figure 6.8, the resistance of

the carbon nanotube sensor increased from 5.55 kΩ in DI water to 7.27 kΩ after exposure to pH8 buffer solution (the change in resistance was about 31%). When the pH7 buffer was introduced into the channel, the resistance of the nanotubes gradually decreased to 6.85 kΩ. As the pH value of the solution decreased, the resistance of the SWNT sensor decreased immediately and reached a stabilized value within a few seconds. The response of continuous pH sensing has the same trend as the data plotted in Figure 6.6. In addition, this real time measurement showed that the response time of the SWNT sensor to pH value of liquid was less than 10 seconds. All the measurements were repeated three times with five different samples to confirm the results.

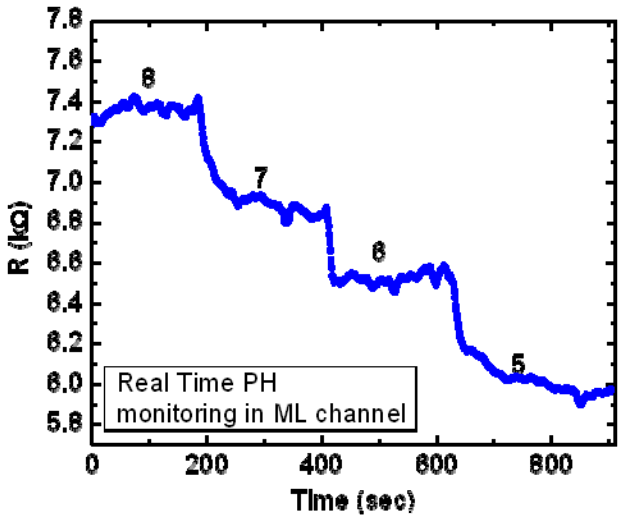

Fig. 6.8: Responses of the SWNT sensor inside the microfluidic chip to continuous liquid flow with different pH values. The solution was continuously changed with pH buffers from 8 to 5 via the microfluidic system. This test confirmed that the system can be used for real-time pH monitoring of liquids.

6.3.2 Detecting TNT in Water

The sensing unit composed of SWNTs integrated with the microfluidic system and the circuitry board with signal processing and transmission capabilities is a versatile platform which can be used for various sensing applications. TNT is the most widely used explosive and is discharged in wastewater during production and purification at munition plants [243]. TNT was detected in soil and water nearby

production waste disposal sites and the loading, assembly, and packing facilities [244, 245]. TNT and its byproducts or derivatives can accumulate in plants and can enter the food chain in terrestrial environments [246]. Humans exposed to TNT tend to experience anemia and abnormal liver functions [247]. Here we utilized the fabricated microfluidic-SWNT sensor to detect TNT with various concentrations in aqueous solutions. Commercially available TNT solution with a concentration of 1mg/ml was obtained from Sigma-Aldrich. Different concentrations of TNT solutions were prepared by diluting the TNT solution with DI water. The resistance of the SWNT sensor during exposure to different concentrations of TNT solutions was measured and is plotted in Figure 6.9. We observed that the SWNTs had a dramatic response to TNT in solution and the change in resistance depended on the concentration of TNT. The change in resistance of the nanosensor increased from 25% to 119% when the concentration of TNT in water increased from 1 ppm to 100 ppm. The response of microfluidic-SWNT sensor to TNT was confirmed independently by three different samples.

The solvent of a commercial TNT solution is composed of 70% acetonitrile and 30% water due to the limited solubility of TNT in pure water. When we diluted this TNT solution with DI water, the concentration of acetonitrile was also diluted. Thus a control experiment with different concentrations of acetonitrile in DI water was conducted and it was found that the SWNT sensor had no significant response to acetonitrile in water. The increase in resistance of the SWN sensor when exposed to TNT solutions was caused by TNT. Since acetonitrile is extremely volatile in air, it will evaporate from the TNT solution and the dissolved TNT will precipitate during testing, especially for highly concentrated TNT solutions such as 50 ppm and 100 ppm. As illustrated in Figure 6.9, the resistance of the SWNT jumped to a high value and then gradually decreased after being exposed to a 100 ppm TNT solution for a few minutes. This phenomenon is consistent with what has been observed by Roberts, et. al. [229]. For TNT solutions with low concentrations (up to 20 ppm) which contain relatively more water solvent and less TNT in them, no TNT precipitation was observed and the response of SWNTs was stable during testing.

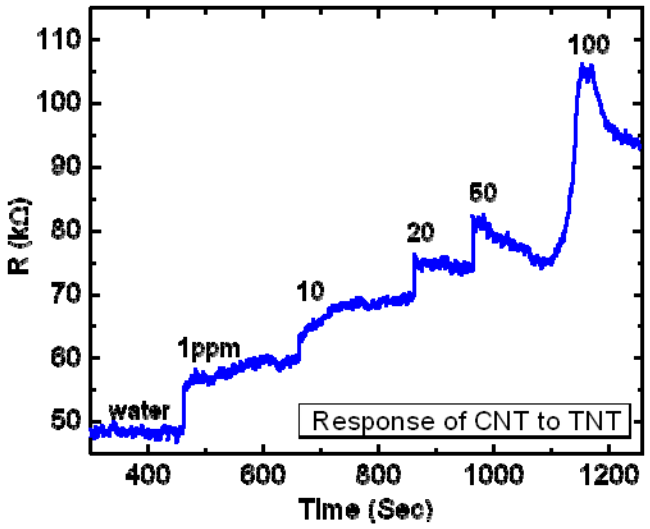

Fig. 6.9: Response of SWNT nanosensor inside a microfluidic channel to different concentrations of TNT solutions.

In conclusion, A remote sensing unit based on the integration of carbon nanotube sensor with microfluidic system for water quality monitoring was demonstrated. SWNT sensor has many superior properties compared to conventional sensing equipment such as high sensitivity, fast response and miniature size. With a microfluidic system used for liquid sampling and manipulation before testing, SWNT sensor can be utilized for autonomous water quality monitoring. The challenge in nanosensor and microfluidic integration is that the plasma treatment used during PDMS bonding will damage the carbon nanotubes on the microdevices. In order to solve this problem, we developed two approaches, assembling SWNTs via DEP process after bonding the microfluidic channel and protecting the assembled SWNTs with a parylene mask before bonding the channel, to integrate the SWNT sensor inside the microfluidic chip. The SWNT-microfluidic sensor was characterized with different pH buffers and a linear relationship between the response of the nanosensor and the pH value of solutions was observed. The sensing results to pH buffers were reversible and repeatable. This sensor platform can be further extended to monitor toxic organics in water. The conductance of the SWNT sensor increased significantly by the addition of TNT in water where the detection limit was down to 1 ppm. Connecting with a signal processing and

wireless transmission unit, the SWNT sensor was developed as an independent sensing unit with a small size which can be placed in rivers or lakes and can be easily installed on various water transportation systems, such as household drains and pipes for real time water quality monitoring.

CHAPTER 7

A STRETCHABLE, FLEXIBLE AND TRANSPARENT SWNT STRAIN SENSOR FOR STRUCTURAL HEALTH MONITORING

There is a growing interest to apply emerging technologies for structural health monitoring. Carbon nanotubes as a unique nanoscale material provide a low cost and simple approach to monitor large stain and cracks in a variety of structural systems. Here a stretchable, flexible and transparent strain sensor composed of single-walled carbon nanotube (SWNT) thin film embedded in thin poly(dimethylsiloxane) (PDMS) films was introduced. The fabricated SWNT networks encapsulated in elastomeric substrates operate as two-terminal resistors which can accommodate up to 35% strain and the amount of strain can be monitored by the change in resistance of SWNT strain sensor. The thickness of the PDMS thin film was 200 μm and was able to extend up to 100% with the elastic modulus of 1.5 MPa. The fabricated SWNT strain sensor was tested with strain ranging from 0.5% to 35% and the change in resistance of SWNT network was monitored during the testing. The electrical response linearly increased with the

applied strain (up to ~5%). Since the nanotubes are extremely sensitive to environmental gases, we encapsulated the CNT strain sensors by coating another 200 μm thick PDMS film on top which eliminated the effect of humidity to SWNTs. The reliability of this sensor was tested with 200 cycling tensile measurements and a linear, repeatable and reversible response of SWNTs to 4% strain was obtained. Our results demonstrate the possibility of using ultrathin SWNT film encapsulated in thin PDMS films as a stretchable, flexible and transparent strain sensor for structural health monitoring.

7.1 INTRODUCTION

Structures, such as bridges, buildings, dams, pipelines, aircraft, ships, are complex engineered systems that ensure society's economic and industrial prosperity [248]. However, structures are often subject to harsh environmental conditions which will result in long-term structural deterioration [249]. It is critical to monitor the structural health for public safety. Structural monitoring systems have been widely applied for monitor the behavior and damages of structures during forced vibration testing or natural excitation, such as earthquakes, winds and live loading [250-252]. Among the monitoring systems, strain sensors have been intensively developed and applied for strain and crack detection in structures for civil and mechanical systems [253-255]. Emerging technologies might provide a new approach to monitoring large strain in structures using a strain sensor with high stretchability and reliability. There is growing interest in making sensors, optoelectronic and electronic devices on flexible and stretchable substrates [256-261]. Even though flexible devices are being explored for some applications, the stretchable devices are not fully studied. Stretchability allows us to realize sensors and devices that can conform and stretch at the same time. Stretchable electronics is an emerging paradigm where researchers use inorganic materials with special structures [262-264] or thin organic films [265, 266] as the stretchable electronics or substrates. Choi et. al. configured 100 nm silicon membrane into a "wavy" structure on elastomeric substrate and the resulting construct can undergo 10% ~20% strain which is 10 to 20 times of the fracture limit of silicon [262]. Kim et. al. achieved stretchable electronics by using buckled, arc-shaped silicon ribbons as the interconnects [264]. This mesh designed structure,

which only bonds on PDMS substrate at the nodes, can move freely out of the plane to accommodate applied strains. Individual aligned SWNTs were transferred onto prestrained (3%~5%) PDMS substrate and formed a "wavy" structure after releasing the prestrain. This mechanically buckled, SWNTs on elastomeric substrate has been applied for up to 4% strain measurements [263]. Some stretchable materials including conductive polymers [266], thin metal films [267] and polymers with conductive dopants [265, 268] were also explored for stretchable electronics.

Carbon nanotubes (CNTs) with their exceptionally high carrier mobility, substantial mechanical strength and unique electromechanical properties are promising materials for the development of novel strain sensors. The conductance of an individual SWNT is extremely sensitive to structural deformation and the electrical response of a nanotube to bending or stretching is reversible and repeatable [29, 269, 270]. Ultrathin film of SWNTs is composed of randomly orientated, entangled CNT network which has superior robustness in terms of bending, stretching and abrasion. In addition, SWNTs can be dispersed in many solvents and deposited easily onto a wide variety of substrates with different shapes or sizes. Thus ultrathin films of SWNTs can be mass produced and cost-effectively scaled to large areas by printing techniques [271, 272]. Recently, Takeo and collaborators have developed a SWNT based strain sensor by stacking multiple SWNT thin films into a highly densely package nanotube mattress and applied the sensor for detecting human motion [261].

Here I report on a flexible, stretchable and transparent strain sensor using ultrathin films of SWNTs as the functional materials. I use the drop casting process to assemble SWNTs onto PDMS substrate and demonstrate a SWNT thin film based stretchable strain sensor embedded in PDMS thin films (Figure 7.1). PDMS thin film is a biocompatible, conformal, flexible and stretchable polymer and is a suitable candidate for the substrate of stretchable electronics. In this work, the effect of strain on the electrical properties of SWNT networks is investigated. In particular, the level of strain, the effect of encapsulation and the device repeatability are studied.

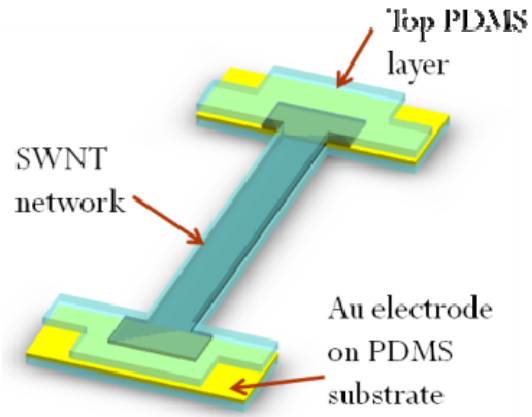

Fig. 7.1: Schematic structure of the encapsulated SWNT strain sensor on the PDMS substrate.

7.2 EXPERIMENTAL PROCEDURES

7.2.1 FABRICATION PROCESS

The fabrication processes of encapsulated SWNT strain sensor in PDMS thin films are schematically illustrated in Figure 7.2. The silicon wafer was first spun coated with a lift off resist (LOR 30B) to make the surface hydrophobic and to reduce the adhesion force between the PDMS thin film and the silicon substrate [273]. This made the fabricated device on PDMS substrate easier to be peeling off from the silicon wafer. PDMS prepolymer was mixed with its curing agent with a ratio of 10:1 by weight (Sylgard 184 elastomer from Dow Corning). The mixed PDMS solution was degassed in vacuum to remove the bubbles inside and then spun coated onto silicon wafers with a speed of 500 rpm for 60 seconds (Figure 7.2a). The spin coated PDMS layers on silicon wafers were cured in a 70 °C oven for 2 hours. The thickness of PDMS films was measured to be 200 μm [274]. 30 nm Cr/150 nm Au electrodes were selectively deposited on the PDMS thin film with a 1mm thick PDMS shadow mask (Figure 7.2b). After lifting off the shadow mask, the PDMS thin film with Au electrodes were roughened by an oxygen plasma generated by the inductively coupled plasma (Plasmatherm 790) reactor. This step increased the hydrophilicity of PDMS thin film and improved the spread of SWNT solution on PDMS substrate. Commercial SWNTs (diameter: 1~2 nm and length: 2~5 μm) dispersed in DI water was sonicated for 2

hours to enhance debundling of the SWNTs. The SWNT solution was drop casted onto the roughened PDMS substrate and dried in air for 2 hours, as shown in Figure 7.2c. The dried SWNT network was attached onto the polymer substrate by a strong van der Waals force [261, 263]. Then another PDMS layer with the thickness of 200 µm was spin coated on top to encapsulate the nanotube network and cured in the 70 °C over for 2 hours (Figure 7.2d). The electrical contacts and excess PDMS layer on silicon wafer were cut by a knife and peeled off manually (Figure 7.2e).

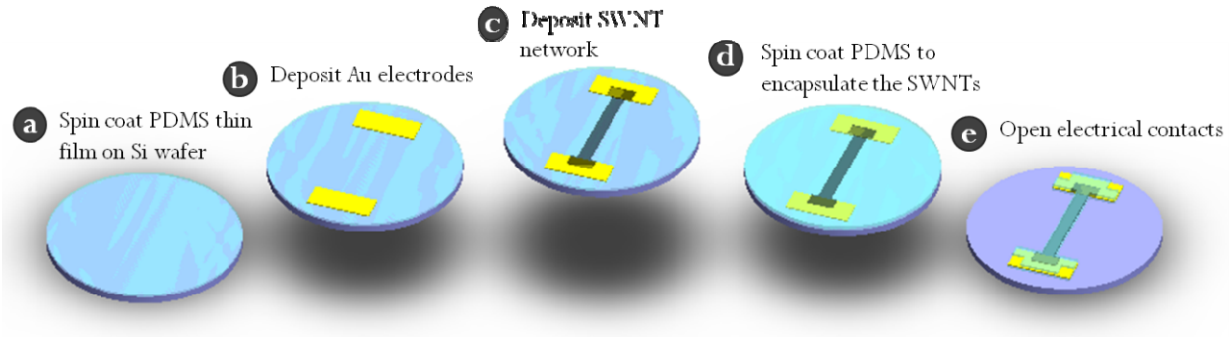

Fig. 7.2: Schematic illustration of the fabrication process for the SWNT strain sensor on a PDMS substrate.

7.2.2 EXPERIMENTAL PROCESS

After fabrication, the stretchable, flexible and transparent SWNT strain sensor was peeled off from the silicon wafer and was ready for mechanical testing. The structure and dimensions of the fabricated strain sensor are shown in Figure 7.3a. The sensing area of the "dog bone" structure is the middle 5mm × 40 mm rectangular area with a thickness of ~ 400 µm. The "dog bone" design will ensure the normal strain was confined in the sensing area when stretched from two ends of the sample [275]. Before testing, the Au pads at the ends of the "dog bone" shaped sample were glued with 250 µm thick cardboards to prevent slippage of the sample from the clamps [275]. The SWNT thin film embedded in PDMS layers is transparent and flexible as shown in Figure 7.3b and a SEM micrograph of the drop casted SWNT network is shown in Figure 7.3c.

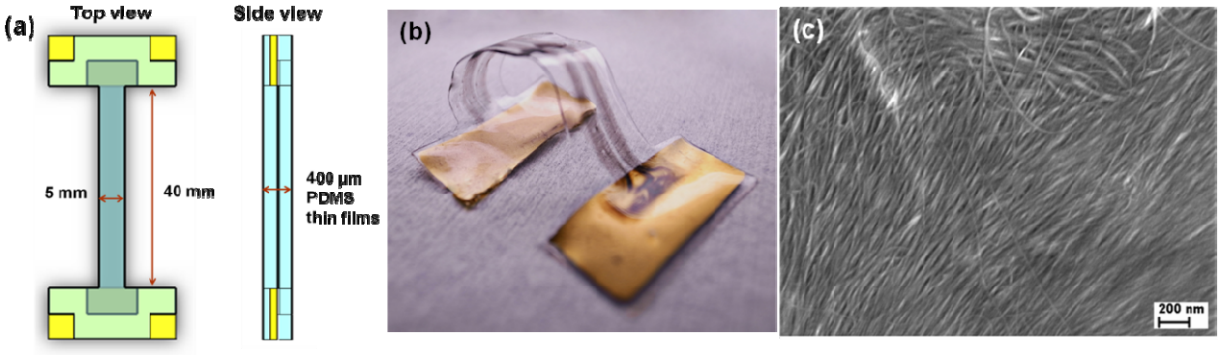

Fig. 7.3: (a) Schematic illustration of the structure and dimensions of the SWNT strain sensor. The testing area is 5mm × 40 mm with the thickness of 400 µm. (b) Photograph of the transparent, flexible and stretchable SWNT network embedded in thin PDMS films. (c) SEM micrograph of SWNT network drop casted on a PDMS substrate.

The tensile testing was conducted by a universal testing machine UMT-2 (CETR, Campbell, CA) in ambient environment. The fabricated SWNT strain sensor was tested with strains ranging from 0.5% to 35% and the change in resistance of SWNT network was monitored with a HP 34401A multimeter and was displayed by a control panel designed by a LabVIEW program.

7.3 RESULTS AND DISCUSSION

7.3.1 SMALL STRAIN MEASUREMENTS

First of all, the fabricated SWNT strain sensors encapsulated in PDMS thin films were applied for the detection of small strain (from 0.5% to 5%). The resistance of nanotubes was measured when the sample was loaded and unloaded with a small strain (ε) for three times and the stress applied on the strain sensor was recorded. In the Figure 7.4 (a), the change in resistance ($\triangle R/R_0$) was plotted versus time when 1% strain was linearly applied on the SWNT sensor at the rate of 0.02 mm/s. The change in resistance increased linearly with time during the loading process (red curve) and linearly decreased with time during unloading process (blue curve) which indicated that the electrical response of SWNT network to small strain is linear. Since the stress applied on the SWNT sensor was perfectly linearly with strain, the

electrical response of nanotubes to small stress was also linear. The gauge factor (GF) can be calculated by Equation 7-1 which was 0.71 for 1% strain.

$$GF = \frac{\Delta R / R_0}{\varepsilon} \tag{7-1}$$

Between each cycle, the sample was recovered to zero force for 30 seconds and the resistance of the nanotubes returned to their initial value (2.2 KΩ) immediately which indicated that the response of SWNT network to small strain is reversible and repeatable. The SWNT strain sensors were further tested with 0.5%, 1%, 1.5%, 2%, 2.5%, 3%, 4% and 5% strain. The changes in resistance of SWNT sensors during loading and unloading are plotted versus time in Figure 7.4 (b). I found that the response of nanotube sensor was almost linear with strains up to 5% during the loading and unloading processes. The resistances of the SWNTs returned to their initial values after unloading when the applied strain was less than 2.5%. When the strain was in range of 3% to 5%, the resistance of SWNT sensor is slightly higher than the initial resistance (increased by 0.2%). Thus I found that the elastic (linear) and reversible region of the SWNT strain sensor was around 5% strain. In this experiment, each testing was repeated three times to confirm the results. The linear, reversible and repeatable electromechanical response of SWNTs to small deformations (< 5%) might be due to the local bonding deformations of the nanotubes when elongated which changed the band gaps of SWNTs [29, 270, 276].

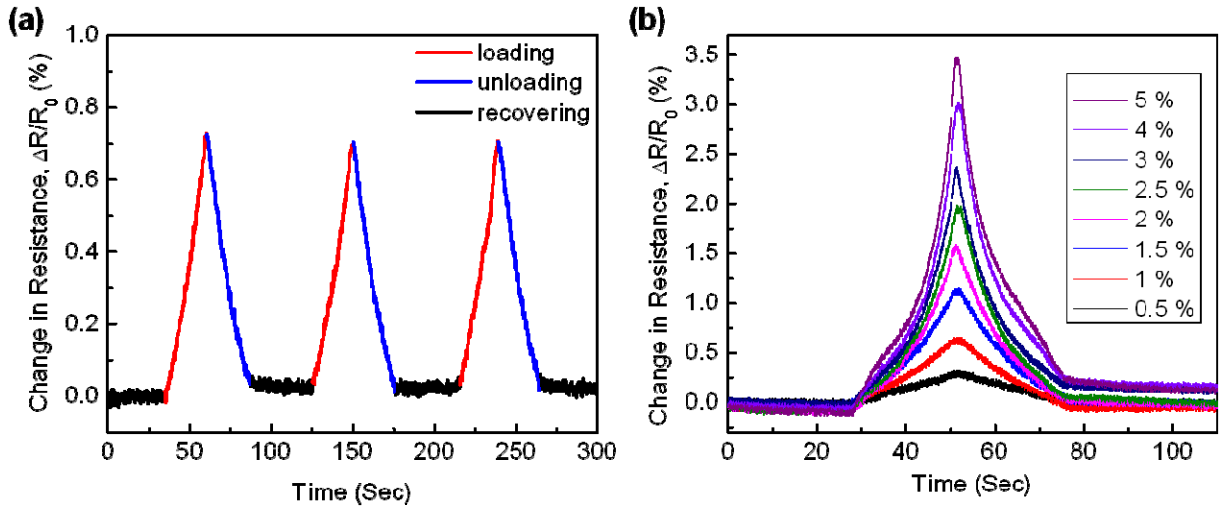

Fig. 7.4: (a) Three cycling measurements of the response of SWNT strain sensor to 1% strain. The change in resistance of nanotubes was plotted versus time. (b) The change in resistance of nanotube when loaded and unloaded with 0.5%, 1%, 1.5%, 2%, 2.5%, 3%, 4% and 5% strain.

7.3.2 Large Strain Measurements

Then, the encapsulated SWNT sensor was tested with a larger strain (10% strain) and the change in resistance during the first loading-unloading cycle was plotted versus strain in Figure 7.5. The loading curve has two linear regions (strain of 0 to ~4% and strain of 5~10%) with different slopes. From 1 to ~4% strain, the slope which represents the gauge factor of the SWNT sensor is about 0.53, while from 5% to 10% strain, the slope is about 6.14. In the unloading process, the resistance of nanotubes was unable to return to its initial resistance (2.83KΩ). This is possibly due to some irreversible deformation being generated in SWNT network by the large strain. I believe that some nanotubes in the network lost contact with others in response to large elongation. The resistance of the SWNT network increased significantly due to the reduced current path in the network [275-277].

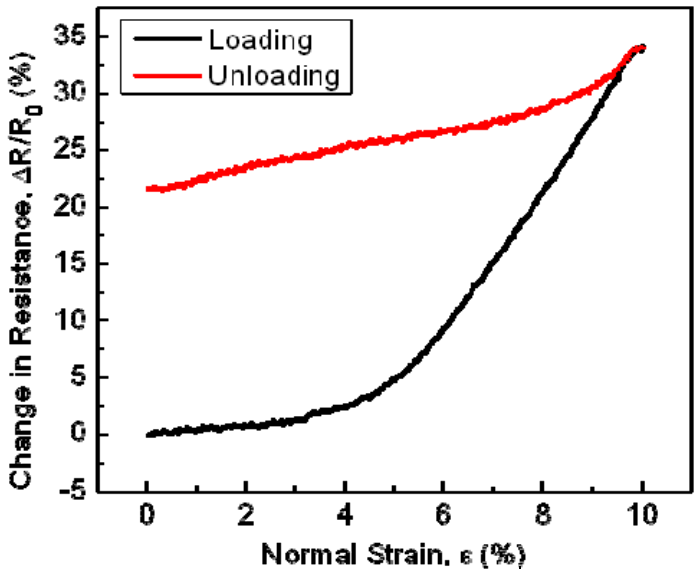

Fig. 7.5: The change in resistance of the SWNTs when loaded (the black curve) and unloaded (the red curve) with 10% strain.

I then increased the strain to 30% and recorded the stress applied onto the SWNT sensor and monitored the resistance of the SWNT network during tensile testing. The sensor was tested with a loading and unloading cycle for three times. The Stress-strain characteristics of the nanotube thin film embedded in PDMS thin films are plotted in Figure 7.6 (a). The stress-strain exhibited a small hysteresis between the loading and unloading curves. However, for multiple loading-unloading processes, the measured loading and unloading curves were basically overlapped with each others. Thus the stress-strain characteristics of SWNT network embedded in PDMS thin films were highly repeatable. The change in resistance of SWNTs when the sensor was loaded and unloaded with 30% strain for three times are plotted in Figure 7.6 (b). The resistance of the nanotubes could not return to its initial value after the first loading-unloading cycle which is consistent with the results obtained with 10% strain. However, the second and third loading-unloading curves almost overlapped with each other and there was a small hysteresis between the loading and unloading curve. I found that the electrical response of SWNTs to

larger strain was not reversible for the first loading-unloading cycle but was highly repeatable for the rest of the loading-unloading tests.

The stress vs. strain, change in resistance vs. strain, change in resistance vs. stress for the second loading with a 30% strain, which can be repeated by multiple testing, were plotted in Figure 7.6 (c), (d) and (e), respectively. The measured stress was shown by the black curve and the elastic range of the curve was linearly fitted by the red curve. The relationship between stress and strain was linear up to 18% strain with a slope of $0.014 \pm 6.27 \times 10^{-5}$. The electrical response of SWNTs to strain is plotted in Figure 7.6 (d) and the elastic region was linearly fitted by the red curve. The slope which represents the gauge factor of SWNT strain sensor was 1.18. The change in resistance almost linearly increased with the normal strain up to 5%. In Figure 7.6 (c), the change in resistance is plotted versus stress corresponding to 30% strain. In the range of 0~0.06 MPa stress (corresponding to 0~5% strain), the change in resistance almost linearly increased in a linear manner with the normal stress with a slope of 90.91. Thus this SWNT thin film based strain sensor can be utilized as a force sensor as well. I further increased the strain and found that this SWNT strain sensor was able to accommodate strain up to 35% and fractured at 40% strain.

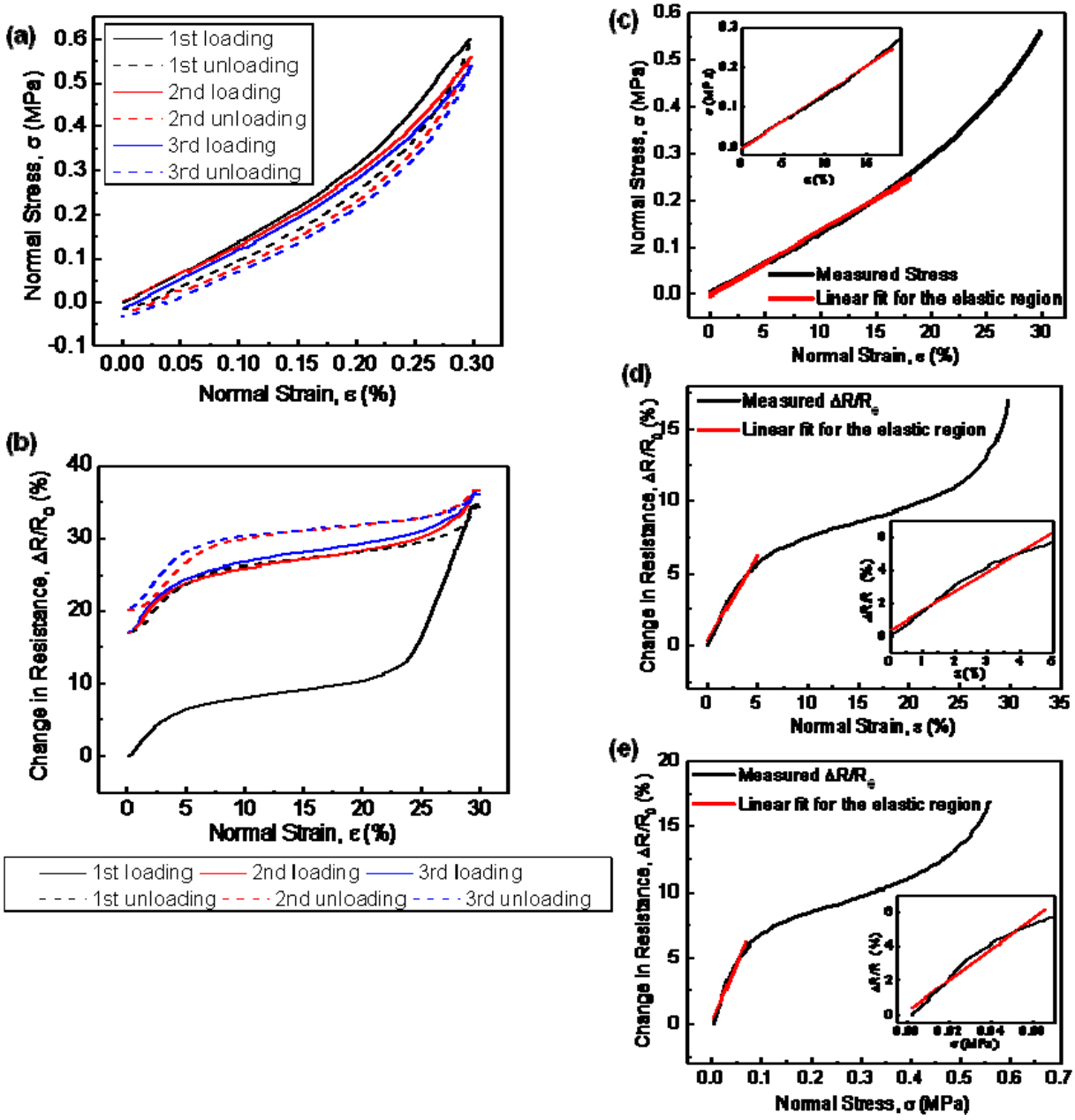

Fig. 7.6: (a) The stress-strain characteristics of SWNT strain sensor to three loading-unloading cycles with 30% strain. (b) The change in resistance of nanotube network when the strain was loaded and unloaded from 0 to 30% for three times. (c) The stress-strain characteristics of SWNT strain sensor to the 2nd loading with 30% strain. (d) The change in resistance of nanotube network when the strain was loaded from 0 to 30% for the 2nd time. (e) The change in resistance of SWNTs versus normal stress for the 2nd loading of 30% strain.

7.3.3 DEVICE ENCAPSULATION

The electrical properties of carbon nanotubes are sensitive to various environmental conductions including temperature and humidity [13, 278]. In addition, carbon nanotubes has been widely investigated for the detection of gases and vapors, such as hydrogen [279], methanol [280] and ammonia [281]. Thus encapsulating SWNTs is necessary to eliminate the effects of gases, vapors in the testing environment which can affect the measured response of SWNT strain sensors. I encapsulated the SWNT network on PDMS substrate with another PDMS thin film on top and compared the response of encapsulated SWNT strain sensor with nonencapsulated SWNT sensor to saturated moisture. As demonstrated in Figure 7.7 (a), the change in resistance of nonencapsulated SWNT sensor was about 20% when exposure to moisture, while the encapsulated SWNT strain sensor barely showed any response to moisture. This result indicates that covering SWNT network with thin PDMS film can effectively eliminate the sensitivity of nanotubes to humidity in ambient environment. The changes in resistance of encapsulated and nonencapsulated SWNT strain sensor are plotted versus strain in Figure 7.7 (b). The electro-mechanical behavior of the sealed nanotube sensor was very similar to that of unsealed strain sensor. In this case, the electrical response of nonencapsulated SWNTs to strain is slightly higher than that of encapsulated SWNTs which might due be to the variations between different samples.

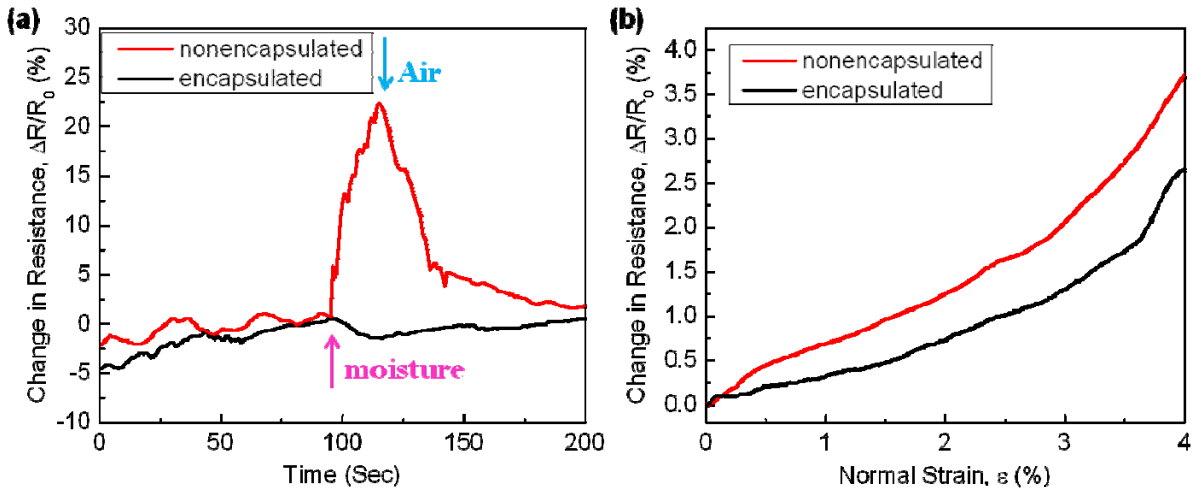

Fig. 7.7: (a) The change in resistance of the encapsulated and nonencapsulated SWNT strain sensors when exposed to saturated moisture. (b) The changes in resistance of the encapsulated and nonencapsulated SWNT strain sensors versus normal strain.

7.3.4 CYCLING MEASUREMENTS

Next, the reliability of the SWNT strain sensor was tested by performing cycling measurements for 200 times with 0~4% strain. The normal stress and the change in resistance as a function of normal strain for the 1st, 50th, 100th, 150th and 200th loading are compared in Figure 7.8. Despite a slightly larger electrical response to strain in the first loading, the changes in resistance of the 50th, 100th, 150th and 200th loading were very close and hysteresis-free. The relationship between the change in resistance of SWNTs and applied strain (up to 4%) for the 50th loading was fitted well with a three ordered polynomial function, $\Delta R/R_0 = -0.0244 + 0.5053\varepsilon - 0.207\varepsilon^2 + 0.0525\varepsilon^3$, as illustrated in Figure 7.8 (b). The normal stress during 200 cycling measurements was perfectly linear with the normal stain. Our results implied that SWNT thin film embedded in PDMS thin films maintained their performances during extended testing.

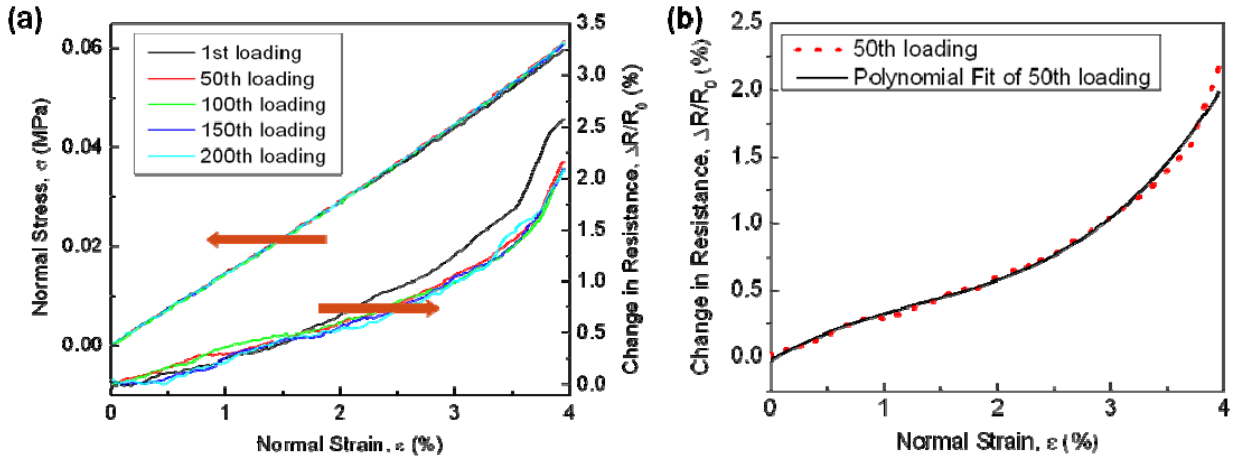

Fig. 7.8: Normal stress and the change in resistance versus strain for the 1st, 50th, 100th, 150th and 200th loading from 0 to 4% strain.

It has been observed that the resistance of SWNTs would decrease with increased temperature [13]. On the other hand, the increased temperature will cause an expansion of PDMS substrate (strain) which will increase the resistance of nanotubes. These two effects compensate each other and affect the measured resistance of the SWNT network on PDMS substrate. Thus temperature as a crucial parameter needs to be calibrated for the nanotube strain sensor.

In summary, I developed a flexible, stretchable and transparent strain sensor composed of ultrathin SWNT film encapsulated in PDMS thin films. The fabricated strain sensor exhibited linear, reversible and repeatable response to up to 5% strain. For larger strains, the electrical response of the SWNTs to strain was irreversible for the first loading-unloading cycle and highly repeatable for the rest of testing. This SWNT network embedded in PDMS thin films could accommodate strains as large as 35% and fractured at 40%. Encapsulating SWNT network by spinning coating another PDMS thin film on the top effectively eliminated the effect of environmental gases and vapors to the conductance of SWNT sensors. The SWNT strain sensor demonstrated consistent results for 200 cycling measurements. The encapsulated SWNT network in PDMS thin films as a robust, flexible, stretchable and transparent composite material might find potential applications in structural health monitoring.

CHAPTER 8

CONCLUSIONS AND FUTURE WORK

In this thesis, I investigated and developed a highly sensitive, efficient and low cost approach for real-time environmental monitoring which include air and water quality monitoring. ssDNA functionalized SWNTs were used as the sensing element and assembled onto microdevices for gas detection. The response of nanotubes was significantly improved by DNA decoration. In addition, the responses of DNA-SWNT sensors depend on the sequences of DNA been utilized and the gases been detected. The sensing characteristics of RNA oligomers functionalized SWNT sensors were investigated. RNAs composed of different sequences have different responses which could be due to the different binding affinities of RNA's nitrogenous bases with the SWNTs. Homo DNA nucleotides with different sequence lengths also exhibit different responses to gases. The optimum DNA sequence length for sensing applications was found to be 24. In order to selectively differentiate the target analyte from a mixture of gases and vapors, a nanosensor array with six channels was developed utilizing SWNTs decorated with different DNA sequences. The fabricated wireless nanosensor array was tested with various kinds of gases and organic vapors and their responses were displayed on a computer by GUI interface. A wireless, single chip sensing unit based on DNA-SWNTs was developed on CMOS chip in order to realize portable, standoff and real-time gas monitoring. Two types of chemical warfare agents (DMMP and DNT) were detected and the changes in resistance as well as gain of amplifier were correlated with the concentration of input vapors. Besides gas monitoring, SWNT sensors were combined with microfluidic system for water quality monitoring. This sensing unit was calibrated by pH buffers ranging from 5-8. Furthermore, different concentrated TNT solution was detected and the change in resistance of SWNTs increased with the concentration of TNT. Polymer thin films as device substrates offer excellent flexibility and stretchability while maintains the electrical properties of conventional electronic devices fabricated on rigid silicon wafer. Here I developed a stretchable and flexible strain sensor composed of carbon nanotubes embedded in PDMS thin films which potentially can be utilized for structural health monitoring. The electrical characteristics in

response to various levels of strain, the effect of encapsulation and the reliability, repeatability of this stretchable sensor were analyzed.

In the future, this thesis can be extended in the following field:

1. The sensing characteristics of DNA decorated SWNT sensor to gases and vapors need to be further explored. Various types of DNA sequences can be designed and applied on nanotube sensor and tested with different gases and vapors. In this way, we can find the DNA sequence which has significant response to certain vapor and the DNA sequence which has very low response to certain vapor. So that the DNA-SWNT nanosensor array can be designed for specific vapor detection. Such as DNA with the sequence of repeated GT bases exhibited a special response (the resistance decrease after exposure) to H_2S comparing to other DNAs (the resistances increased after detection).
2. In the aspect of data analysis, after achieving the responses of nanosensor array to certain vapor wirelessly, the collected data from six channels can be plotted in the same figure and the specific sensing characteristics to certain vapor can be differentiated by pattern recognition.
3. The nanosensor integrated with microfluidic channel as a platform can be extended to various types of chemical sensing and biosensing in liquid. The SWNTs inside the microfluidic channel can be decorated with antibodies which can bind antigens in the solution, can be functionalized with DNA nucleotides and applied to detection DNA with the complimentary sequence, can be decorated with DNA containing T-T mismatches which can selectively response to mercury in the liquid and so on. In addition, the microfluidic system can be designed to filter and separate various components in liquid sample and then guide them to multiple nanosensors for analysis. The eventual goal is to develop a lab-on-a-chip device which performs water quality monitoring that normally done in a lab by human effort and bulky equipments on a single autonomous microdevice (A schematic illustration of the lab-on-a-chip device was shown in Figure 8.2)

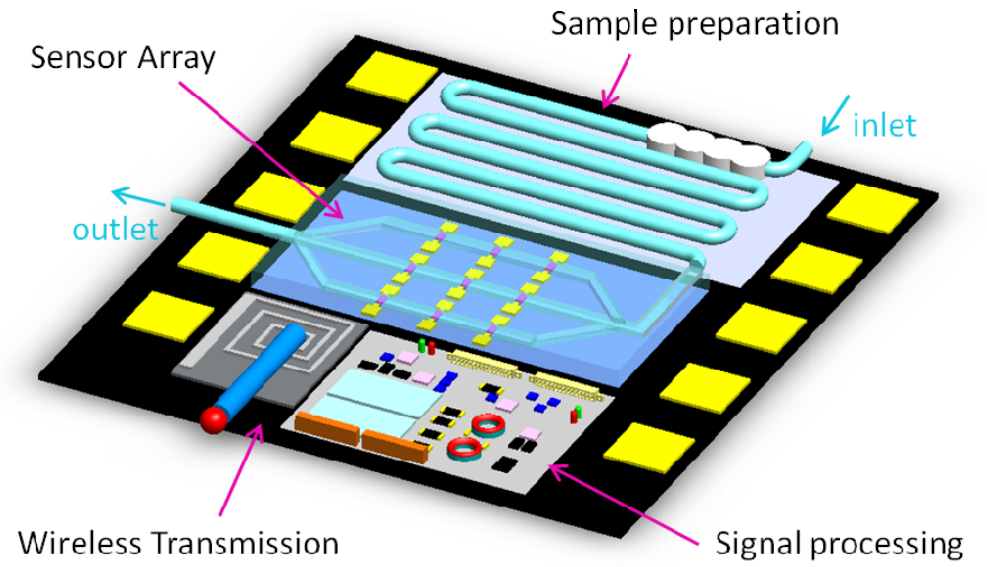

Fig. 8.1: Schematic illustration of a lab-on-a-chip sensor for remote water quality monitoring. The sample preparation, detection, signal processing and wireless transmission are integrated on a single chip.

4. The stretchable and flexible sensor composed of SWNT network embedded inside PDMS thin films can be extended to many types of wearable sensors for diagnostic and medical applications, such as a strain sensor measuring human motion, a pressure sensor placed in shoes measuring the steps during walking, a strain sensor measuring the beating of heart, a strain sensor measuring the displacement of bones and so on.

APPENDIX A

FABRICATE 2D ELECTRODES WITH 1 MICROMETER GAP

1. Clean the Si Wafer

1.1 The Si wafers used in this experiment is from University Wafers with the parameters:

DIA	TYPE	ORIENT	RES	THK	GRADE	SURFACE
3”	P	<100>	0-100	500	Virgin Test	1S polished

1.2 Immerse the wafers in Piranha solution at 90 °C for 10 mins to remove metal ions; Rinse with DI water

1.3 Immerse the wafers in HF solution at 115 °C for 15 sec to remove the oxide layer formed on top of silicon wafers; Rinse with DI water

1.4 Dehydration bake at 150 °C for 10 mins

2. Define the 1μm pattern with photolithography

2.1. Spin coat PR 1805 with Brewer 100 CB at 4000 rpm for 45 sec

2.2. Prebake on a hot plate at 115 °C for 1 min

2.3. UV exposure with Quintel Aligner for 5 sec

2.4. Develop in MF 319 for 20 sec with strong agitation

2.5. Rinse in DI water for 5 mins and blow dry with N_2

3. Inspect the pattern with Nikon Optiphot 200D

4. Deposit 20 nm Cr and 150 nm with E-beam Deposition System

5. Lift off process

5.1. Soak the wafers in Acetone overnight

5.2. Remove the excess Au layer and photoresist with N_2 air

APPENDIX B

SIX CHANNEL WIRELESS SENSOR ARRAY

1. Write a program on the wireless circuitry board to control data transmission

Set the wireless board to read data from A/D converter and send the data to receiver by C program

2. Design the GUI interface

The GUI interface was designed by LabWindows by C program

3. Prepare the nanosensor array
   - 3.1 The silicon chip with microelectrodes was wire bonded using MEI 1024B Ball Bonder onto a ceramic chip holder
   - 3.2 Assemble SWNTs onto the microelectrodes by DEP assembly
   - 3.3 Decorate ssDNA onto the SWNTs
   - 3.4 Insert the chip holder onto the socket soldered on a PCB board with testing components
4. Record and display the data
   - 4.1 Push the start button on the wireless transmission board and open the GUI interface
   - 4.2 Open proprietary serial port. If successfully, go to next step
   - 4.3 If there is data store in the buffer of serial port, read the data. If not, wait until there is data stored in the buffer
   - 4.4 Save the data into the file; In the mean while, the data will be plotted in the GUI interface.

APPENDIX C

TESTING SETUP FOR GAS SENSORS

The schematic testing setup for gas sensors is shown below:

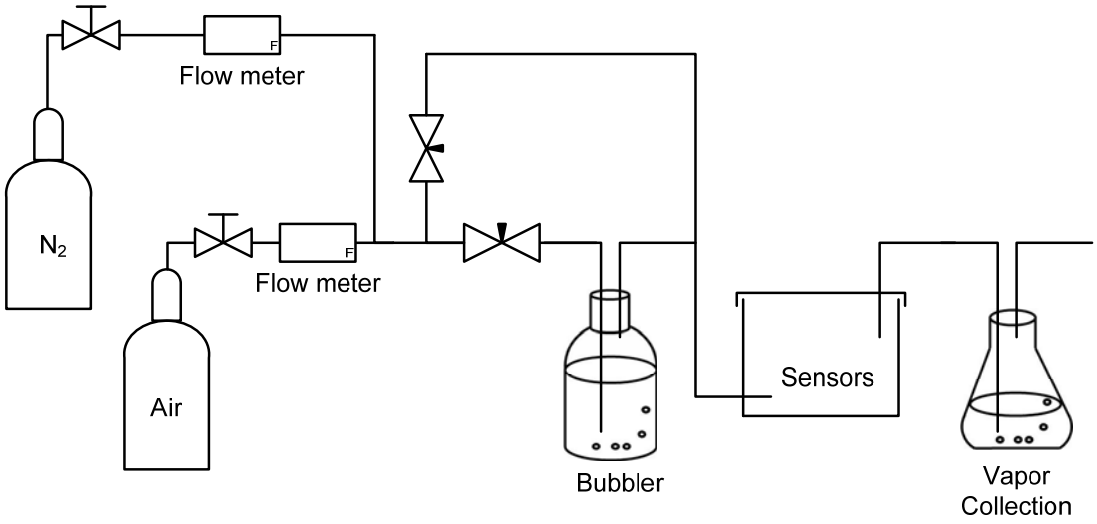

1. The gas to carry organic vapors could be N_2 or air
2. Gas with controlled flowing rate will pass through the bubbler and carrier organic vapors out and deliver the vapors into a sealed chamber with nanosensors inside;
3. After detection, the gas and vapors inside the chamber will be pushed into the waste collection area. For example, if the vapor is DNT, using basic solution such as NaOH inside the waste collection bottle can effectively decompose the DNT vapor and prevent its release to the environment.
4. After detection, the clean gas without any vapor will be injected into the chamber and the vapors on nanosensors will be desorbed
5. The vapor pressures of organics are highly sensitive to temperature. Here I used a thermal bath to heat the organic solution in the bubbler. The water inside the thermal bath is driven to the double jacket chamber by a mechanical pump.

The photoimages of the testing setup are shown below:

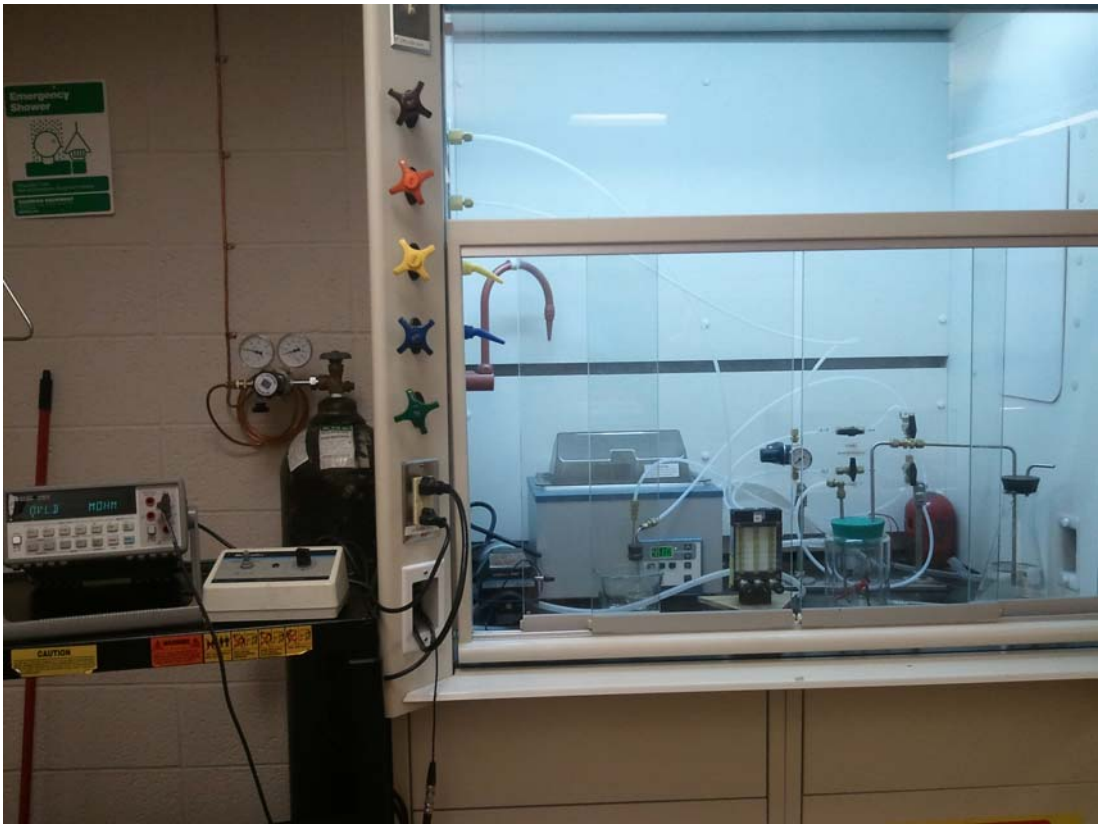

APPENDIX D

INTEGRATE SWNT SENSORS WITH MICROFLUIDIC SYSTEMS

Appendix C-1 Fabrication Process for SU8 mode

1. Clean the Si Wafer

   1.1 The Si wafers used in this experiment is from University Wafers with the parameters:

DIA	TYPE	ORIENT	RES	THK	GRADE	SURFACE
3”	P	<100>	0-100	500	Virgin Test	1S polished

   1.2 Immerse the wafers in Piranha solution at 90 °C for 10 mins to remove metal ions; Rinse with DI water

   1.3 Immerse the wafers in HF solution at 115 °C for 15 sec to remove the oxide layer formed on top of silicon wafers; Rinse with DI water

   1.4 Dehydration bake at 150 °C for 10 mins

2. Define SU8 Pattern by Photolithography

   2.1 Spin coat SU8-100 by Laurell Spinner with the speed of 500 rpm for 10 sec; then with the speed of 1300 rpm for 30 sec. The obtained film thickness is around 200 μm;

   2.2 Prebake the wafer on a hot plate at 65 °C for 25 mins; Then soft bake the wafer on a hot plate at 95 °C for 70 mins

   2.3 Leave the wafer dry in air overnight

   2.4 Exposure SU8 under mask for 36 sec using Quintel Aligner

   2.5 Post exposure, the wafer was baked at 65 °C for 2 mins then baked at 95 °C for 18 mins

   2.6 Develop in SU8 developer for 18 mins with strong agitation.

   2.7 Rinse briefly with IPA (10 sec) then blow dry with N_2

2.8 Inspect the pattern with Nikon Optiphot 200D and calibrate the thickness with Dektak

Appendix C-2 Fabrication Process for Microfluidic Channel

1. Mix PDMS prepolymer

   1.1 The silicone elastomer kit, Sylgard 184, contains two parts: the polymer base and the curing agent. The Polymer base and the curing agent were mixed with a ratio of 10:1 by weight.

   1.2 Stirring the mixture with a tip until the solution looks milky.

2. Degas PDMS prepolymer

   2.1 Put the mixed PDMS solution into a vacuum chamber and degas for 20 mins until no bubbles can be observed.

3. Cure the PDMS on SU8 mode

   3.1 When the PDMS prepolymer is completely degassed, pour the solution onto the SU8 mode displaced in a petridish.

   3.2 Cure the PDMS solution inside the petridish in a 70 °C oven for 4 hours

4. Peel off the PDMS layer

   Gently peel off PDMS layer from SU8 mode

Appendix C-3 Bonding Microfluidic Channel onto Silicon Chip

1. Cut the PDMS film with microfluidic channels into small rectangular slabs and each slab contains one microfluidic channel
2. Use syringe needle to punch holes on the slab
3. Put the PDMS slab with microfluidic channel and a silicon chip with microelectrodes into the chamber of ICP (Plasma Therm 790) and run RoughenYL for 30 sec

4. Put the microfluidic channel on top of silicon chip with DI water in between. Place the device on a 150 °C for 15 mins
5. Insert tygon tubes into the holes on microfluidic channel
6. Inject SWNT solution into the microfluidic channel; Assemble SWNTs between the Au electrodes through the microfluidic channel

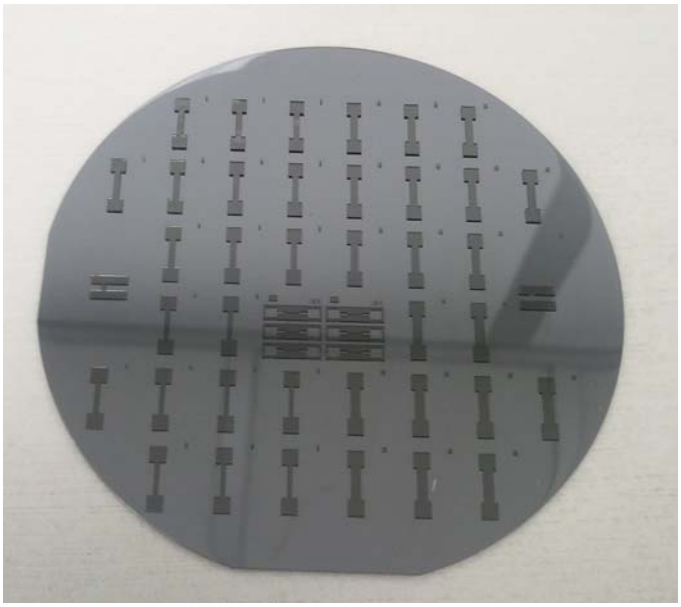

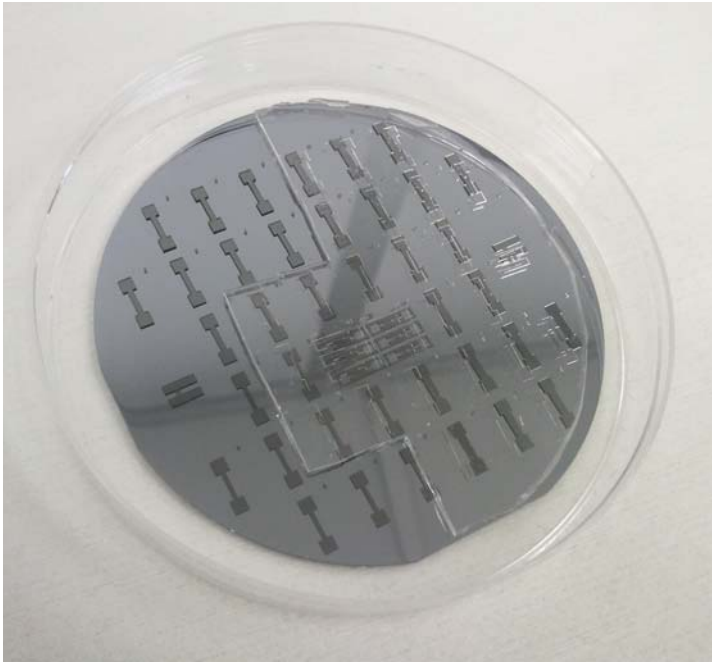

Appendix C-3 Bonding Microfluidic Channel onto Nanotube Device

1. For silicon chip with SWNTs assembled between the microelectrodes, cover 10 μm parylene-C film on the top of SWNTs
2. Put the PDMS slab with microfluidic channel and the nanotube device protected by parylene into the chamber of ICP (Plasma Therm 790) and run RoughenYL for 30 sec
3. Gently peel off the parylene film; check the resistance of SWNTs by a multimeter
4. Put the microfluidic channel on top of silicon chip with DI water in between. Place the device on a 150 °C for 15 mins
5. Insert Tygon tubes into the holes on microfluidic channel; check the resistance of SWNTs by a multimeter

APPENDIX E

FLEXIBLE AND STRETCHABLE SWNT DEVICE EMBEDDED IN PDMS THIN FILMS

1. Clean the Si Wafer

   1.1 The Si wafers used in this experiment is from University Wafers with the parameters:

DIA	TYPE	ORIENT	RES	THK	GRADE	SURFACE
3”	P	<100>	0-100	500	Virgin Test	1S polished

   1.2 Immerse the wafers in Piranha solution at 90 °C for 10 mins to remove metal ions; Rinse with DI water

   1.2 Immerse the wafers in HF solution at 115 °C for 15 sec to remove the oxide layer formed on top of silicon wafers; Rinse with DI water

   1.4 Dehydration bake at 200 °C for 5 mins

2. Fabricate PDMS thin film

   2.1 Spin coat adhesion primer onto clean Si wafer with Laurell Spinner with the speed of 3000 rpm for 45 sec;

   2.2 Bake the wafer at 170 °C for 5 mins

   2.3 Spin coat degassed PDMS prepolymer onto Si wafer with Laurell Spinner with the speed of 500 rpm for 60 sec;

   2.2 Cure the spin coated PDMS thin film in a 70 °C oven for 2 hours

3. Deposit electrodes on PDMS layer

   3.1 Create a shadow mask with thick PDMS film

   3.2 Cover the shadow mask onto Si wafer with PDMS thin film

   3.3 Deposit 30 nm Cr and 150 nm Au layers with MRC 8667 Sputtering

3.4 Remove the shadow mask

4. Drop cast SWNT network between the electrodes

   4.1 Roughen the surface of PDMS film with ICP (Plasma Therm 790) for 30 sec

   4.2 Drop cast well dispersed SWNT solution onto the PDMS film

   4.3 Dry the SWNT solution in air for 4 hours

   4.4 Check the resistance of SWNT network between Au electrodes

5. Encapsulate SWNT network with PDMS layer

   5.1 Spin coat degassed PDMS prepolymer onto Si wafer with Laurell Spinner with the speed of 500 rpm for 60 sec;

   5.2 Cure the spin coated PDMS thin film in a 70 °C oven for 2 hours

6. Manually cut off the excess PDMS films on Si wafer and peel off the PDMS films covered on the open contact area of Au electrode

7. Gently peel off the device from Si wafer

APPENDIX F

SYNTHESIS POLYANILINE ON SWNTS

1. Chemical polymerization:

   1.1 Dip SWNT device into Aniline solution for 12 hours

   1.2 Drop APS solution into aniline solution. The reaction finishes vary fast (within 1 min). Green flakes, powders are observed in the solution. Also a thick green layer is covered on the top of SWNT device

   1.3 Rinse with DI water

   1.4 Inspect the formation of Polyaniline (PANi) under microscope

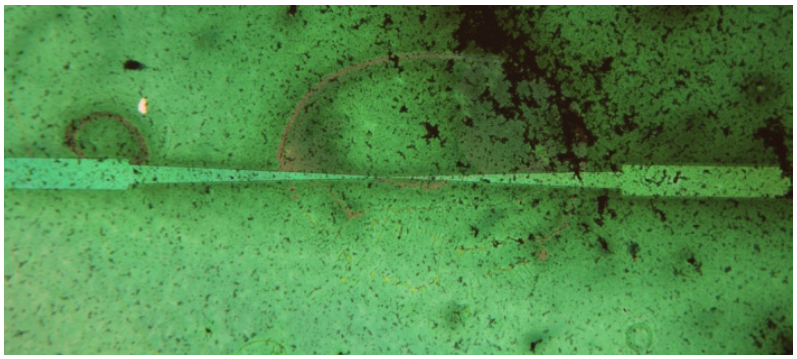

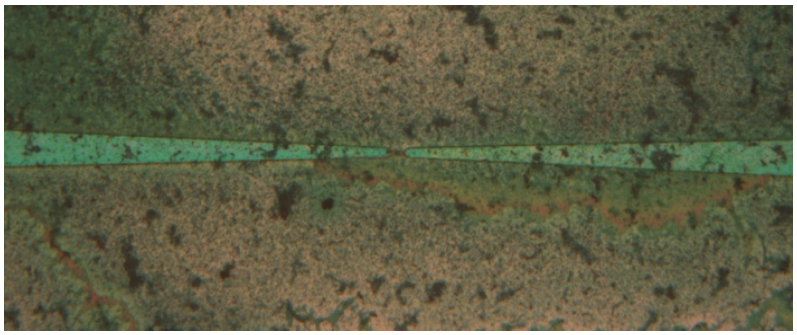

   1.5 Dip SWNT device into Aniline solution for 12 hours and then take device out and rinse with 1 M HCl solution to remove excess aniline stick on the device.

   1.6 Drop APS solution on the top of device; wait for 4 hour for the reaction.

   1.7 Rinse with DI water

   1.8 Inspect the formation of PANi under microscope

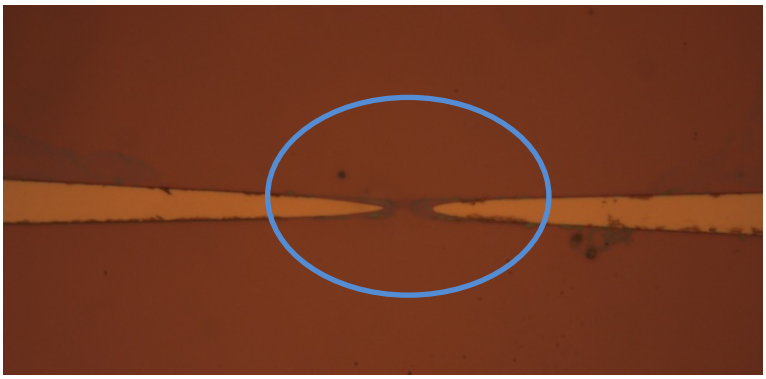

1.9 Inspect the formation of PANi under SEM

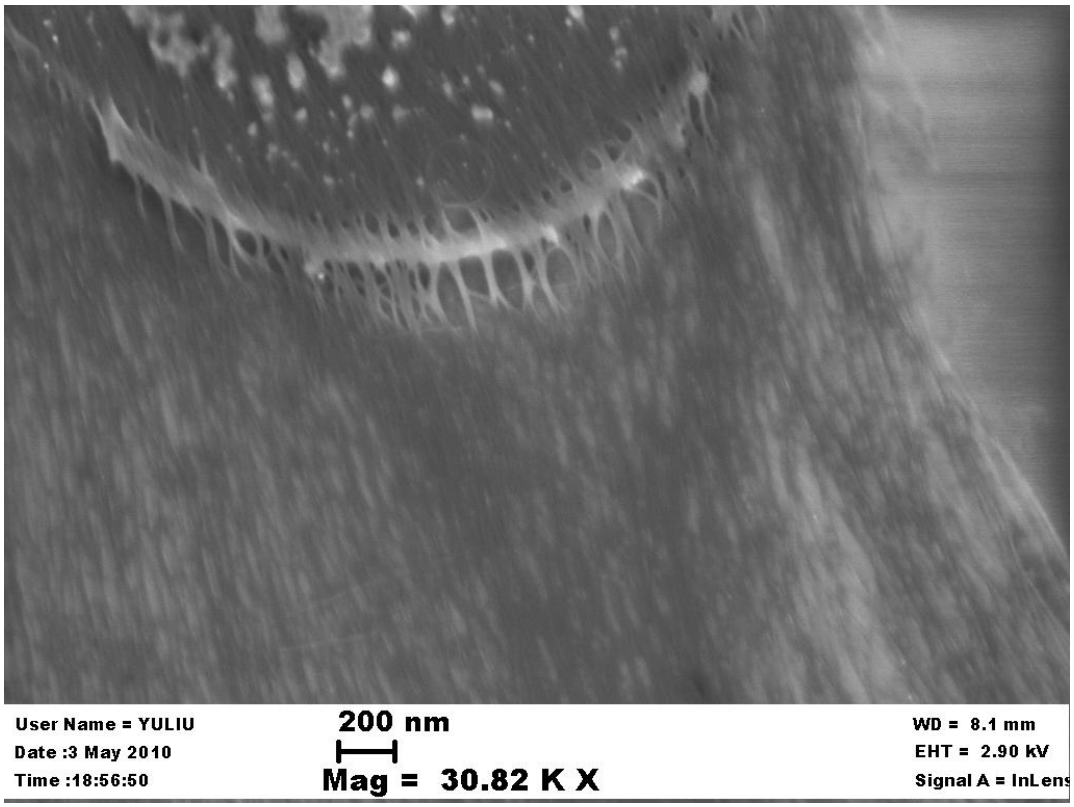

APPENDIX G

FUNCTIONALIZE SWNTS WITH ANTIBODY

1. SWNT devices in 5mM 1-pyrenebutanoic acid succinimidyl ester in dry dimethylformamide (DMF) overnight at room temperature
2. Incubate the SWNT device in a PBS solution of anti-PSA monoclonalantibody for 12h at room temperature
3. Inspect the decoration of Antibodies by SEM

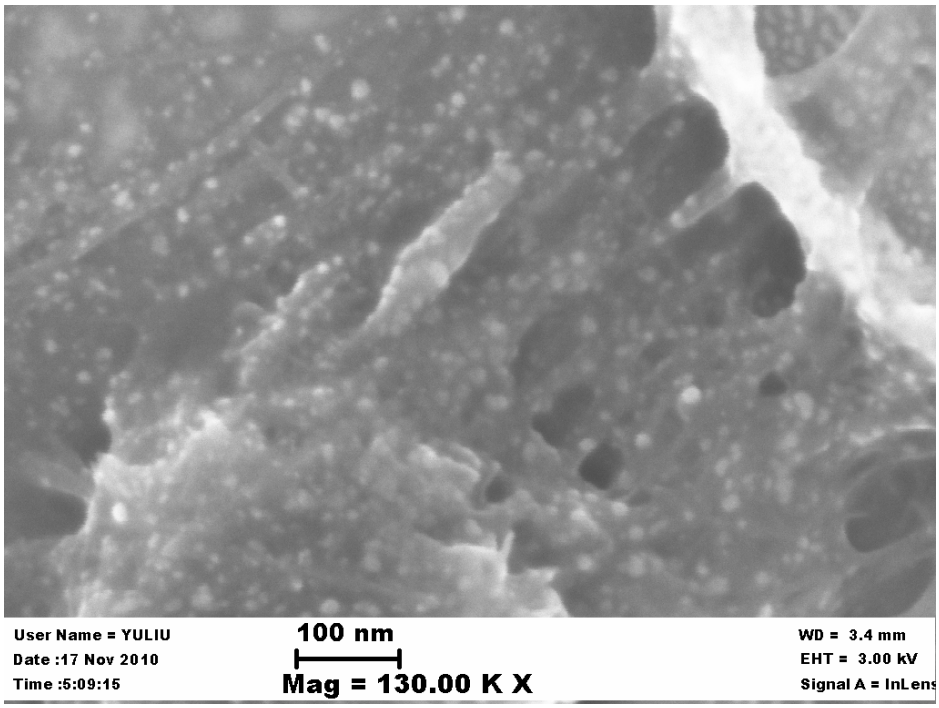

Appendix H

Control Program for Agilent LCR 4263B by LabVIEW

A control panel was design by LabVIEW to record and display data obtain from LCR 4263B. Below is a screen captured image of the control panel.

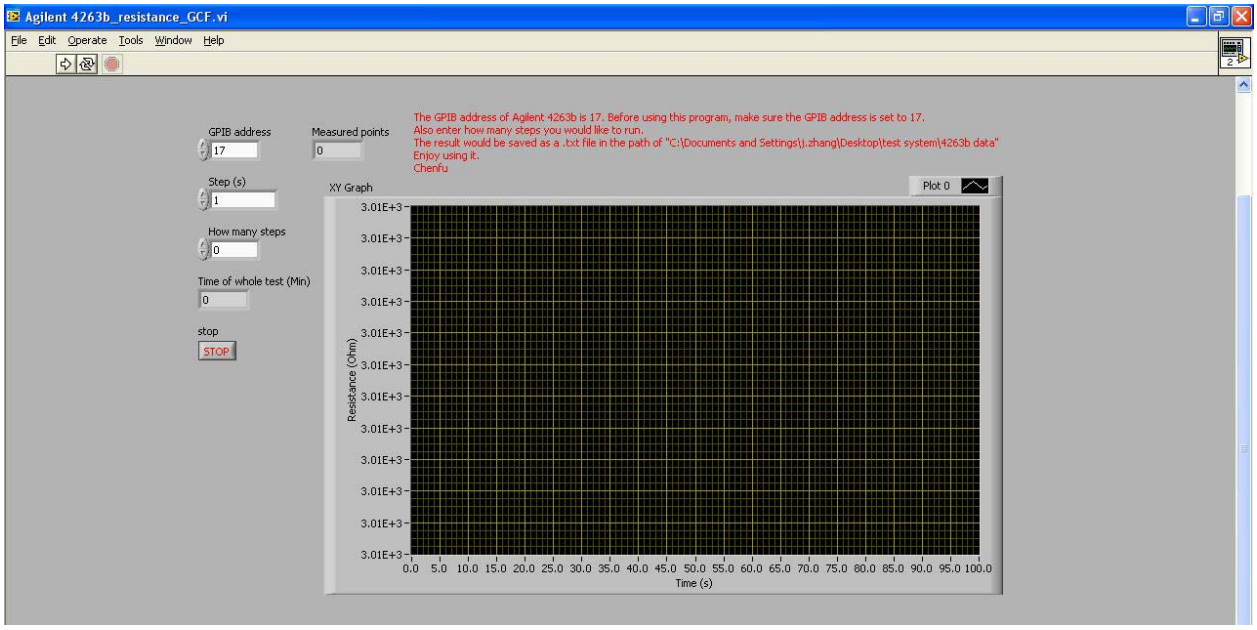

Case 0: Connect LabVIEW to Agilent LCR 4263B and configure the equipment including clear all data, send data from the LCR meter to LabView via the designated GPIB address.

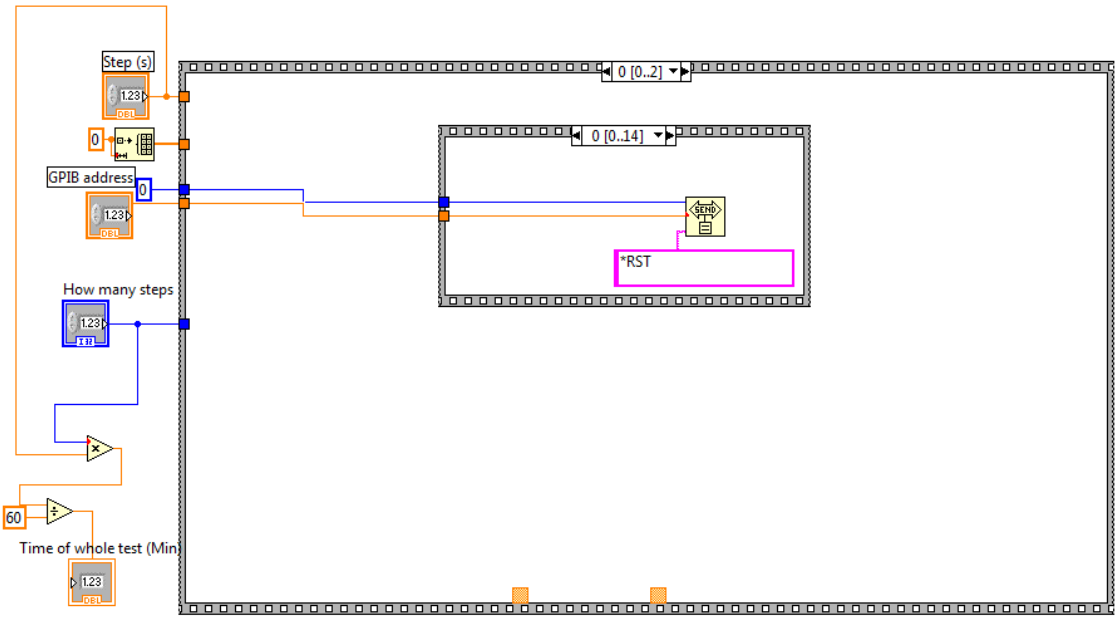

Case 1-0: Set the timer for individual data recall to be 1000 miliseconds.

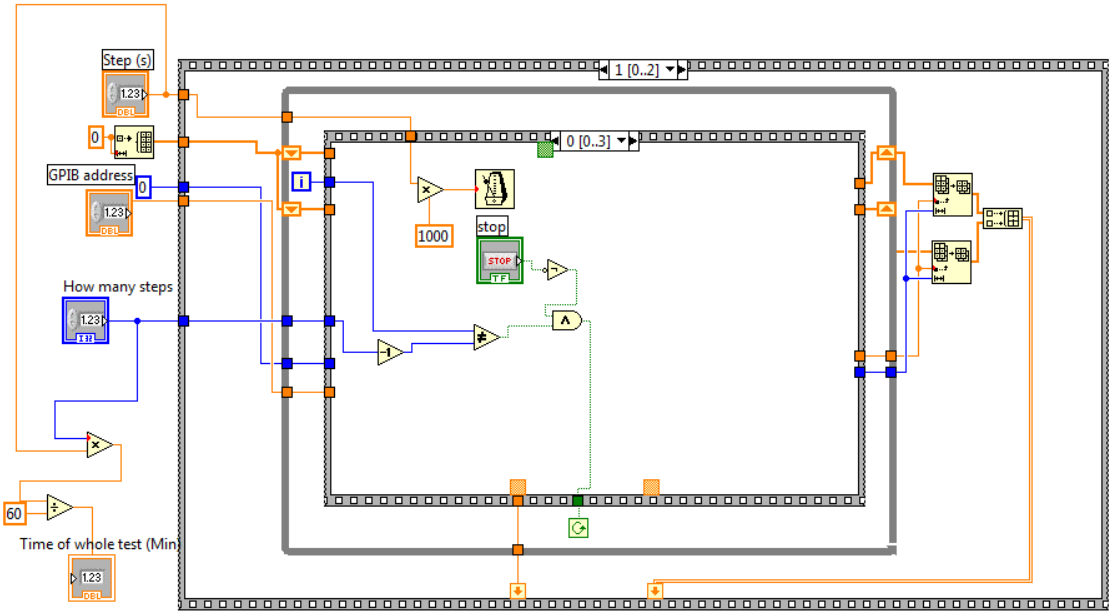

Case 1-1: Form 2D data arrays which record the number of measurements and the data read from LCR meter. Combine the 2D data arrays into one file and display the data in the X-Y graph.

Note: Out of the while loop, there is a redundancy loop which keeps saving the data (on the right side)

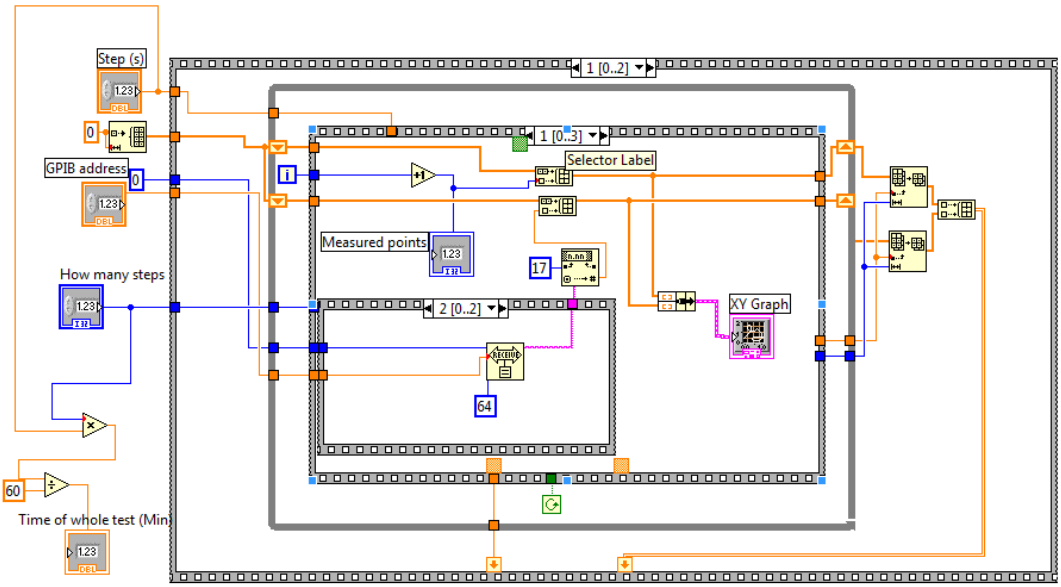

Case 1-2: If the number of measurements reaches the input number of steps, the accumulated data in one subarray will be combined with the number of measurements in other subarray into a 2D array

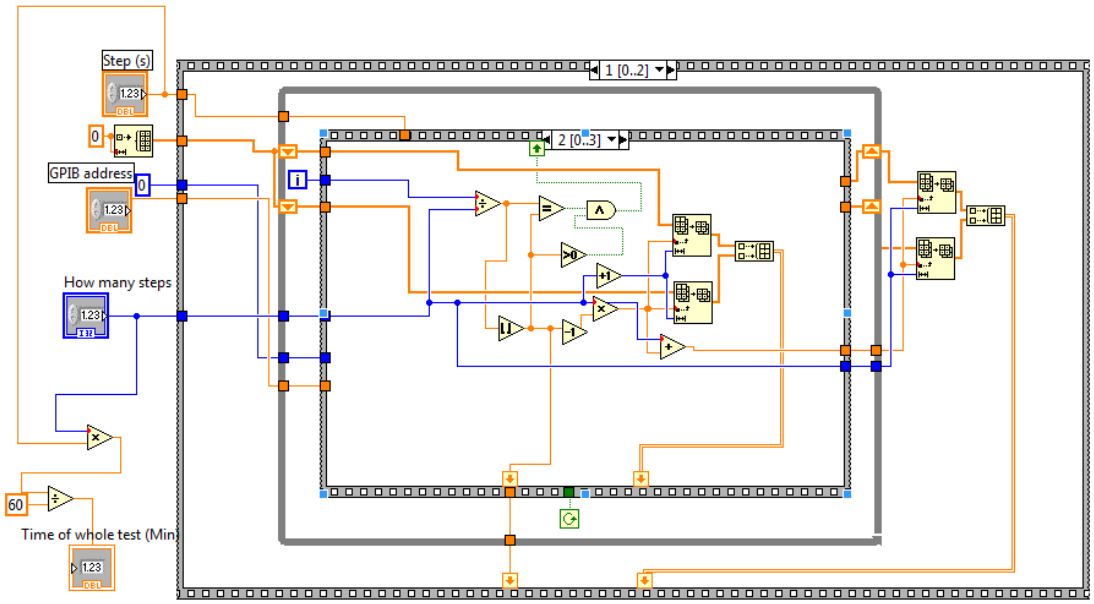

Case 1-3: Save the 2D data array as a text file to the designated path defined by users.

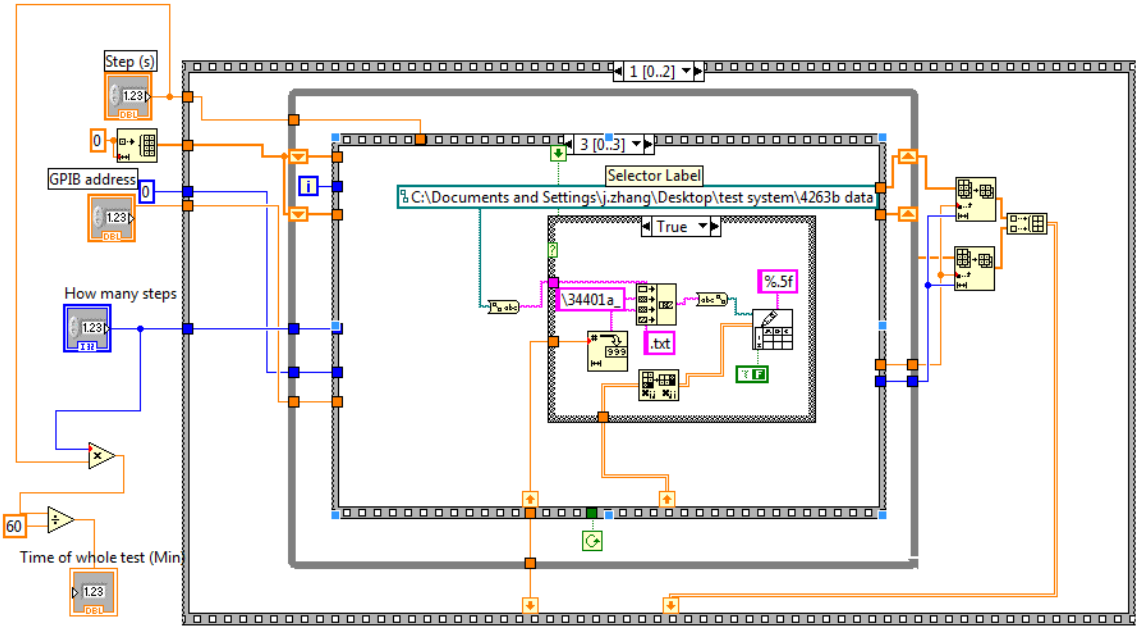

Case 2: The redundancy loop for saving data is defined here. If the program is terminated, the data recorded in the two subarrays and combined in case 1-1 will be saved into the designated path defined by users.

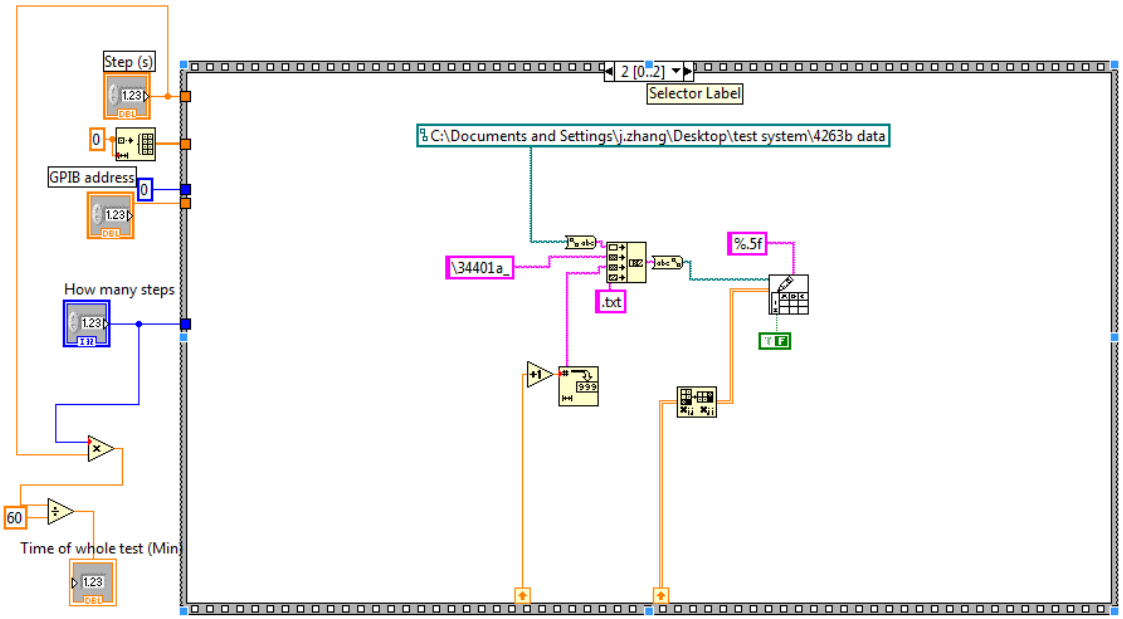

REFERENCES

[1] S. Iijima, Helical microtubules of graphitic carbon, Nature, 354 (1991) 56-58.
[2] R.E. Smalley, Formation and properties of C_{60} and the fullerenes, in: National Institute of Standards and Technology, 1990.
[3] M.S. Dresselhaus, in: Oral presentation at fullerene workshop, University of Pennsylvania, 1991.
[4] S. Iijima, Ichihashi, T., Single-shell carbon nanotubes of 1-nm diameter, Nature, 363 (1993) 603-605.
[5] D.S. Bethune, C.H. Klang, M.S. de Vries, G. Gorman, R. Savoy, J. Vazquez, R. Beyers, Cobalt-catalysed growth of carbon nanotubes with single-atomic-layer walls, Nature, 363 (1993) 605-607.
[6] H. Dai, Nanotube Growth and Characterization, in: Proc. Springer, Berlin, 2001.
[7] T.W. Ebbesen, P.M. Ajayan, Large-scale synthesis of carbon nanotubes, Nature, 358 (1992) 220-222.
[8] A. Thess, R. Lee, P. Nikolaev, H.J. Dai, P. Petit, J. Robert, C.H. Xu, Y.H. Lee, S.G. Kim, A.G. Rinzler, D.T. Colbert, G.E. Scuseria, D. Tomanek, J.E. Fischer, R.E. Smalley, Crystalline Ropes of Metallic Carbon Nanotubes, Science, 273 (1996) 483-487.
[9] D. Takagi, Y. Homma, H. Hibino, S. Suzuki, Y. Kobayashi, Single-Walled Carbon Nanotube Growth From Highly Activated Metal Nanoparticles, Nano Lett., 6 (2006) 2642-2645.
[10] H.J. Dai, Carbon nanotubes: Synthesis, integration, and properties, Accounts Chem Res, 35 (2002) 1035-1044.
[11] J.W.G. Wildoer, L.C. Venema, A.G. Rinzler, R.E. Smalley, C. Dekker, Electronic structure of atomically resolved carbon nanotubes, Nature, 391 (1998) 59-62.
[12] K. Maehashi, Y. Ohno, K. Inoue, K. Matsumoto, Chirality selection of single-walled carbon nanotubes by laser resonance chirality selection method, Appl Phys Lett, 85 (2004) 858-860.
[13] C.L. Kane, E.J. Mele, R.S. Lee, J.E. Fischer, P. Petit, H. Dai, A. Thess, R.E. Smalley, A.R.M. Verschueren, S.J. Tans, C. Dekker, Temperature-dependent resistivity of single-wall carbon nanotubes, Europhys Lett, 41 (1998) 683-688.
[14] A. Bachtold, M.S. Fuhrer, S. Plyasunov, M. Forero, E.H. Anderson, A. Zettl, P.L. McEuen, Scanned probe microscopy of electronic transport in carbon nanotubes, Phys Rev Lett, 84 (2000) 6082-6085.
[15] P. Avouris, Supertubes, in: IEEE Spectrum, 2004, pp. 40-45.
[16] B. Mahar, C. Laslau, R. Yip, Y. Sun, Development of carbon nanotube-based sensors - A review, Ieee Sens J, 7 (2007) 266-284.
[17] A.M. Rao, E. Richter, S. Bandow, B. Chase, P.C. Eklund, K.A. Williams, S. Fang, K.R. Subbaswamy, M. Menon, A. Thess, R.E. Smalley, G. Dresselhaus, M.S. Dresselhaus, Diameter-selective Raman scattering from vibrational modes in carbon nanotubes, Science, 275 (1997) 187-191.
[18] S.M. Bachilo, M.S. Strano, C. Kittrell, R.H. Hauge, R.E. Smalley, R.B. Weisman, Structure-assigned optical spectra of single-walled carbon nanotubes, Science, 298 (2002) 2361-2366.
[19] A. Hagen, T. Hertel, Quantitative analysis of optical spectra from individual single-wall carbon nanotubes, Nano Lett, 3 (2003) 383-388.
[20] A. Hartschuh, H.N. Pedrosa, L. Novotny, T.D. Krauss, Simultaneous fluorescence and Raman scattering from single carbon nanotubes, Science, 301 (2003) 1354-1356.
[21] M. Freitag, Y. Martin, J.A. Misewich, R. Martel, P.H. Avouris, Photoconductivity of single carbon nanotubes, Nano Lett, 3 (2003) 1067-1071.
[22] J.A. Misewich, R. Martel, P. Avouris, J.C. Tsang, S. Heinze, J. Tersoff, Electrically induced optical emission from a carbon nanotube FET, Science, 300 (2003) 783-786.

[23] J.P. Salvetat, G.A.D. Briggs, J.M. Bonard, R.R. Bacsa, A.J. Kulik, T. Stockli, N.A. Burnham, L. Forro, Elastic and shear moduli of single-walled carbon nanotube ropes, Phys Rev Lett, 82 (1999) 944-947.
[24] J. Bernholc, D. Brenner, M.B. Nardelli, V. Meunier, C. Roland, Mechanical and electrical properties of nanotubes, Annu Rev Mater Res, 32 (2002) 347-375.
[25] I. Palaci, S. Fedrigo, H. Brune, C. Klinke, M. Chen, E. Riedo, Radial elasticity of multiwalled carbon nanotubes, Phys Rev Lett, 94 (2005) -.
[26] X.J. Xu, M.M. Thwe, C. Shearwood, K. Liao, Mechanical properties and interfacial characteristics of carbon-nanotube-reinforced epoxy thin films, Appl Phys Lett, 81 (2002) 2833-2835.
[27] T. Laha, A. Agarwal, T. McKechnie, S. Seal, Synthesis and characterization of plasma spray formed carbon nanotube reinforced aluminum composite, Mat Sci Eng a-Struct, 381 (2004) 249-258.
[28] R. Andrews, D. Jacques, A.M. Rao, T. Rantell, F. Derbyshire, Y. Chen, J. Chen, R.C. Haddon, Nanotube composite carbon fibers, Appl Phys Lett, 75 (1999) 1329-1331.
[29] T.W. Tombler, C.W. Zhou, L. Alexseyev, J. Kong, H.J. Dai, L. Lei, C.S. Jayanthi, M.J. Tang, S.Y. Wu, Reversible electromechanical characteristics of carbon nanotubes under local-probe manipulation, Nature, 405 (2000) 769-772.
[30] J. Cao, Q. Wang, H.J. Dai, Electromechanical properties of metallic, quasimetallic, and semiconducting carbon nanotubes under stretching, Phys Rev Lett, 90 (2003) -.
[31] R.C. Haddon, Chemistry of the Fullerenes - the Manifestation of Strain in a Class of Continuous Aromatic-Molecules, Science, 261 (1993) 1545-1550.
[32] R.C. Haddon, Measure of nonplanarity in conjugated organic molecules: Which structurally charaterized molecules displays the highest degree of pyramidalization?, J. Am. Chem. Soc., 112 (1990) 3385-3389.
[33] B.R. Weedon, R.C. Haddon, H.P. Spielmann, M.S. Meier, Fulleroid Addition Regiochemistry is Driven by pi-Orbital Misalignment, J. Am. Chem. Soc., 121 (1999) 335-340.
[34] D. Srivastava, D.W. Brenner, J.D. Schall, K.D. Ausman, M. Yu, R.S. Ruoff, Predictions of Enhanced Chemical Reactivity to Regions of Local Conformational Strain on Carbon Nanotubes: Kinky Chemistry, J. Phys. Chem. B, 103 (1999) 4330-4337.
[35] T.W. Ebbesen, H. Hiura, M.E. Bisher, M.M.J. Treacy, J.L. ShreeveKeyer, R.C. Haushalter, Decoration of carbon nanotubes, Adv Mater, 8 (1996) 155-&.
[36] A. Koshio, M. Yudasaka, M. Zhang, S. Iijima, A Simple Way to Chemically React Single-Wall Carbon Nanotubes with Organic Materials Using Ultrasonication, Nano Lett., 1 (2001) 361-363.
[37] M. Monthioux, B.W. Smith, B. Burteaux, A. Claye, J.E. Fischer, D.E. Luzzi, Sensitivity of single-wall carbon nanotubes to chemical processing: an electron microscopy investigation, Carbon, 39 (2001) 1251-1272.
[38] J. Li, Y.J. Lu, Q. Ye, M. Cinke, J. Han, M. Meyyappan, Carbon nanotube sensors for gas and organic vapor detection, Nano Lett, 3 (2003) 929-933.
[39] M. Meyyappan, Carbon nanotubes: science and applications, CRC Press LLC, 2005.
[40] J. Zhao, A. Buldum, J. Han, J.P. Lu, Gas molecule adsorption in carbon nanotubes and nanotube bundles, Nanotechnology, 13 (2002) 195-200.
[41] J. Zhao, J.P. Lu, J. Han, C.-K. Yang, Noncovalent functionalization of carbon nanotubes by aromatic organic molecules, Appl. Phys. Lett., 82 (2003) 3746-3748.
[42] B. Gao, A. Kleinhammes, X.P. Tang, C. Bower, L. Fleming, Y. Wu, O. Zhou, Electrochemical intercalation of single-walled carbon nanotubes with lithium, Chem Phys Lett, 307 (1999) 153-157.
[43] J. Hone, M. Whitney, C. Piskoti, A. Zettl, Thermal conductivity of single-walled carbon nanotubes, Phys Rev B, 59 (1999) R2514-R2516.

[44] W. Yi, L. Lu, D.L. Zhang, Z.W. Pan, S.S. Xie, Linear specific heat of carbon nanotubes, Phys Rev B, 59 (1999) R9015-R9018.
[45] P. Kim, L. Shi, A. Majumdar, P.L. McEuen, Thermal transport measurements of individual multiwalled nanotubes, Phys Rev Lett, 8721 (2001) -.
[46] L. Lindsay, D.A. Broido, N. Mingo, Diameter dependence of carbon nanotube thermal conductivity and extension to the graphene limit, Phys Rev B, 82 (2010) -.
[47] J. Kong, N.R. Franklin, C.W. Zhou, M.G. Chapline, S. Peng, K.J. Cho, H.J. Dai, Nanotube molecular wires as chemical sensors, Science, 287 (2000) 622-625.
[48] S. Chopra, K. McGuire, N. Gothard, A.M. Rao, A. Pham, Selective gas detection using a carbon nanotube sensor, Appl Phys Lett, 83 (2003) 2280-2282.
[49] Q.F. Pengfei, O. Vermesh, M. Grecu, A. Javey, O. Wang, H.J. Dai, S. Peng, K.J. Cho, Toward large arrays of multiplex functionalized carbon nanotube sensors for highly sensitive and selective molecular detection, Nano Lett, 3 (2003) 347-351.
[50] E. Bekyarova, M. Davis, T. Burch, M.E. Itkis, B. Zhao, S. Sunshine, R.C. Haddon, Chemically functionalized single-walled carbon nanotubes as ammonia sensors, J Phys Chem B, 108 (2004) 19717-19720.
[51] T. Zhang, M.B. Nix, B.Y. Yoo, M.A. Deshusses, N.V. Myung, Electrochemically functionalized single-walled carbon nanotube gas sensor, Electroanal, 18 (2006) 1153-1158.
[52] N.H. Quang, M. Van Trinh, B.H. Lee, J.S. Huh, Effect of NH3 gas on the electrical properties of single-walled carbon nanotube bundles, Sensor Actuat B-Chem, 113 (2006) 341-346.
[53] H.Q. Nguyen, J.S. Huh, Behavior of single-walled carbon nanotube-based gas sensors at various temperatures of treatment and operation, Sensor Actuat B-Chem, 117 (2006) 426-430.
[54] O.K. Varghese, P.D. Kichambre, D. Gong, K.G. Ong, E.C. Dickey, C.A. Grimes, Gas sensing characteristics of multi-wall carbon nanotubes, Sensor Actuat B-Chem, 81 (2001) 32-41.
[55] L.H. Nguyen, T.V. Phi, P.Q. Phan, H.N. Vu, C. Nguyen-Duc, F. Fossard, Synthesis of multi-walled carbon nanotubes for NH3 gas detection, Physica E, 37 (2007) 54-57.
[56] S.I. Moon, K.K. Paek, Y.H. Lee, H.K. Park, J.K. Kim, S.W. Kim, B.K. Ju, Bias-heating recovery of MWCNT gas sensor, Mater Lett, 62 (2008) 2422-2425.
[57] J. Suehiro, G.B. Zhou, M. Hara, Detection of partial discharge in SF6 gas using a carbon nanotube-based gas sensor, Sensor Actuat B-Chem, 105 (2005) 164-169.
[58] G.Z. Sun, S.W. Liu, K.F. Hua, X.Y. Lv, L. Huang, Y.J. Wang, Electrochemical chlorine sensor with multi-walled carbon nanotubes as electrocatalysts, Electrochem Commun, 9 (2007) 2436-2440.
[59] L. Valentini, C. Cantalini, I. Armentano, J.M. Kenny, L. Lozzi, S. Santucci, Highly sensitive and selective sensors based on carbon nanotubes thin films for molecular detection, Diam Relat Mater, 13 (2004) 1301-1305.
[60] W.S. Cho, S.I. Moon, K.K. Paek, Y.H. Lee, J.H. Park, B.K. Ju, Patterned multiwall carbon nanotube films as materials of NO2 gas sensors, Sensor Actuat B-Chem, 119 (2006) 180-185.
[61] T. Ueda, M.M.H. Bhulyan, H. Norimatsu, S. Katsuki, T. Ikegami, F. Mitsugi, Development of carbon nanotube-based gas sensors for NOx gas detection working at low temperature, Physica E, 40 (2008) 2272-2277.
[62] N.D. Hoa, N. Van Quy, Y. Cho, D. Kim, An ammonia gas sensor based on non-catalytically synthesized carbon nanotubes on an anodic aluminum oxide template, Sensor Actuat B-Chem, 127 (2007) 447-454.
[63] C.S. Huang, B.R. Huang, Y.H. Jang, M.S. Tsai, C.Y. Yeh, Three-terminal CNTs gas sensor for N-2 detection, Diam Relat Mater, 14 (2005) 1872-1875.
[64] T. Zhang, S. Mubeen, E. Bekyarova, B.Y. Yoo, R.C. Haddon, N.V. Myung, M.A. Deshusses, Poly(m-aminobenzene sulfonic acid) functionalized single-walled carbon nanotubes based gas sensor, Nanotechnology, 18 (2007) -.

[65] K.H. An, S.Y. Jeong, H.R. Hwang, Y.H. Lee, Enhanced sensitivity of a gas sensor incorporating single-walled carbon nanotube-polypyrrole nanocomposites, Adv Mater, 16 (2004) 1005-+.
[66] X.L. Liu, J. Ly, S. Han, D.H. Zhang, A. Requicha, M.E. Thompson, C.W. Zhou, Synthesis and electronic properties of individual single-walled carbon nanotube/polypyrrole composite nanocables, Adv Mater, 17 (2005) 2727-+.
[67] P. Santhosh, K.M. Manesh, A. Gopalan, K.P. Lee, Novel amperometric carbon monoxide sensor based on multi-wall carbon nanotubes grafted with polydiphenylamine - Fabrication and performance, Sensor Actuat B-Chem, 125 (2007) 92-99.
[68] J.K. Abraham, B. Philip, A. Witchurch, V.K. Varadan, C.C. Reddy, A compact wireless gas sensor using a carbon nanotube/PMMA thin film chemiresistor, Smart Mater Struct, 13 (2004) 1045-1049.
[69] K.S.V. Santhanam, R. Sangoi, L. Fuller, A chemical sensor for chloromethanes using a nanocomposite of multiwalled carbon nanotubes with poly(3-methylthiophene), Sensor Actuat B-Chem, 106 (2005) 766-771.
[70] B. Zhang, R.W. Fu, M.Q. Zhang, X.M. Dong, P.L. Lan, J.S. Qiu, Preparation and characterization of gas-sensitive composites from multi-walled carbon nanotubes/polystyrene, Sensor Actuat B-Chem, 109 (2005) 323-328.
[71] L. Niu, Y.L. Luo, Z.Q. Li, A highly selective chemical gas sensor based on functionalization of multi-walled carbon nanotubes with poly(ethylene glycol), Sensor Actuat B-Chem, 126 (2007) 361-367.
[72] L. Valentini, V. Bavastrello, E. Stura, I. Armentano, C. Nicolini, J.M. Kenny, Sensors for inorganic vapor detection based on carbon nanotubes and poly(o-anisidine) nanocomposite material, Chem Phys Lett, 383 (2004) 617-622.
[73] C. Wei, L.M. Dai, A. Roy, T.B. Tolle, Multifunctional chemical vapor sensors of aligned carbon nanotube and polymer composites, J Am Chem Soc, 128 (2006) 1412-1413.
[74] J. Kong, M.G. Chapline, H.J. Dai, Functionalized carbon nanotubes for molecular hydrogen sensors, Adv Mater, 13 (2001) 1384-1386.
[75] I. Sayago, E. Terrado, M. Aleixandre, M.C. Horrillo, M.J. Fernandez, J. Lozano, E. Lafuente, W.K. Maser, A.M. Benito, M.T. Martinez, J. Gutierrez, E. Munoz, Novel selective sensors based on carbon nanotube films for hydrogen detection, Sensor Actuat B-Chem, 122 (2007) 75-80.
[76] S. Mubeen, T. Zhang, B. Yoo, M.A. Deshusses, N.V. Myung, Palladium nanoparticles decorated single-walled carbon nanotube hydrogen sensor, J Phys Chem C, 111 (2007) 6321-6327.
[77] Y.G. Sun, H.H. Wang, Electrodeposition of Pd nanoparticles on single-walled carbon nanotubes for flexible hydrogen sensors, Appl Phys Lett, 90 (2007) -.
[78] J. Sippel-Oakley, H.T. Wang, B.S. Kang, Z.C. Wu, F. Ren, A.G. Rinzler, S.J. Pearton, Carbon nanotube films for room temperature hydrogen sensing, Nanotechnology, 16 (2005) 2218-2221.
[79] D.Y. Ding, Z. Chen, S. Rajaputra, V. Singh, Hydrogen sensors based on aligned carbon nanotubes in an anodic aluminum oxide template with palladium as a top electrode, Sensor Actuat B-Chem, 124 (2007) 12-17.
[80] Y.J. Lu, J. Li, J. Han, H.T. Ng, C. Binder, C. Partridge, M. Meyyappan, Room temperature methane detection using palladium loaded single-walled carbon nanotube sensors, Chem Phys Lett, 391 (2004) 344-348.
[81] Y. Li, H.C. Wang, Y.S. Chen, M.J. Yang, A multi-walled carbon nanotube/palladium nanocomposite prepared by a facile method for the detection of methane at room temperature, Sensor Actuat B-Chem, 132 (2008) 155-158.
[82] M.K. Kumar, S. Ramaprabhu, Nanostructured Pt functionlized multiwalled carbon nanotube based hydrogen sensor, J Phys Chem B, 110 (2006) 11291-11298.

[83] M.K. Kumar, S. Ramaprabhu, Palladium dispersed multiwalled carbon nanotube based hydrogen sensor for fuel cell applications, Int J Hydrogen Energ, 32 (2007) 2518-2526.
[84] M.K. Kumar, A.L.M. Reddy, S. Ramaprabhu, Exfoliated single-walled carbon nanotube-based hydrogen sensor, Sensor Actuat B-Chem, 130 (2008) 653-660.
[85] G.V. Kamarchuk, I.G. Kolobov, A.V. Khotkevich, I.K. Yanson, A.P. Pospelov, I.A. Levitsky, W.B. Euler, New chemical sensors based on point heterocontact between single wall carbon nanotubes and gold wires, Sensor Actuat B-Chem, 134 (2008) 1022-1026.
[86] M. Penza, G. Cassano, R. Rossi, M. Alvisi, A. Rizzo, M.A. Signore, T. Dikonimos, E. Serra, R. Giorgi, Enhancement of sensitivity in gas chemiresistors based on carbon nanotube surface functionalized with noble metal (Au, Pt) nanoclusters, Appl Phys Lett, 90 (2007) -.
[87] E.H. Espinosa, R. Lonescu, C. Bittencourt, A. Felten, R. Erni, G. Van Tendeloo, J.J. Pireaux, E. Llobet, Metal-decorated multi-wall carbon nanotubes for low temperature gas sensing, Thin Solid Films, 515 (2007) 8322-8327.
[88] A. Star, V. Joshi, S. Skarupo, D. Thomas, J.C.P. Gabriel, Gas sensor array based on metal-decorated carbon nanotubes, J Phys Chem B, 110 (2006) 21014-21020.
[89] Y.J. Lu, C. Partridge, M. Meyyappan, J. Li, A carbon nanotube sensor array for sensitive gas discrimination using principal component analysis, J Electroanal Chem, 593 (2006) 105-110.
[90] B.Y. Wei, M.C. Hsu, P.G. Su, H.M. Lin, R.J. Wu, H.J. Lai, A novel SnO2 gas sensor doped with carbon nanotubes operating at room temperature, Sensor Actuat B-Chem, 101 (2004) 81-89.
[91] J.W. Gong, J.R. Sun, Q.F. Chen, Micromachined sol-gel carbon nanotube/SnO2 nanocomposite hydrogen sensor, Sensor Actuat B-Chem, 130 (2008) 829-835.
[92] N.D. Hoa, N. Van Quy, Y.S. Cho, D. Kim, Nanocomposite of SWNTs and SnO2 fabricated by soldering process for ammonia gas sensor application, Physica Status Solidi a-Applications and Materials Science, 204 (2007) 1820-1824.
[93] Y.L. Liu, H.F. Yang, Y. Yang, Z.M. Liu, G.L. Shen, R.Q. Yu, Gas sensing properties of tin dioxide coated onto multi-walled carbon nanotubes, Thin Solid Films, 497 (2006) 355-360.
[94] Y.J. Chen, C.L. Zhu, T.H. Wang, The enhanced ethanol sensing properties of multi-walled carbon nanotubes/SnO2 core/shell nanostructures, Nanotechnology, 17 (2006) 3012-3017.
[95] E.H. Espinosa, R. Ionescu, B. Chambon, G. Bedis, E. Sotter, C. Bittencourt, A. Felten, J.J. Pireaux, X. Correig, E. Llobet, Hybrid metal oxide and multiwall carbon nanotube films for low temperature gas sensing, Sensor Actuat B-Chem, 127 (2007) 137-142.
[96] N. Van Hieu, L.T.B. Thuy, N.D. Chien, Highly sensitive thin film NH3 gas sensor operating at room temperature based on SnO2/MWCNTs composite, Sensor Actuat B-Chem, 129 (2008) 888-895.
[97] J. Wang, L. Liu, S.Y. Cong, J.Q. Qi, B.K. Xu, An enrichment method to detect low concentration formaldehyde, Sensor Actuat B-Chem, 134 (2008) 1010-1015.
[98] C. Bittencourt, A. Felten, E.H. Espinosa, R. Ionescu, E. Llobet, X. Corteig, J.J. Pireaux, WO3 films modified with functionalised multi-wall carbon nanotubes: Morphological, compositional and gas response studies, Sensor Actuat B-Chem, 115 (2006) 33-41.
[99] M. Sanchez, R. Guirado, M.E. Rincon, Multiwalled carbon nanotubes embedded in sol-gel derived TiO2 matrices and their use as room temperature gas sensors, J Mater Sci-Mater El, 18 (2007) 1131-1136.
[100] E. Llobet, E.H. Espinosa, E. Sotter, R. Ionescu, X. Vilanova, J. Torres, A. Felten, J.J. Pireaux, X. Ke, G. Van Tendeloo, F. Renaux, Y. Paint, M. Hecq, C. Bittencourt, Carbon nanotube-TiO2 hybrid films for detecting traces of O-2, Nanotechnology, 19 (2008) -.
[101] V.D. Nguyen, V.H. Nguyen, T.H. Pham, D.C. Nguyen, M. Thamilselvan, J. Yi, Mixed SnO2/TiO2 included with carbon nanotubes for gas-sensing application, Physica E, 41 (2008) 258-263.
[102] M. Trojanowicz, Analytical applications of carbon nanotubes: a review, Trac-Trend Anal Chem, 25 (2006) 480-489.

[103] J. Wang, Stripping analysis at bismuth electrodes: A review, Electroanal, 17 (2005) 1341-1346.
[104] L.M. Dai, P.G. He, S.N. Li, Functionalized surfaces based on polymers and carbon nanotubes for some biomedical and optoelectronic applications, Nanotechnology, 14 (2003) 1081-1097.
[105] F.L. Cheng, S. Du, B.K. Jin, Electrochemical studies of cytochrome c on electrodes modified by single-wall carbon nanotubes, Chinese J Chem, 21 (2003) 436-441.
[106] Y.D. Zhao, Y.H. Bi, W.D. Zhang, Q.M. Luo, The interface behavior of hemoglobin at carbon nanotube and the detection for H2O2, Talanta, 65 (2005) 489-494.
[107] R.J. Chen, Y.G. Zhang, D.W. Wang, H.J. Dai, Noncovalent sidewall functionalization of single-walled carbon nanotubes for protein immobilization, J Am Chem Soc, 123 (2001) 3838-3839.
[108] C. Li, M. Curreli, H. Lin, B. Lei, F.N. Ishikawa, R. Datar, R.J. Cote, M.E. Thompson, C.W. Zhou, Complementary detection of prostate-specific antigen using ln(2)O(3) nanowires and carbon nanotubes, J Am Chem Soc, 127 (2005) 12484-12485.
[109] A. Star, Y. Liu, K. Grant, L. Ridvan, J.F. Stoddart, D.W. Steuerman, M.R. Diehl, A. Boukai, J.R. Heath, Noncovalent side-wall functionalization of single-walled carbon nanotubes, Macromolecules, 36 (2003) 553-560.
[110] A. Star, J.F. Stoddart, D. Steuerman, M. Diehl, A. Boukai, E.W. Wong, X. Yang, S.W. Chung, H. Choi, J.R. Heath, Preparation and properties of polymer-wrapped single-walled carbon nanotubes, Angew Chem Int Edit, 40 (2001) 1721-1725.
[111] M. Shim, N.W.S. Kam, R.J. Chen, Y.M. Li, H.J. Dai, Functionalization of carbon nanotubes for biocompatibility and biomolecular recognition, Nano Lett, 2 (2002) 285-288.
[112] Y. Lin, S. Taylor, H.P. Li, K.A.S. Fernando, L.W. Qu, W. Wang, L.R. Gu, B. Zhou, Y.P. Sun, Advances toward bioapplications of carbon nanotubes, J Mater Chem, 14 (2004) 527-541.
[113] K. Besteman, J.O. Lee, F.G.M. Wiertz, H.A. Heering, C. Dekker, Enzyme-coated carbon nanotubes as single-molecule biosensors, Nano Lett, 3 (2003) 727-730.
[114] M. Zheng, A. Jagota, E.D. Semke, B.A. Diner, R.S. Mclean, S.R. Lustig, R.E. Richardson, N.G. Tassi, DNA-assisted dispersion and separation of carbon nanotubes, Nat Mater, 2 (2003) 338-342.
[115] A.T.C. Johnson, C. Staii, M. Chen, S. Khamis, R. Johnson, M.L. Klein, A. Gelperin, DNA-decorated carbon nanotubes for chemical sensing, Semicond Sci Tech, 21 (2006) S17-S21.
[116] K. Maehashi, K. Matsumoto, K. Kerman, Y. Takamura, E. Tamiya, Ultrasensitive detection of DNA hybridization using carbon nanotube field-effect transistors, Jpn J Appl Phys 2, 43 (2004) L1558-L1560.
[117] X.W. Tang, S. Bansaruntip, N. Nakayama, E. Yenilmez, Y.L. Chang, Q. Wang, Carbon nanotube DNA sensor and sensing mechanism, Nano Lett, 6 (2006) 1632-1636.
[118] K. Maehashi, T. Katsura, K. Kerman, Y. Takamura, K. Matsumoto, E. Tamiya, Label-free protein biosensor based on aptamer-modified carbon nanotube field-effect transistors, Anal Chem, 79 (2007) 782-787.
[119] P. Debye, Dieletric Properties of Pure Liquids, Chem. Rev., 19 (1936) 171-182.
[120] P. Kral, M. Shapiro, Nanotube electron drag in flowing liquids, Phys Rev Lett, 86 (2001) 131-134.
[121] S. Ghosh, A.K. Sood, N. Kumar, Carbon nanotube flow sensors, Science, 299 (2003) 1042-1044.
[122] J.R. Wood, H.D. Wagner, Single-wall carbon nanotubes as molecular pressure sensors, Appl Phys Lett, 76 (2000) 2883-2885.
[123] C.K.M. Fung, M.Q.H. Zhang, R.H.M. Chan, W.J. Li, A PMMA-based micro pressure sensor chip using carbon nanotubes as sensing elements, in: Proc. 18th IEEE Conf. Micro Electro Mechanical Systems, 2005, pp. 251.

[124] C.M.K.M. Fung, V.T.S. Wong, R.H.M. Chan, W.J. Li, Dielectrophoretic batch fabrication of bundled carbon nanotube thermal sensors, Ieee T Nanotechnol, 3 (2004) 395-403.
[125] H.Y. Chiu, P. Hung, H.W.C. Postma, M. Bockrath, Atomic-Scale Mass Sensing Using Carbon Nanotube Resonators, Nano Lett, 8 (2008) 4342-4346.
[126] K. Jensen, K. Kim, A. Zettl, An atomic-resolution nanomechanical mass sensor, Nat Nanotechnol, 3 (2008) 533-537.
[127] J. Watson, F. Crick, Molecular structure of nucleic acids: a structure for deoxyribose nucleic acid, Nature, 171 (1953) 737-738.
[128] H.J. Gao, Y. Kong, Simulation of DNA-nanotube interactions, Annu Rev Mater Res, 34 (2004) 123-150.
[129] D.M.J. Lilley, Understanding DNA - the Molecule and How It Works - Calladine,Cr, Drew,Hr, Nature, 367 (1994) 330-331.
[130] W. Saenger, Principles of Nucleic Acid Structure, in: Springer, Berlin, 1988.
[131] T.R. Strick, M.N. Dessinges, G. Charvin, N.H. Dekker, J.F. Allemand, D. Bensimon, V. Croquette, Stretching of macromolecules and proteins, Rep Prog Phys, 66 (2003) 1-45.
[132] R. Wheeler, A-DNA, B-DNA and Z-DNA, in, Zephyris at en.wikipedia, 2007.
[133] R.V. Anthony, J.D. Cantlon, Ribonucleic acid interference: A new approach to the in vivo study of gene function, J Anim Sci, 85 (2007) E18-E19.
[134] Ribonucleic acid, in, Wikipedia.
[135] E. Generalic, Ribonucleic Acid, in: C.-E.C.D. Glossary (Ed.), 2011.
[136] Z.J. Tan, S.J. Chen, Salt dependence of nucleic acid hairpin stability, Biophys J, 95 (2008) 738-752.
[137] D.H. Mathews, M.D. Disney, J.L. Childs, S.J. Schroeder, M. Zuker, D.H. Turner, Incorporating chemical modification constraints into a dynamic programming algorithm for prediction of RNA secondary structure, P Natl Acad Sci USA, 101 (2004) 7287-7292.
[138] R.R. Johnson, A.T.C. Johnson, M.L. Klein, Probing the structure of DNA-carbon nanotube hybrids with molecular dynamics, Nano Lett, 8 (2008) 69-75.
[139] H.J. Gao, Y. Kong, D.X. Cui, C.S. Ozkan, Spontaneous insertion of DNA oligonucleotides into carbon nanotubes, Nano Lett, 3 (2003) 471-473.
[140] G.I. Dovbeshko, O.P. Repnytska, E.D. Obraztsova, Y.V. Shtogun, DNA interaction with single-walled carbon nanotubes: a SEIRA study, Chem Phys Lett, 372 (2003) 432-437.
[141] M.J. O'Connell, P. Boul, L.M. Ericson, C. Huffman, Y.H. Wang, E. Haroz, C. Kuper, J. Tour, K.D. Ausman, R.E. Smalley, Reversible water-solubilization of single-walled carbon nanotubes by polymer wrapping, Chem Phys Lett, 342 (2001) 265-271.
[142] D.A. Heller, E.S. Jeng, T.K. Yeung, B.M. Martinez, A.E. Moll, J.B. Gastala, M.S. Strano, Optical detection of DNA conformational polymorphism on single-walled carbon nanotubes, Science, 311 (2006) 508-511.
[143] C. Staii, A.T. Johnson, DNA-decorated carbon nanotubes for chemical sensing, Nano Lett, 5 (2005) 1774-1778.
[144] L.B. Zhang, L. Tao, B.L. Li, L. Jing, E.K. Wang, Carbon nanotube-DNA hybrid fluorescent sensor for sensitive and selective detection of mercury(II) ion, Chem Commun, 46 (2010) 1476-1478.
[145] X.C. Dong, D.L. Fu, Y.P. Xu, J.Q. Wei, Y.M. Shi, P. Chen, L.J. Li, Label-free electronic detection of DNA using simple double-walled carbon nanotube resistors, J Phys Chem C, 112 (2008) 9891-9895.
[146] R.H. Yang, J.Y. Jin, Y. Chen, N. Shao, H.Z. Kang, Z. Xiao, Z.W. Tang, Y.R. Wu, Z. Zhu, W.H. Tan, Carbon nanotube-quenched fluorescent oligonucleotides: Probes that fluoresce upon hybridization, J Am Chem Soc, 130 (2008) 8351-8358.
[147] Y. Xu, P.E. Pehrsson, L.W. Chen, R. Zhang, W. Zhao, Double-stranded DNA single-walled carbon nanotube hybrids for optical hydrogen peroxide and glucose sensing, J Phys Chem C, 111 (2007) 8638-8643.

[148] Y. Xu, P.E. Pehrsson, L.W. Chen, W. Zhao, Controllable redox reaction of chemically purified DNA-single walled carbon nanotube hybrids with hydrogen peroxide, J Am Chem Soc, 130 (2008) 10054-+.
[149] P.D. Tam, V.N. Hieu, N.D. Chien, A.T. Le, M.A. Tuan, DNA sensor development based on multi-wall carbon nanotubes for label-free influenza virus (type A) detection, J Immunol Methods, 350 (2009) 118-124.
[150] C.W. Liu, C.C. Huang, H.T. Chang, Highly Selective DNA-Based Sensor for Lead(II) and Mercury(II) Ions, Anal Chem, 81 (2009) 2383-2387.
[151] Y. Ataseven, E. Olhan, Environmental Evaluation of Pollutions Due to Agricultural Activities in Drinking Water Basins, J Environ Prot Ecol, 11 (2010) 1253-1263.
[152] D. Oberson, D. Lafon, Environmental pollutions and effects on reproduction: A glance at the past, Arch Mal Prof Enviro, 71 (2010) 141-150.
[153] H.L. Alaoui, K. Oufdou, N. Mezrioui, Environmental pollutions impacts on the bacteriological and physicochemical quality of suburban and rural groundwater supplies in Marrakesh area (Morocco), Environ Monit Assess, 145 (2008) 195-207.
[154] J.J. Berger, Environmental Restoration: Science and strategies for restoring the earth, Island Press, Washington, D.C., 1990.
[155] Environmental Pollution and Impacts on Public Health: Implications of the Dandora Municipal Dumping Site in Nairobi, Kenya, in: U.N.E.P.U. Urban Environment Unit (Ed.), Urban Environment Unit, United Nations Environment Programme (UNEP).
[156] Sicence and Technology of United States Environmental Protection Agency for Air Quality monitoring, in.
[157] EPA, Learn the Issues: Emergencies, in: U.S.E.P. Agency (Ed.), 2012.
[158] E.A. Johnson, H.F. Lam, L.S. Katafygiotis, J.L. Beck, A benchmark problem for structural health monitoring and damage detection, in: Fabio Casciati, G. Magonette (Eds.) Structural Control for Civil and Infrastructure Engineering, World Scientific, 2001, pp. 317.
[159] J. Appenzeller, R. Martel, V. Derycke, M. Radosavjevic, S. Wind, D. Neumayer, P. Avouris, Carbon nanotubes as potential building blocks for future nanoelectronics, Microelectron Eng, 64 (2002) 391-397.
[160] A. Tanioka, K. Suzuki, H. Matsumoto, M. Minagawa, Y. Hayashi, K. Fukuzono, G.A.J. Amaratunga, Carbon nanotubes on carbon fabrics for flexible field emitter arrays, Appl Phys Lett, 93 (2008).
[161] Y. Battie, O. Ducloux, P. Thobois, N. Dorval, J.S. Lauret, B. Attal-Tretout, A. Loiseau, Gas sensors based on thick films of semi-conducting single walled carbon nanotubes, Carbon, 49 (2011) 3544-3552.
[162] R.V. Gelamo, F.P. Rouxinol, C. Verissimo, M.A.B. de Moraes, S.A. Moshkalev, Gas and Pressure Sensors Based on Multi-Wall Carbon Nanotubes: Study of Sensing Mechanisms, Sensor Lett, 8 (2010) 488-492.
[163] A. Javey, J. Guo, Q. Wang, M. Lundstrom, H.J. Dai, Ballistic carbon nanotube field-effect transistors, Nature, 424 (2003) 654-657.
[164] S. Iijima, Carbon nanotubes: past, present, and future, Physica B, 323 (2002) 1-5.
[165] Y.G. Sun, H.H. Wang, High-performance, flexible hydrogen sensors that use carbon nanotubes decorated with palladium nanoparticles, Adv Mater, 19 (2007) 2818-+.
[166] A.A. Tomchenko, G.P. Harmer, B.T. Marquis, J.W. Allen, Semiconducting metal oxide sensor array for the selective detection of combustion gases, Sensor Actuat B-Chem, 93 (2003) 126-134.
[167] Y.T. Jang, S.I. Moon, J.H. Ahn, Y.H. Lee, B.K. Ju, A simple approach in fabricating chemical sensor using laterally grown multi-walled carbon nanotubes, Sensor Actuat B-Chem, 99 (2004) 118-122.

[168] R.J. Chen, H.C. Choi, S. Bangsaruntip, E. Yenilmez, X.W. Tang, Q. Wang, Y.L. Chang, H.J. Dai, An investigation of the mechanisms of electronic sensing of protein adsorption on carbon nanotube devices, J Am Chem Soc, 126 (2004) 1563-1568.
[169] Y.H. Lin, F. Lu, Y. Tu, Z.F. Ren, Glucose biosensors based on carbon nanotube nanoelectrode ensembles, Nano Lett, 4 (2004) 191-195.
[170] M. Chen, S. Datta, S. Khamis, J.E. Fischer, A.T. Johnson, RNA Functionalized Carbon Nanotube for Chemical Sensing, in: NIST-nanotechnology, 2010, pp. 191-194.
[171] J.J. Zhao, H.K. Park, J. Han, J.P. Lu, Electronic properties of carbon nanotubes with covalent sidewall functionalization, J Phys Chem B, 108 (2004) 4227-4230.
[172] S.M. Khamis, R.R. Johnson, Z.T. Luo, A.T.C. Johnson, Homo-DNA functionalized carbon nanotube chemical sensors, J Phys Chem Solids, 71 (2010) 476-479.
[173] A. Fraser, RNA Interface: Human Genes Hit the Big Screen, Nature, 428 (2004) 375-378.
[174] G.L. Conn, D.E. Draper, RNA structure, Curr Opin Struc Biol, 8 (1998) 278-285.
[175] M. Afshar, C.D. Prescott, G. Varani, Structure-based and combinatorial search for new RNA-binding drugs, Curr Opin Biotech, 10 (1999) 59-63.
[176] H.M. So, D.W. Park, E.K. Jeon, Y.H. Kim, B.S. Kim, C.K. Lee, S.Y. Choi, S.C. Kim, H. Chang, J.O. Lee, Detection and titer estimation of Escherichia coli using aptamer-functionalized single-walled carbon-nanotube field-effect transistors, Small, 4 (2008) 197-201.
[177] C.L. Chen, C.F. Yang, V. Agarwal, T. Kim, S. Sonkusale, A. Busnaina, M. Chen, M.R. Dokmeci, DNA-decorated carbon-nanotube-based chemical sensors on complementary metal oxide semiconductor circuitry, Nanotechnology, 21 (2010) -.
[178] C. Zhao, Y.H. Peng, Y.J. Song, J.S. Ren, X.G. Qu, Self-assembly of single-stranded RNA on carbon nanotube: Polyadenylic acid to form a duplex structure, Small, 4 (2008) 656-661.
[179] C. Lamprecht, I. Liashkovich, V. Neves, J. Danzberger, E. Heister, M. Rangl, H.M. Coley, J. McFadden, E. Flahaut, H.J. Gruber, P. Hinterdorfer, F. Kienberger, A. Ebner, AFM imaging of functionalized carbon nanotubes on biological membranes, Nanotechnology, 20 (2009) -.
[180] R. Rao, J. Lee, Q. Lu, G. Keskar, K.O. Freedman, W.C. Floyd, A.M. Rao, P.C. Ke, Single-molecule fluorescence microscopy and Raman spectroscopy studies of RNA bound carbon nanotubes, Appl Phys Lett, 85 (2004) 4228-4230.
[181] H. William, CRC Handbook of Chemistry and Physics, CRC Press, 2010.
[182] X. Zhao, J.K. Johnson, Simulation of adsorption of DNA on carbon nanotubes, J Am Chem Soc, 129 (2007) 10438-10445.
[183] Y. Liu, M. Chen, M.L. Wang, M.R. Dokmeci, Sensing Characteristics of RNA Oligomer Coated SWNT Gas Sensors, in: Proceedings of the 16th international Conference on Solid-State Sensors, Actuators and Microsystems (Transducers '11), Beijing, China, 2011.
[184] E.A. Lesnik, S.M. Freier, Relative Thermodynamic Stability of DNA, Rna, and DNA-Rna Hybrid Duplexes - Relationship with Base Composition and Structure, Biochemistry-Us, 34 (1995) 10807-10815.
[185] A. Star, E. Tu, J. Niemann, J.C.P. Gabriel, C.S. Joiner, C. Valcke, Label-free detection of DNA hybridization using carbon nanotube network field-effect transistors, P Natl Acad Sci USA, 103 (2006) 921-926.
[186] N.N. Zhu, Y.Q. Lin, P. Yu, L. Su, L.Q. Mao, Label-free and sequence-specific DNA detection down to a picomolar level with carbon nanotubes as support for probe DNA, Anal Chim Acta, 650 (2009) 44-48.
[187] P.C. Ke, R. Qiao, Carbon nanomaterials in biological systems, J Phys-Condens Mat, 19 (2007).
[188] X.G. Qu, X. Li, Y.H. Peng, Carbon nanotubes selective destabilization of duplex and triplex DNA and inducing B-A transition in solution, Nucleic Acids Res, 34 (2006) 3670-3676.
[189] E.S. Jeng, P.W. Barone, J.D. Nelson, M.S. Strano, Hybridization kinetics and thermodynamics of DNA adsorbed to individually dispersed single-walled carbon nanotubes, Small, 3 (2007) 1602-1609.

[190] E.L. Gui, L.J. Li, P.S. Lee, A. Lohani, S.G. Mhaisalkar, Q. Cao, S.J. Kang, J.A. Rogers, N.C. Tansil, Z.Q. Gao, Electrical detection of hybridization and threading intercalation of deoxyribonucleic acid using carbon nanotube network field-effect transistors, Appl Phys Lett, 89 (2006).
[191] X.D. Cui, M. Freitag, R. Martel, L. Brus, P. Avouris, Controlling energy-level alignments at carbon nanotube/Au contacts, Nano Lett, 3 (2003) 783-787.
[192] Y. Liu, M. Chen, M. Mohebbi, M.L. Wang, M.R. Dokmeci, The Effect of Sequence Length on DNA Decorated CNT Gas Sensors, in: Proceedings of the 16th international Conference on Solid-State Sensors, Actuators and Microsystems (Transducers '11), Beijing, China, 2011.
[193] V. Dusastre, Electronic noses: Principles and applications, Nature, 402 (1999) 351-352.
[194] J. Mizsei, V. Lantto, Air-Pollution Monitoring with a Semiconductor Gas Sensor Array System, Sensor Actuat B-Chem, 6 (1992) 223-227.
[195] S. Capone, P. Siciliano, N. Barsan, U. Weimar, L. Vasanelli, Analysis of CO and CH4 gas mixtures by using a micromachined sensor array, Sensor Actuat B-Chem, 78 (2001) 40-48.
[196] L. Fernandez, A. Gutierrez-Galvez, J. Fonollosa, S. Marco, A biomimetic gas sensor array system designed to test computational olfaction models, Chem Senses, 36 (2011) E16-E17.
[197] A.K. Srivastava, Detection of volatile organic compounds (VOCs) using SnO2 gas-sensor array and artificial neural network, Sensor Actuat B-Chem, 96 (2003) 24-37.
[198] K.D. Mitzner, J. Sternhagen, D.W. Galipeau, Development of a micromachined hazardous gas sensor array, Sensor Actuat B-Chem, 93 (2003) 92-99.
[199] C.J. Lu, J. Whiting, R.D. Sacks, E.T. Zellers, Portable gas chromatograph with tunable retention and sensor array detection for determination of complex vapor mixtures, Anal Chem, 75 (2003) 1400-1409.
[200] K.M. Lee, J.B. Yu, H.K. Jun, J.O. Lim, D.D. Lee, H.G. Byun, J.S. Huh, Volatile organic gas recognition using conducting polymer sensor array, Eco-Materials Processing & Design, 439 (2003) 344-351.
[201] A.L. Kukla, A.S. Pavluchenko, Y.M. Shirshov, N.V. Konoshchuk, O.Y. Posudievsky, Application of sensor arrays based on thin films of conducting polymers for chemical recognition of volatile organic solvents, Sensor Actuat B-Chem, 135 (2009) 541-551.
[202] C. Viespe, C. Grigoriu, C. Toader, I.M. Popescu, Nanocomposite Coated Surface Acoustic Wave Sensor for Chemical Warfare Agent Detections, U Politeh Buch Ser A, 73 (2011) 195-200.
[203] S.G. Chen, J. Mao, B.X. Han, N.F. Chen, Scent analysis of Rosa laevigata through metal oxide sensor array electronic nose, Rev Bras Farmacogn, 21 (2011) 1150-1154.
[204] H.P. Lang, R. Berger, F. Battiston, J.P. Ramseyer, E. Meyer, C. Andreoli, J. Brugger, P. Vettiger, M. Despont, T. Mezzacasa, L. Scandella, H.J. Guntherodt, C. Gerber, J.K. Gimzewski, A chemical sensor based on a micromechanical cantilever array for the identification of gases and vapors, Appl Phys a-Mater, 66 (1998) S61-S64.
[205] Changjun Hou, Jiangjie Li, Danqun Huo, Xiaogang Luo, Jiale Dong, Mei Yang, X. Shi, A portable embedded toxic gas detection device based on a cross-responsive sensor array, Sensor Actuat B-Chem, 161 (2012) 244-250.
[206] H.L. Tai, Y.D. Jiang, G.Z. Xie, J.S. Yu, M.J. Zhao, Self-assembly of TiO2/polypyrrole nanocomposite ultrathin films and application for an NH3 gas sensor, Int J Environ an Ch, 87 (2007) 539-551.
[207] E.N. Dattoli, A.V. Davydov, K.D. Benkstein, Tin oxide nanowire sensor with integrated temperature and gate control for multi-gas recognition, Nanoscale, 4 (2012) 1760-1769.
[208] Y.W. Cheng, Z. Yang, H. Wei, Y.Y. Wang, L.M. Wei, Y.F. Zhang, Progress in Carbon Nanotube Gas Sensor Research, Acta Phys-Chim Sin, 26 (2010) 3127-3142.
[209] M. Castro, B. Kumar, J.F. Feller, Z. Haddi, A. Amari, B. Bouchikhi, Novel e-nose for the discrimination of volatile organic biomarkers with an array of carbon nanotubes (CNT) conductive polymer nanocomposites (CPC) sensors, Sensor Actuat B-Chem, 159 (2011) 213-219.

[210] M. Penza, G. Cassano, P. Aversa, A. Cusano, A. Cutolo, M. Giordano, L. Nicolais, Carbon nanotube acoustic and optical sensors for volatile organic compound detection, Nanotechnology, 16 (2005) 2536-2547.
[211] P. Makaram, S. Selvarasah, X.G. Xiong, C.L. Chen, A. Busnaina, N. Khanduja, M.R. Dokmeci, Three-dimensional assembly of single-walled carbon nanotube interconnects using dielectrophoresis, Nanotechnology, 18 (2007) -.
[212] K.L. Shepard, S. Sorgenfrei, C.Y. Chiu, R.L. Gonzalez, Y.J. Yu, P. Kim, C. Nuckolls, Label-free single-molecule detection of DNA-hybridization kinetics with a carbon nanotube field-effect transistor, Nat Nanotechnol, 6 (2011) 125-131.
[213] D.K. Dubey, D. Pardasani, A. Purohit, A. Mazumder, Gas chromatography-mass spectrometric analysis of trimethylsilyl derivatives of toxic hydrolyzed products of nerve agent VX and its analogues for verification of Chemical Weapons Convention, Anal Methods-Uk, 2 (2010) 661-667.
[214] R.G. Cooks, I. Cotte-Rodriguez, D.R. Justes, S.C. Nanita, R.J. Noll, C.C. Mulligan, N.L. Sanders, Analysis of gaseous toxic industrial compounds and chemical warfare agent simulants by atmospheric pressure ionization mass spectrometry, Analyst, 131 (2006) 579-589.
[215] G.A. Eiceman, Ion mobility spectrometry as detector and sensor for chemical warfare agents and toxic industrial chemicals., Abstr Pap Am Chem S, 224 (2002) U145-U145.
[216] L. Valentini, I. Armentano, J.M. Kenny, C. Cantalini, L. Lozzi, S. Santucci, Sensors for sub-ppm NO2 gas detection based on carbon nanotube thin films, Appl Phys Lett, 82 (2003) 961-963.
[217] H. Nanto, T. Minami, S. Takata, Zinc-Oxide Thin-Film Ammonia Gas Sensors with High-Sensitivity and Excellent Selectivity, J Appl Phys, 60 (1986) 482-484.
[218] M. Park, L.N. Cella, W.F. Chen, N.V. Myung, A. Mulchandani, Carbon nanotubes-based chemiresistive immunosensor for small molecules: Detection of nitroaromatic explosives, Biosens Bioelectron, 26 (2010) 1297-1301.
[219] X.Q. Lu, Y.L. Quan, Z.H. Xue, B.W. Wu, H.T. Qi, D. Liu, Determination of explosives based on novel type of sensor using porphyrin functionalized carbon nanotubes, Colloid Surface B, 88 (2011) 396-401.
[220] J.P. Novak, E.S. Snow, E.J. Houser, D. Park, J.L. Stepnowski, R.A. McGill, Nerve agent detection using networks of single-walled carbon nanotubes, Appl Phys Lett, 83 (2003) 4026-4028.
[221] C.J. Hou, J.L. Dong, D.Q. Huo, Y.J. Duan, W. Luo, ANYL 268-Novel self-assembled films of porphyrin-functionalized single-wall carbon nanotubes for DMMP detection, Abstr Pap Am Chem S, 236 (2008).
[222] Y.Y. Wang, Z.H. Zhou, Z. Yang, X.H. Chen, D. Xu, Y.F. Zhang, Gas sensors based on deposited single-walled carbon nanotube networks for DMMP detection, Nanotechnology, 20 (2009).
[223] P.G. Collins, M.S. Fuhrer, A. Zettl, 1/f noise in carbon nanotubes, Appl Phys Lett, 76 (2000) 894-896.
[224] S. Reza, Q.T. Huynh, G. Bosman, J. Sippel-Oakley, A.G. Rinzler, 1/f noise in metallic and semiconducting carbon nanotubes, J Appl Phys, 100 (2006).
[225] Y.M. Lin, J. Appenzeller, Z.H. Chen, P. Avouris, Electrical transport and 1/f noise in semiconducting carbon nanotubes, Physica E, 37 (2007) 72-77.
[226] H.B. Glasgow, J.M. Burkholder, R.E. Reed, A.J. Lewitus, J.E. Kleinman, Real-time remote monitoring of water quality: a review of current applications, and advancements in sensor, telemetry, and computing technologies, J Exp Mar Biol Ecol, 300 (2004) 409-448.
[227] F.J. Rawson, D.J. Garrett, D. Leech, A.J. Downard, K.H.R. Baronian, Electron transfer from Proteus vulgaris to a covalently assembled, single walled carbon nanotube electrode functionalised with osmium bipyridine complex: Application to a whole cell biosensor, Biosens Bioelectron, 26 (2011) 2383-2389.

[228] M. Kaempgen, S. Roth, Transparent and flexible carbon nanotube/polyaniline pH sensors, J Electroanal Chem, 586 (2006) 72-76.
[229] M.E. Roberts, M.C. LeMieux, Z.N. Bao, Sorted and Aligned Single-Walled Carbon Nanotube Networks for Transistor-Based Aqueous Chemical Sensors, Acs Nano, 3 (2009) 3287-3293.
[230] E.S. Forzani, X.L. Li, P.M. Zhang, N.J. Tao, R. Zhang, I. Amlani, R. Tsui, L.A. Nagahara, Tuning the chemical selectivity of SWNT-FETs for detection of heavy-metal ions, Small, 2 (2006) 1283-1291.
[231] R.H. Zhou, P. Wang, H.C. Chang, Bacteria capture, concentration and detection by alternating current dielectrophoresis and self-assembly of dispersed single-wall carbon nanotubes, Electrophoresis, 27 (2006) 1376-1385.
[232] M. Bhattacharya, S. Hong, D. Lee, T. Cui, S.M. Goyal, Carbon nanotube based sensors for the detection of viruses, Sensor Actuat B-Chem, In press (2010) 8.
[233] G.M. Whitesides, The origins and the future of microfluidics, Nature, 442 (2006) 368-373.
[234] Y.C. Toh, C. Zhang, J. Zhang, Y.M. Khong, S. Chang, V.D. Samper, D. van Noort, D.W. Hutmacher, H.R. Yu, A novel 3D mammalian cell perfusion-culture system in microfluidic channels, Lab Chip, 7 (2007) 302-309.
[235] Y.C. Tan, J.S. Fisher, A.I. Lee, V. Cristini, A.P. Lee, Design of microfluidic channel geometries for the control of droplet volume, chemical concentration, and sorting, Lab Chip, 4 (2004) 292-298.
[236] J. Liu, Q. Fu, Integrated single-walled carbon nanotube/microfluidic devices for the study of the sensing mechanism of nanotube sensors, J Phys Chem B, 109 (2005) 13406-13408.
[237] B. Bourlon, J. Wong, C. Miko, L. Forro, M. Bockrath, A nanoscale probe for fluidic and ionic transport, Nat Nanotechnol, 2 (2007) 104-107.
[238] G.M. Whitesides, J.C. McDonald, Poly(dimethylsiloxane) as a material for fabricating microfluidic devices, Accounts Chem Res, 35 (2002) 491-499.
[239] M.R. Dokmeci, S. Selvarasah, S.H. Chao, C.L. Chen, S. Sridhar, A. Busnaina, A. Khademhosseini, A reusable high aspect ratio parylene-C shadow mask technology for diverse micropatterning applications, Sensor Actuat a-Phys, 145 (2008) 306-315.
[240] Y. Woo, G.S. Duesberg, S. Roth, Reduced contact resistance between an individual single-walled carbon nanotube and a metal electrode by a local point annealing, Nanotechnology, 18 (2007).
[241] LCRA, Water quality indicators-Key measures provide a snapshot of conditions in: E.w.a.c.s.f.C. Texas (Ed.), Energy water and community services for Central Texas Austin, Texas, 2011.
[242] S.R. Lustig, A. Jagota, C. Khripin, M. Zheng, Theory of structure-based carbon nanotube separations by ion-exchange chromatography of DNA/CNT hybrids, J Phys Chem B, 109 (2005) 2559-2566.
[243] L. Gordon, W.R. Hartley, Drinking water health advisory: Munitions, in: O.o.D.W.H.A.a.U.S.E.P. Agency (Ed.), Lewis, Boca Raton, FL, 1992, pp. 327-398.
[244] R.H. Ross, W.R. Hartley, Comparison of Water-Quality Criteria and Health Advisories for 2,4,6-Trinitrotoluene, Regul Toxicol Pharm, 11 (1990) 114-117.
[245] M.G. Ryon, R.H. Ross, Water-Quality Criteria for 2,4,6-Trinitrotoluene, Regul Toxicol Pharm, 11 (1990) 104-113.
[246] S.D. Harvey, R.J. Fellows, D.A. Cataldo, R.M. Bean, Analysis of 2,4,6-Trinitrotoluene and Its Transformation Products in Soils and Plant-Tissues by High-Performance Liquid-Chromatography, J Chromatogr, 518 (1990) 361-374.
[247] B.S. Levine, E.M. Furedi, D.E. Gordon, J.J. Barkley, P.M. Lish, Toxic Interactions of the Munitions Compounds Tnt and Rdx in F344 Rats, Fund Appl Toxicol, 15 (1990) 373-380.
[248] J.P. Lynch, K.J. Loh, A Summary Review of Wireless Sensors and Sensor Networks for Structural Health Monitoring, The Shock and Vibration Digest, 38 (2006) 91-128.

[249] Heng-lin Lv, Cheng-ming Zhao, Lei Song, Ying Ma, C.-h. Xu, Damage and deterioration mechanism and curing technique of concrete structure in main coal cleaning plants, Mining Science and Technology (China), 19 (2009) 750-755.
[250] R.A. Esmaeel, J. Briand, F. Taheri, Computational simulation and experimental verification of a new vibration-based structural health monitoring approach using piezoelectric sensors, Struct Health Monit, 11 (2012) 237-250.
[251] J. Kullaa, Distinguishing between sensor fault, structural damage, and environmental or operational effects in structural health monitoring, Mech Syst Signal Pr, 25 (2011) 2976-2989.
[252] W.I. Liao, J.X. Wang, G. Song, H. Gu, C. Olmi, Y.L. Mo, K.C. Chang, C.H. Loh, Structural health monitoring of concrete columns subjected to seismic excitations using piezoceramic-based sensors, Smart Mater Struct, 20 (2011).
[253] B. Torres, I. Paya-Zaforteza, P.A. Calderon, J.M. Adam, Analysis of the strain transfer in a new FBG sensor for Structural Health Monitoring, Eng Struct, 33 (2011) 539-548.
[254] I.P. Kang, M.J. Schulz, J.H. Kim, V. Shanov, D.L. Shi, A carbon nanotube strain sensor for structural health monitoring, Smart Mater Struct, 15 (2006) 737-748.
[255] G. Hegde, A. Asundi, Performance analysis of all-fiber polarimetric strain sensor for composites structural health monitoring, Ndt&E Int, 39 (2006) 320-327.
[256] D.P.J. Cotton, I.M. Graz, S.P. Lacour, A Multifunctional Capacitive Sensor for Stretchable Electronic Skins, Ieee Sens J, 9 (2009) 2008-2009.
[257] C.J. Yu, Z.Y. Wang, H.Y. Yu, H.Q. Jiang, A stretchable temperature sensor based on elastically buckled thin film devices on elastomeric substrates, Appl Phys Lett, 95 (2009).
[258] K.L. Lin, K. Jain, Design and Fabrication of Stretchable Multilayer Self-Aligned Interconnects for flexible Electronics and Large-Area Sensor Arrays Using Excimer Laser Photoablation, Ieee Electr Device L, 30 (2009) 14-17.
[259] T. Sekitani, H. Nakajima, H. Maeda, T. Fukushima, T. Aida, K. Hata, T. Someya, Stretchable active-matrix organic light-emitting diode display using printable elastic conductors, Nat Mater, 8 (2009) 494-499.
[260] S. Cheng, Z.G. Wu, A Microfluidic, Reversibly Stretchable, Large-Area Wireless Strain Sensor, Adv Funct Mater, 21 (2011) 2282-2290.
[261] T. Yamada, Y. Hayamizu, Y. Yamamoto, Y. Yomogida, A. Izadi-Najafabadi, D.N. Futaba, K. Hata, A stretchable carbon nanotube strain sensor for human-motion detection, Nat Nanotechnol, 6 (2011) 296-301.
[262] W.M. Choi, J.Z. Song, D.Y. Khang, H.Q. Jiang, Y.Y. Huang, J.A. Rogers, Biaxially stretchable "Wavy" silicon nanomembranes, Nano Lett, 7 (2007) 1655-1663.
[263] D.Y. Khang, J.L. Xiao, C. Kocabas, S. MacLaren, T. Banks, H.Q. Jiang, Y.Y.G. Huang, J.A. Rogers, Molecular scale buckling mechanics on individual aligned single-wall carbon nanotubes on elastomeric substrates, Nano Lett, 8 (2008) 124-130.
[264] D.H. Kim, J.Z. Song, W.M. Choi, H.S. Kim, R.H. Kim, Z.J. Liu, Y.Y. Huang, K.C. Hwang, Y.W. Zhang, J.A. Rogers, Materials and noncoplanar mesh designs for integrated circuits with linear elastic responses to extreme mechanical deformations, P Natl Acad Sci USA, 105 (2008) 18675-18680.
[265] T. Sekitani, Y. Noguchi, K. Hata, T. Fukushima, T. Aida, T. Someya, A rubberlike stretchable active matrix using elastic conductors, Science, 321 (2008) 1468-1472.
[266] T.S. Hansen, K. West, O. Hassager, N.B. Larsen, Highly stretchable and conductive polymer material made from poly (3,4-ethylenedioxythiophene) and polyurethane elastomers, Adv Funct Mater, 17 (2007) 3069-3073.
[267] J. Jones, S.P. Lacour, S. Wagner, Z.G. Suo, Stretchable wavy metal interconnects, Journal of Vacuum Science & Technology A, 22 (2004) 1723-1725.
[268] D.C. Hyun, M. Park, C. Park, B. Kim, Y. Xia, J.H. Hur, J.M. Kim, J.J. Park, U. Jeong, Ordered Zigzag Stripes of Polymer Gel/Metal Nanoparticle Composites for Highly Stretchable Conductive Electrodes, Adv Mater, 23 (2011) 2946-+.

[269] N.K. Chang, C.C. Su, S.H. Chang, Fabrication of single-walled carbon nanotube flexible strain sensors with high sensitivity, Appl Phys Lett, 92 (2008).
[270] E.D. Minot, Y. Yaish, V. Sazonova, J.Y. Park, M. Brink, P.L. McEuen, Tuning carbon nanotube band gaps with strain, Phys Rev Lett, 90 (2003).
[271] H. Jung, D.J. Lee, H.T. Chun, N.J. Koh, Y.R. Cho, D.G. Lee, Carbon nanotube field emitters for display applications using screen printing, Pricm 5: The Fifth Pacific Rim International Conference on Advanced Materials and Processing, Pts 1-5, 475-479 (2005) 1889-1892.
[272] S. Tawfick, K. O'Brien, A.J. Hart, Flexible High-Conductivity Carbon-Nanotube Interconnects Made by Rolling and Printing, Small, 5 (2009) 2467-2473.
[273] G. Keulemans, F. Ceyssens, M. De Volder, J.W. Seo, R. Puers, Fabrication and Characterisation of carbon nanotube composites for strain sensor applications, in: MME 2010 edition:21 location:Entschede, The Netherlands date:27-29 September 2010, Proceedings of the 21st Micromechanics and Micro systems Europe Workshop, Entschede, The Netherlands, 2010.
[274] G.Y. Yang, V.J. Bailey, Y.-H. Wen, G. Lin;, W.C. Tang, J.H. Keyak, Fabrication and characterization of microscale sensors for bone surface strain measurement, in: Sensors, 2004. Proceedings of IEEE Vienna, Austria, 2004, pp. 1355 - 1358.
[275] C.L. Chen, E. Lopez, Y.J. Jung, S. Muftu, S. Selvarasah, M.R. Dokmeci, Mechanical and electrical evaluation of parylene-C encapsulated carbon nanotube networks on a flexible substrate, Appl Phys Lett, 93 (2008).
[276] H. Maune, M. Bockrath, Elastomeric carbon nanotube circuits for local strain sensing, Appl Phys Lett, 89 (2006).
[277] Q. Cao, J.A. Rogers, Ultrathin Films of Single-Walled Carbon Nanotubes for Electronics and Sensors: A Review of Fundamental and Applied Aspects, Adv Mater, 21 (2009) 29-53.
[278] P.S. Na, H.J. Kim, H.M. So, K.J. Kong, H.J. Chang, B.H. Ryu, Y.M. Choi, J.O. Lee, B.K. Kim, J.J. Kim, J.H. Kim, Investigation of the humidity effect on the electrical properties of single-walled carbon nanotube transistors, Appl Phys Lett, 87 (2005) -.
[279] C.W. Bauschlicher, High coverages of hydrogen on a (10,0) carbon nanotube, Nano Lett, 1 (2001) 223-226.
[280] Z.R. Tang, The adsorption of methanol at the defective site of single-walled carbon nanotube, Physica B, 405 (2010) 770-773.
[281] S. Chopra, A. Pham, J. Gaillard, A. Parker, A.M. Rao, Carbon-nanotube-based resonant-circuit sensor for ammonia, Appl Phys Lett, 80 (2002) 4632-4634.

PUBLICATIONS

Journal

1. Y. Liu, H. H. Wang, J. E. Indacochea, M. L. Wang, "A Colorimetric Sensor Based on Anodized Aluminum Oxide (AAO) Substrate for the Detection of Nitroaromatics", *Sensors and Actuators B: Chemical, 160, 1149-1158, 2011*.
2. Y. Liu, C.-L. Chen, Y. Zhang, S. Sonkusale, M. L. Wang and M. R. Dokmeci, "SWNT based Nanosensors for Wireless Detection of Explosives and Chemical Warfare Agents," *Sensors Journal, IEEE*, 2011-submitted.
3. Y. Liu, M. Chen, M. Mohebbi, M. L. Wang and M. R. Dokmeci, "The Effect of Sequence Length on Gas Sensing Characteristics of DNA Decorated SWNT Sensors", *Sensors and Actuators B: Chemical*, 2011 – under revision.
4. X. Li, S. Selvarasah, Y. Liu, M. Mohebbi and M. R. Dokmeci, "Highly Sensitive Single-stranded DNA decorated Single-Walled Carbon Nanotube Gas Sensors on Plastic Substrates", *Micro and Nano Lett.*, 2011-accepted.
5. Y. Liu, M. L. Wang, M. R. Dokmeci, "Integration of Single-Walled Carbon Nanotube Sensor inside Microfluidic Device for Remote Water Quality Monitoring", to be submitted to *Nanotechnology*.
6. Y. Liu, M. L. Wang, M. R. Dokmeci, "Analyzing the Gas Sensing Characteristics of RNA Functionalized SWNT Sensor", to be submitted to *Appl. Phys. Lett.*
7. Y. Liu, Q. Sheng, S. Muftu, M. L. Wang, M. R. Dokmeci, "A Stretchable, Flexible and Transparent SWNT Strain Sensor Embedded in PDMS Thin Films"-to be submitted to *Nano Lett*.
8. Y. Liu, Y. Zhang, M. R. Dokmeci, M. L. Wang, "Wireless Sensor Array based on DNA Decorated Single-Walled Carbon Nanotubes for Gas Monitorng", *Proceedings of SPIE, vol. 7981, Sensors and Smart Structures Technologies for Civil, Mechanical, and Aerospace Systems*, San Diego, CA, March 11-15, 2012.
9. Y. Liu, Y. Zhang, M. R. Dokmeci, M. L. Wang, "Direct (DEP) Assembly of Single-Walled Carbon Nanotubes as Sensor Array for Wireless Gas Monitoring Applications", *Proceedings of the 2011 World Congress on Advances in Structural Engineering and Mechanics (ASEM11 plus), Mini Symposium-Multifunctional Thin Film*, Seoul, Korean, Sep. 18-22, 2011.
10. Y. Liu, C.-L. Chen, V. Agarwal, S. Sonkusale, M. L. Wang, M. R. Dokmeci, "Single Chip Nanotube Sensors for Chemical Agent Monitoring", *Proceedings of the 16th international Conference on Solid-State Sensors, Actuators and Microsystems (Transducers '11)*, Beijing, China, 02-116, June 5-9, 2011.
11. Y. Liu, M. Chen, M. L. Wang, M. R. Dokmeci, "Sensing Characteristics of RNA Oligomer Coated SWNT Gas Sensors", *Proceedings of the 16th international Conference on Solid-State Sensors, Actuators and Microsystems (Transducers '11)*, Beijing, China, 02-117, June 5-9, 2011.
12. Y. Liu, M. Chen, M. Mohebbi, M. L. Wang, M. R. Dokmeci, "The Effect of Sequence Length on DNA Decorated CNT Gas Sensors", *Proceedings of the 16th international Conference on Solid-State Sensors, Actuators and Microsystems (Transducers '11)*, Beijing, China, 03-158, June 5-9, 2011.
13. Y. Liu, X. Li, M. R. Dokmeci, M. L. Wang, "Carbon Nanotube Sensors Integrated Inside a Microfluidic channel for Water Quality Monitoring", to appear in *Proceedings of SPIE, vol. 7981, Sensors and Smart Structures Technologies for Civil, Mechanical, and Aerospace Systems*, San Diego, CA, March 6-10, 2011.

14. X. Li, S. Selvarasah, Y. Liu, C. Yang, and M. R. Dokmeci, "Highly Sensitive Single-Walled Carbon Nanotubes based Gas Sensors on Plastic Substrates," *Bio Sensors, Materials Research Society Fall Meeting*, Boston, MA, November 30 - December 2, 2010.
15. C.-L. Chen, Y. Liu, V. Agarwal, S. Sonkusale, A. Busnaina, M. Chen, and M. R. Dokmeci, "Single-Walled Carbon Nanotube Gas Sensors Integrated on Complementary Metal Oxide Semiconductor Circuitry," *Proceedings of the 13th NSTI Nanotechnology Conference*, Anaheim, CA, June 21-24, 2010.
16. Y. Liu, C.-L. Chen, V. Agarwal, Xinghui Li, S. Sonkusale, M. R. Dokmeci, and M. Wang, "Carbon Nanotube Sensors on CMOS circuitry for Environmental Monitoring," to appear in *Proceedings of SPIE, vol. 7647, Sensors and Smart Structures Technologies for Civil, Mechanical, and Aerospace Systems,* San Diego, CA, March 7-11, 2010.
17. B. Zientek; H. H. Wang; J. E. Indacochea; Y. Liu; M. L. Wang, " Development of nanowell based sensors for the detection of improvised explosive devices," to appear in *Proceedings of SPIE, vol. 7647, Sensors and Smart Structures Technologies for Civil, Mechanical, and Aerospace Systems,* San Diego, CA, March 7-11, 2010.
18. Y. Liu, M. R. Dokmeci, and M. Wang, " Sensor Protocol Made of DNA Assembled Carbon Nanotube on CMOS Chip for Environmental Monitoring," to appear in *Proceedings of The US-Korea Workshop on Multi-scale Mechanics and Multi-functional Materials for Smart Sensing and Actuation*, Jeju, Korea, May 30-June 3, 2010.
19. Y. Liu, M. L. Wang, J. E. Indacochea, H. H. Wang, "Interference color of anodized aluminum oxide (AAO) films for sensor application," to appear in *Proceedings of SPIE, vol. 7647, Sensors and Smart Structures Technologies for Civil, Mechanical, and Aerospace Systems,* San Diego, CA, March 7-11, 2009.
20. Y. Liu, M. L. Wang, J. E. Indacochea, H. H. Wang, "Colorimetric Detection of Nitroaromatics," to appear in *Proceedings of ANCRiSST, The Fifth International Workshop on Advanced Smart Structures and Technology*, Boston, MA, July 29-31, 2009.